ADDITIVE LAYER MANUFACTURED SINTER-STYLE ALUMINIUM/AMMONIA HEAT PIPES

SEIED MASOUD AMELI

PhD

2013

ADDITIVE LAYER MANUFACTURED SINTER-STYLE ALUMINIUM/AMMONIA HEAT PIPES

Seied Masoud Ameli

The thesis submitted in partial fulfilment of the requirements of the University of Northumbria at Newcastle for the degree of Doctor of Philosophy

Faculty of Engineering and Environment

Research undertaken in the Faculty of Engineering and Environment in collaboration with Thermacore Europe

September 2013

Abstract

A novel heat pipe (HP) manufacturing method has been developed based on an additive layer manufacturing technique called "selective laser melting" or SLM. This innovation is expected to benefit current applications of aluminium/ammonia heat pipes in space and terrestrial projects as well as many new HP applications.

The project was jointly sponsored by the Northumbria University and Thermacore, a world leading heat pipe manufacturing company in the UK, and formed the feasibility stage of a much larger program in Thermacore aiming to develop the next generation of HPs for space applications. In this project, sinter-style aluminium SLM HPs have been produced and tested to prove their functionality and to provide an overall image of the new production process with regard to the major involved parameters.

It is believed that this is the first time that functional heat pipes are produced with this method and also the first time that functional aluminium HPs are produced with a sinter-style wick structure. Currently, aluminium heat pipes with aluminium sintered wick do not exist due to the impracticality of sintering aluminium powders on the internal walls of a heat pipe.

During the project several properties of the new heat pipes e.g. wick porosity, permeability and pore size; wall density, hardness, vibration resistance and optimum SLM build parameters have also been determined by the existing or especially developed rigs in Thermacore or Northumbria University laboratories including scanning electronic microscope (SEM), vibration table, permeability measurement rig, etc. Converting the SLM products into functional heat pipes involves many other steps which have also been completed and explained.

At the end of the project two successful functional samples were obtained and clear and precise answers were found to the project questions. SLM process was proved to be capable of producing functional heat pipes. Functional sinter-style heat pipes are proved to be producible by SLM. A numerical design tool is now available to evaluate SLM produced heat pipes and major challenges of this new HP production process including the density of the solid structures and possible contamination of the materials have been identified. Also a reasonably good overall image of this new HP production process and the new HPs has been provided in this project through the conducted measurements and experiments. The contribution of this project to knowledge is supported by two papers published in prestigious heat pipe journals and one paper presented in the 16th international heat pipe conference.

Table of Contents

List of figures

List of Tables

- Ameli, M., Agnew, B., Leung, P. S., Ng, B., Sutcliffe, C. J., Singh, J., McGlen, R., (2013). "A novel method for manufacturing sintered aluminum heat pipes (SAHP)", Applied Thermal Engineering 52: 498-504.
- Ameli M., Agnew B., Leung P. S., McGlen R. J., Sutcliffe C. J., (2013). "Ammonia Heat Pipes for Built Environment Applications", Heat Pipe Science and Technology - An International Journal (Awaiting publication)
- Ameli M, Agnew B, Ng B, McGlen R J, Sutcliffe C J, Singh J, (2012). "Sintered Aluminium Heat pipe (SAHP)", proceedings of the 16th International Heat Pipe conference (16th IHPC), May 20-24, Lyon, France.

PREFACE

This project's original idea was formed in Thermacore Europe. Thermacore specializes in design and development of thermal management systems for mission-critical applications across a diversified set of markets including military and aerospace and is a world leading heat pipe patent holder and manufacturer.

This PhD is part of a much bigger program in Thermacore to develop the next generation of heat pipes for space applications in response to the European space agency (ESA) call. An additive layer manufacturing laser technology had been identified by Thermacore with a possible capability to produce aluminium heat pipes that would improve the performance of the space-used aluminium/ammonia heat pipes in some aspects.

Once it was proposed that the improvements could also benefit many terrestrial applications of ammonia heat pipes, a joint venture was formed between Thermacore and the department of engineering and environment of Northumbria University to do a feasibility study in the scope of a PhD project.

Having a mechanical/thermal academic background and work experience including five years work experience in Thermacore during my MPhil degree and then as an R&D engineer, I was successful to be accepted to work on this interesting project.

Today, at the end of this project, the idea has been proved to be indeed feasible. Prompted by the results of this project, the work is continuing in a much larger scale with access to many more resources to complete the very long way ahead before the identified challenges are overcome and this new innovation is fully characterized and qualified especially for critical applications.

ACKNOWLEDGMENTS

I think the best things in life are;

- Having my late-father's ambitiousness, my supervisor's astuteness, Iranian patience and British politeness and then
- To do a PhD in England
- To live in Asia
- And to work in Middle East

Having lived in England for eleven years and having concluded this project I hope I have ticked the first two with the other two planned for the rest of my life and I thank each and everyone who supported me through this. The completion of this PhD was possible by the support of several people.

My sincere gratitude goes to my supervisor, Professor Brian Agnew for insightful discussions and consistent encouragement throughout the work and through all these years. I feel really privileged to know him. He is one of the smartest people I know. Fulfilment of the numerous tasks involved in the project was possible because of the support provided by Thermacore and its excellent facilities and personnel especially Dr. Ryan McGlen for his treasured suggestions and friendship, engineering manager Kevin Lynn for his unconditional support and all the technicians. I do hereby acknowledge all of them and will forever be thankful to Thermacore.

I would like to thank my second supervisor, Dr. Ken Leung for his support all through the project. I thank Dr. Singh and the team in Liverpool University to make the samples and prototypes for us. I also have to thank the members of my annual review PhD committee, Professor Bob Giddings and Professor Christopher Underwood for their very constructive comments that helped to keep the project in the right track to meet both its academic and industrial objectives. The dedication of them to their work and research by their continuous presence in the school is an example to follow in my future careers.

I appreciate the interest shown to my project by my fellow PhD researchers and colleagues including Paula Drew, Benjamin Shaw, Sonia Zahiroddini and Joshua Fong, to name a few, who made the journey more fun. And last but not least I am grateful for all the love that I received from my family whom I cannot wait to meet again.

I declare that work contained in this thesis has not been submitted for any other award and that it is all my own work. I also confirm that this work fully acknowledges opinions, ideas and contributions from work of others. The work was done in collaboration with Thermacore Europe Company based in Ashington, UK.

The project has had a laboratory and experimental based nature and did not require direct participation from anyone other than the researcher. The IP issues, publication rights etc. have been dealt with in a mutual contract between the University and Thermacore Europe.

Seied Masoud Ameli

30 July 2013

Chapter I : INTRODUCTION

Heat pipes (HP) are passive two-phase heat transfer devices to transfer heat from one point to another. There is a wide variety of HPs based on the structure, material, geometry and operating inclination angle and temperature. With respect to their internal structure, HPs are classified into three major groups of "sintered", "grooved" and "screen mesh" HPs, each characterized by certain technological traits.

Sintered heat pipes' main characteristics are a wide range of operating inclination angle and higher input heat flux handling capability compared to the other two groups. Currently there is a lack of sintered aluminium heat pipes due to the restrictions of the conventional manufacturing methods. This project aims to investigate a novel method for producing these heat pipes that can also be applicable to other types of heat pipe. This novel method is based on an additive layer manufacturing technique called selective laser melting or SLM.

A typical heat pipe is a hermetically sealed cylindrical tube with a capillary structure or "wick" on its internal wall filled with a small amount of a working fluid. Inside the tube, the working fluid is always in, or very close to its saturated state. When a section of the tube is heated the fluid evaporates and travels to the other parts of the tube which are colder. By rejecting the heat at these parts the vapour condenses and the condensate is returned back to the hot section by capillary pumping force of the wick and/or gravity and the cycle continues.

An absolute majority of the currently available aluminium heat pipes are extruded aluminium profiles with internal grooves or axially grooved heat pipes (AGHP) as shown in figure 1-1, that are filled with ammonia and are used in space and some terrestrial applications.

Figure 1- 1 Aluminium axially grooved heat pipe (AGHP)

Grooves do not supply high capillary pumping forces thus the use of these HPs in near-zero-gravity space applications or in applications where the hot source is below the cold medium and gravity aids to return the condensate back to the hot section and therefore the capillary force is not of prime importance. When a HP works against gravity or with its hot section above the cold part, the wick's capillary action is the only driving force to return the condensate to the hot section. Maximum capillary pumping force is achieved by using sintered wicks that have many tiny interconnected pores. In the conventional HP manufacturing methods sintered wicks are fabricated by sintering metal powders together and to the HP internal wall so the name "sintered heat pipes". Figure 1-2.

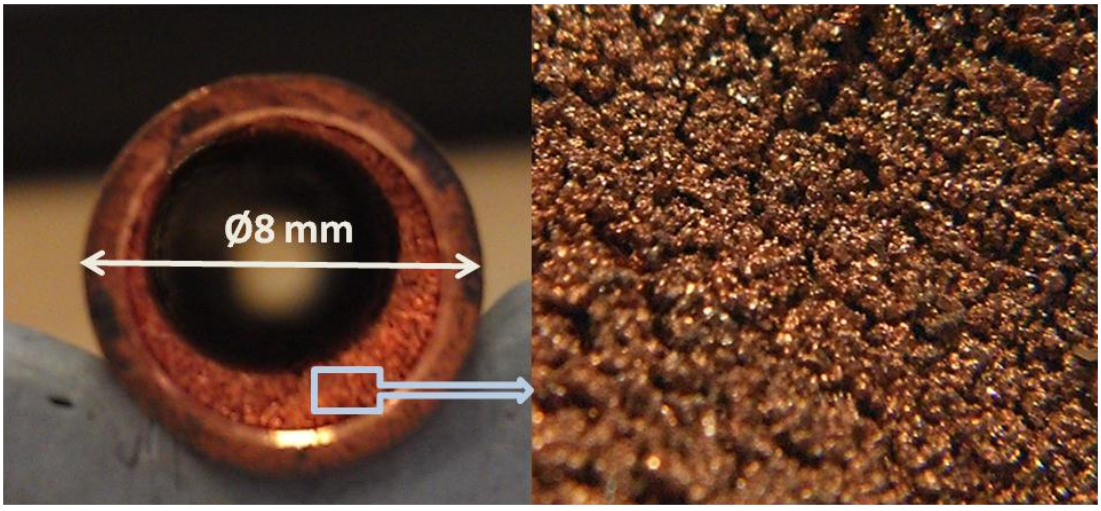

Figure 1- 2 Sintered copper heat pipe

This fabrication method can not be used for production of sintered aluminium heat pipes. Aluminium reacts with oxygen very quickly to form Al2O3. An alumina film forms on an aluminium surface which is exposed to even small amount of atmospheric oxygen or water vapour. Conventional aluminium sintering methods all either use a force to break this alumina layer and bring the aluminium atoms close to each other by compacting the aluminium powder or use a sintering aid. None of these methods are practical to build heat pipe wicks. A new method for sintering aluminium is presented in U.S. Pat. No. 7,517,492 B2 issued to Jianxin Liu

on April 14, 2009, "Processes for Sintering Aluminium and Aluminium Alloy Components", which is based on sintering aluminium powder together in a nitrogen atmosphere which contains a partial pressure of water vapour without using a sintering aid or pressing the aluminium powder together by mechanical force to rupture the alumina film prior to or during the heat of the powder. But, to the knowledge of the author, this invention has never been used to generate aluminium wick structures for heat pipes.

Selective laser melting (SLM) is capable of producing similar porous structures from an array of tiny octahedral geometries formed into a lattice structure (henceforth called "sinter-style" in this project) (Figure 1-3). SLM uses a high power laser beam in a controlled environment that melts aluminium powders together as defined in a CAD model.

Figure 1- 3 SLM produced sinter-style structure

SLM can also produce solid walls by fully melting the powders together in an area therefore the heat pipe wall and end caps, and consequently the entire heat pipe, can be produced by SLM.

This project represents the first time SLM is being investigated for production of sinter-style aluminium heat pipes. SLM produced HP samples will be converted into functional heat pipes through a long conversion process of machining, welding, cleaning and filling and will be tested by the especial test rigs that also need to be designed and fabricated. The feasibility of the SLM HP is to be verified and sinter-style samples are to be demonstrated to posses the main characteristics of the conventional sintered heat pipes (such as sintered copper heat pipes) including the ability to work against gravity and high input heat flux handling capability.

Two innovations are intended to be claimed by the project; the first functional heat pipe ever produced by an additive layer manufacturing technique and the first functional aluminium heat pipe with an aluminium sinter-style wick structure. The first claim will be realised by producing

and processing the samples and comparing their heat transfer capacity versus a pure solid conductor to demonstrate that they work as heat pipes and the latter will be supported by comparing the processed sinter-style SLM HP samples' thermal performance with that of a geometrically-identical extruded axially grooved heat pipe (AGHP).

An overall clear image of the entire process and the key issues will be drawn through measurements on the critical parameters and a numerical model will be developed that enables theoretical evaluation of the new SLM HPs.

Background and motives of the project

Ammonia heat pipes have been in use since 1960s. They have a superior performance compared to other types of heat pipes at a temperature range of -40 to +30 °C and were first developed for unmanned spacecraft, an application which still dedicates the majority of ammonia heat pipe applications. In space, ammonia HPs are used for either iso-thermalization of the side panels or transferring the heat from cables and electronics to the radiative panels. Almost all these pipes use aluminium as the container material and the majority have a grooved wick structure.

Ammonia HPs have also been implemented in several terrestrial applications including thermo-stabilization of permafrost, de-icing of infrastructures, refrigeration systems and waste heat recovery heat exchangers with a potential for the use in other applications such as low grade geothermal conversion, catering, solar collectors, air conditioning and dehumidification heat exchangers. Existing terrestrial ammonia HPs have either carbon steel or aluminium containers and grooved wick structure although in some major permafrost applications wickless ammonia HPs (Thermosyphone) have been employed.

A process that allows production of sintered (or sinter-style) aluminium heat pipes especially a flexible process such as SLM that enables generation of fully controlled sinter-style wicks at selected regions of a heat pipe, will benefit most of these applications. Currently, the major challenge for the space ammonia HPs is improving their heat flux handling capability to meet the thermal control demands of the next generation of satellites and spacecrafts. To address this, activities so far have been focused on using composite wick structures which is difficult to achieve in practice.

Conceivable improvements to the terrestrial ammonia heat pipes by the new SLM production process are envisaged in different aspects depending on the type of the application. Firstly an ammonia heat pipe capable of operating at high inclination angles against gravity opens up a whole new range of possible applications for these pipes. It seems that the problem of the lack

of these pipes, so far has been avoided by using ammonia HPs only in gravity aided situations. Secondly, the new SLM based process can benefit many of the current applications by offering ammonia heat pipe that have graded sinter-style wick at selected heat removal and disposal regions of the pipe to achieve higher heat flux handling capability. Moreover a graded/tailored sinter-style wick applied to the evaporator (hot) region of a heat pipe provides a better circumferential distribution of the working fluid which is highly desired especially in large diameter heat pipes. So far different approaches have been suggested to overcome this latest issue, as discussed in the next chapter, but none is as effective and, perhaps economically viable, as this.

Project objectives/development plan

There are four main objectives for the project.

1. To prove the feasibility of producing operational heat pipes by SLM. Accomplishment of this objective will be measured by producing the samples, converting them to functional heat pipes and comparing the temperature drop along the pipe in charged and uncharged states.
2. To demonstrate that sinter-style aluminium heat pipes can be produced by SLM and to verify that they have the main attributes of the conventional sintered heat pipes including the ability to work at high inclination angles against gravity and high input heat flux. Accomplishment of this objective will be measured by comparing the performance of the processed SLM HP samples against identical grooved heat pipes at the same conditions.
3. To develop a numerical design tool for theoretical design and evaluation of the new sinter-style SLM heat pipes. The tool will predict the performance of a SLM HP based on the user input specs to check whether it will meet the requirement of the intended application or not.
4. To identify the main challenges and critical issues of the new production process and the new heat pipes to direct the future investigations.

Successful conclusion of the objectives will depend on several other lateral actions to be undertaken. Raw SLM heat pipes need to go through a long process before becoming functional. This process involves a range of equipment including welding fixtures and filling rigs that must be developed for the special shape of the samples.

Several other measurements should be performed on critical parameters that are either essential for successful production of the samples or to identify possible critical issues and challenging problems. Also several test rigs should be designed and fabricated for the specific produced SLM samples for performance evaluation or characterization. Completion of these tasks stimulates access to and exploitation of different resources in Thermacore, the University or third parties. The project objectives and development plan is shown in figure 1-4 schematically.

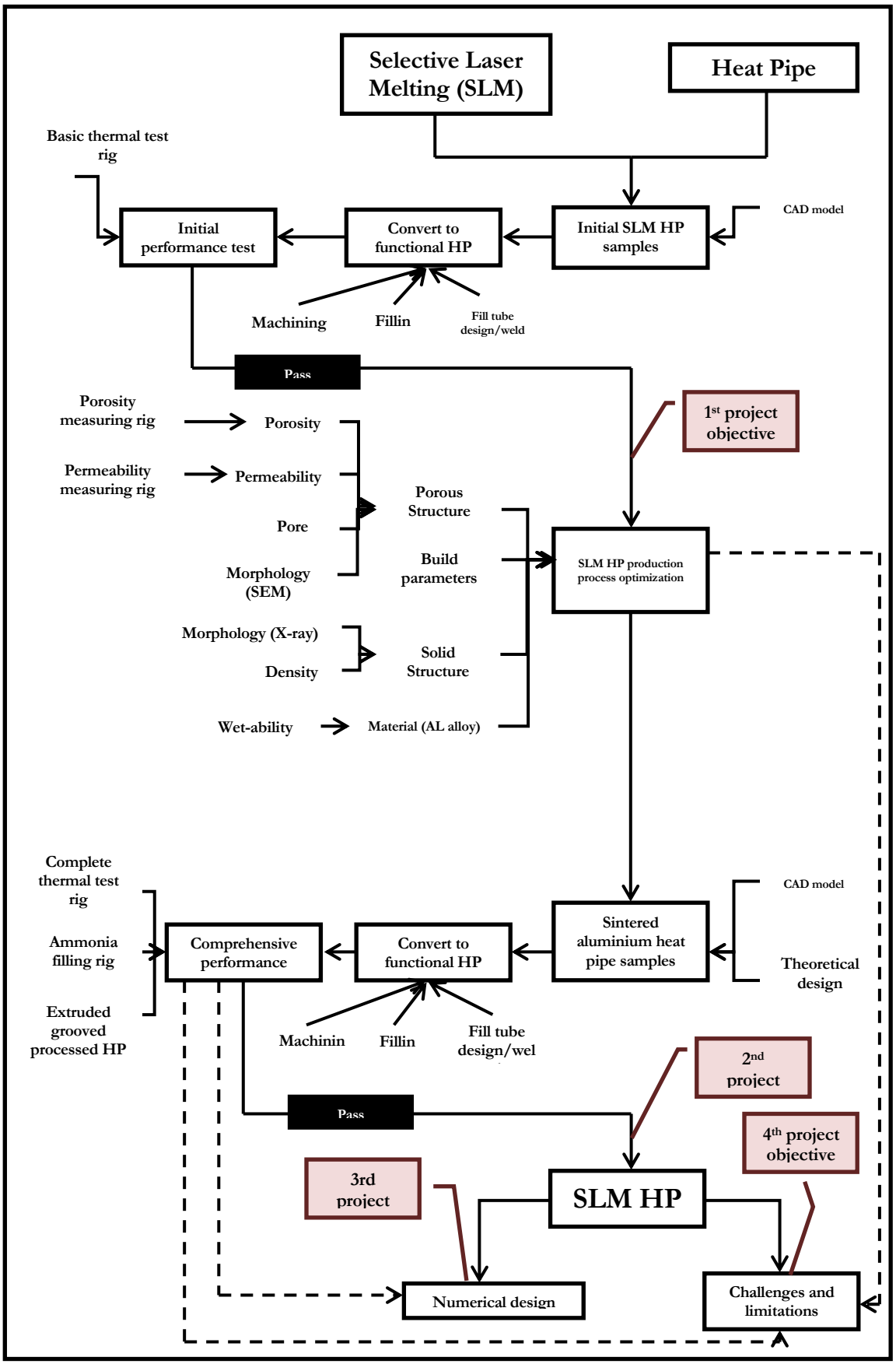

Figure 1- 4 Project objectives achievement plan

Contribution to knowledge

Two innovations are to be claimed by this project. SLM technique is to be introduced as a novel heat pipe production method and aluminium heat pipes are to be produced, for the first time, with a sinter-style wick structure using this method.

The new production process is likely to be advantageous to a much wider range of heat pipes not limited to aluminium HPs. When proved feasible, the same process can be applied to any heat pipe made of materials that are suitable for SLM process. Also, extreme flexibility and controllability of the SLM build process can help the ideas to fly to break new grounds in heat transfer behaviour of the heat pipes by using complex wick structures.

If prompted by the project's results, the new capabilities of aluminium/ammonia heat pipes will allow more demanding applications with higher heat intensities to function as well as new applications with different positioning of the hot and cold medium.

Thesis layout

The thesis is divided into six chapters. This chapter introduces the idea of the project, project objectives and motives, original contribution to knowledge and the background.

Chapter two is a review of the available literature and applications of aluminium/ammonia heat pipes to specify their characteristics and the extent to which they have been implemented. The review highlights how the new idea, which is being evaluated and developed in this project, would help to improve the current applications' performance.

A relatively comprehensive theoretical basis has been given in chapter three which has later formed the core of the developed numerical design tool. Exemplary calculation process to verify the initial samples' build parameters is also described in this chapter as well as the numerical designing tool which has been developed through the project.

The very long length of the fourth chapter is a representative of the amount of the work that has gone into this section. It is a relatively detailed description of the process and methodology of building the prototypes, hardware and the test rigs and the measurements on the critical parameters. It illustrates the entire process up to the point that the final SLM HP prototypes have been ready for experiment which is the subject of its following chapter. This chapter can be quickly reviewed before reading its following chapters and only be referred to again when it is needed.

Experimental results on the actual SLM HP prototypes are presented in chapter five.

The identified challenged and critical issues are discussed in the last chapter along with the conclusions and side notes including the economics of the SLM HP production process.

2-1) Introduction

Increasing powers and heat fluxes of micro-electronic devices has produced the requirement for more efficient next generation electronics cooling techniques to dissipate the waste heat generated. Current satellite systems deploy aluminium ammonia axially grooved heat pipes (AGHP) to transport the heat from the electronics to the radiator. AGHPs are very appropriate devices for space applications: they do not need electric power, have no moving parts, have a very effective thermal conductance and have a long operational life (Vlassov, de Sousa, et al. 2006). But the low surface heat flux of AGHP is now limiting deployment of high specification electronic components, which in turn limits the capabilities of the space-based sensing and communications systems.

Yet the next generation of spacecraft and satellites will be even more heat dissipative. The maximum conductive dissipation of the communication module of a telecommunication satellite can reach 6.5 kW (McGlen, 2011). This thermal control requirement directly concerns heat pipes networks. Thus, there is a need for a technology development cycle to face these new thermal specifications and to meet the future thermal control requirements on telecommunication and scientific satellites. According to Hoa, Demolder, et al. (2003) one of the main objectives to reach and the technical challenges to overcome is to achieve higher surface heat densities.

By replacing the capillary grooves of an AGHP with a sintered powder capillary structure to form a sintered aluminium heat pipe (SAHP), the input heat flux across the evaporator region of the AGHP could be increased from the current value of less than 3 W/cm2 to in excess of 50 W/cm2, allowing for a step change in thermal performance of the heat pipe specially where heat pipes are needed to work against gravity while keeping the low weight advantage of the aluminium (McGeln, 2011). It is very difficult to sinter an aluminium structure using conventional manufacturing techniques due to the existence of aluminium oxide on the powder surface and the wide, yet relatively low melting point range of aluminium. An additive layer manufacturing technique called selective laser melting (SLM) locally melts and fuses metal powders to form complex 3D structures. This project aims to assess the feasibility of the SLM technique to manufacture sinter-style aluminium capillary structures and ultimately sinter-style aluminium heat pipes. These structures are generated from a CAD model allowing them to be graded / tailored to meet the needs of the specific application.

Moreover, current manufacturing methods for heat pipe porous wick structures have exposed many restrictions on the shape and complexity of the wick. As a result of this, most of the research on the thermal and mechanical properties of the porous wicks has focused on these limited shapes and structures. The fact that porous structures can be produced by SLM with literally no limit enables the ideas to fly and the research to further focus on optimizing the structural and functional performance of the wick for each application regardless of its complication.

Apart from the space, SAHPs and other SLM HPs can also benefit many current terrestrial applications of ammonia heat pipes not limited to heat pipe-based heat recovery heat exchangers, permafrost stabilization and de-icing applications. The terrestrial applications cover a wider variety of ammonia heat pipes than space applications. In space, an absolute majority of heat pipes are aluminium AGHPs filled with ammonia while current terrestrial applications of ammonia heat pipes use either aluminium or carbon steel pipes in a wickless form or with axially grooved or composite wicks. In this project these relatively wide range of heat pipes have been grouped and studied together under the common name of ammonia heat pipes.

There are several advantages attributed to SLM ammonia HPs (Inc. SAHPs) compared to the existing ammonia heat pipes (Inc. AGHPs). Higher heat flux density, the ability to work against gravity, better working fluid distribution in the evaporator (which leads to better overall thermal performance) and flexibility in terms of the shape and structure of the porous wick are some of these advantages. Each current application of ammonia heat pipes is believed to benefit from one or more of these new improvements.

For instance in an space used AGHP, replacing the grooves with an SLM sintered structure in the evaporator section increases the heat flux density considerably while using a steel sinter-style wick in the evaporator section of a currently-wickless permafrost ammonia Thrmosyphon (wickless heat pipe) can provide a better overall performance by distributing the working fluid in the evaporator more evenly. Or in a heat recovery heat exchanger having a sinter-style wick all along the aluminium heat pipe (instead of the grooves) will enable the pipe to work at inclination angles against gravity.

This project does not recommend SAHP as a direct replacement for all the AGHPs or other types of ammonia heat pipes but SLM HPs (including SAHP) are introduced as a new generation of heat pipes with several advantages that can benefit most of the current applications of ammonia heat pipe in one way or another.

In this chapter current applications where ammonia heat pipes have been implemented are reviewed in two main categories of space and terrestrial applications and the specifications of the reported ammonia heat pipes are summarized. This review aims to, firstly, highlight the fact that almost all the available ammonia heat pipes are either AGHPs or without a wick structure (what is known as Thermosyphon) and then to clarify how each group of applications can benefit from one or more advantages attributed to the new SLM HPs including design flexibility, higher heat flux density, wider operation angle and better overall performance. It should be noted that the focus of this literature review and this project is only on the heat pipe in its most conventional shape. Other types of heat pipes such as capillary pumped loops, loop heat pipes, micro and miniature heat pipes, flat heat pipes and oscillating and variable conductance heat pipes are out of the scope of this project.

It should also be reminded that, although the ultimate use of the new heat pipes is expected to be in aluminium/ammonia HP applications, all the experiments of this project have been conducted using acetone since the required ammonia filling rig was not completed until the very end of the project. However this change of the working fluid makes no difference in the concluded results whatsoever. The main concerns in using a new working fluid in a HP is the efficient working temperature of the new fluid and, more importantly, its compatibility with the HP container material but it does not affect the operability and working principles of the pipe. Aluminium heat pipes are compatible with both ammonia and acetone and a comparison of the performance of the two is reported in some literatures e.g. Vlassov, de Sousa, et al. (2006) and Munzel & Savage, (1975).

2-2) Ammonia heat pipes in space applications

As a highly effective heat transfer element, heat pipes have been gradually recognized, and are playing a more and more important role in almost all industrial fields (Zhang & Zhuang, 2003). Typically, ammonia heat pipes have an operational temperature range from -40°C to 80 °C. Although there are reports of elevated temperature ammonia pipes able to operate up to 125°C (Prado, Mishkinis, et al., 2012), the highest efficiency is achieved between -40°C and +30 °C.. This temperature range well suits many of the un-manned space applications.

The first investigations on using ammonia as a working fluid for heat pipes was done in the late 60s (Cotter, 1965) and the first onboard spacecraft experiments of an ammonia heat pipe was in early 70's as reported by Harwell & Mcintosh, (1981). To date, nearly all space radiator systems have used grooved aluminium/ammonia heat pipes or loop heat pipes (Vlassov, de Sousa, et al. 2006).

Other types of heat pipes have also been used or investigated for the use in some space applications e.g. high temperature sodium heat pipes for space nuclear power (Rosenfeld & Sanzi, 2012), but ammonia is the most common HP working fluid for space and more ammonia heat pipes have been used in space than all the other applications together.

In space, ammonia heat pipes are used for either iso-thermalization of the side panels e.g. in Ollendorf, McIntosch, et al. (1973), or transferring the heat from cables and electronics to the radiative panels e.g. in Jones (1983), Barantsevich & Shabalkin (2003) and Valssov, de Sousa, et al. (2006).

In the latter, the heat from electronics is transmitted to the external surface of the ring radiator as shown in figure 2-1;

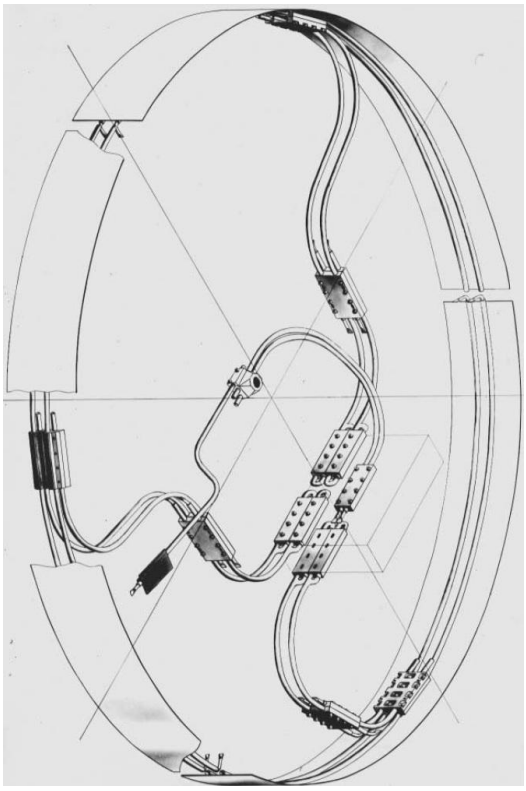

Figure 2- 1 Ammonia heat pipes are used to transfer heat from electronics to the radiative panels. (Vasiliev, 1998)

Maydanik (2005); Riehl & Dutra, (2005); Vasiliev & Vasiliev (2005); Vlassov, de Sousa, et al. (2006); Bai, Lin, et al. (2009); Kaya (2009) and Dobre, Pârvulescu, et al. (2010) are only some more examples of the very rich literature on this type of applications.

Axially grooved heat pipes are the most common heat pipes used in space. They offer relatively simple industrial fabrication and greater reliability than other wick designs, such as artery heat

pipes. Most of these were first designed with rectangular grooves but then trapezoidal grooves have been developed as they have shown better performances (Hoa, Demolder, et al., 2003).

Longitudinal grooves in the walls of a heat pipe are mainly extruded and aluminium is the most suitable material for extrusion. Grooves can also be threaded inside the pipe for the purpose of good liquid distribution on the circumference. An oil filled ball spinning process to machine the axially inner micro grooves by extruding the tube with fixed multi-tooth mandrel is presented by Li, Xiao, et al. (2008).

Aluminium is not the only material and axial grooves are not the only wick structure used for space ammonia heat pipes. Artery heat pipes have different passages for the working fluid condensate and the vapour inside the pipe in order to avoid vapour-condensate interaction which is a performance limiting factor in AGHPs. They mainly achieve this by using a rolled screen mesh over the tip of the grooves inside the pipe to minimize this interaction. Examples of this type of space ammonia heat pipes can be seen at Munzel & Savage (1976) who reports the life test results of ammonia aluminium and SS double artery heat pipes flight-tested aboard a sounding rocket or at Kreeb, Groll, et al. (1973) who presents the life test results for an ammonia HP with SS 321 container, 250 Al mesh, Ø14 OD and 50mm length.

Regardless of the material and wick structure, in space, heat pipes work in a zero or micro gravity environment and as such the higher capillary force of a sinter-style SLM HP is not of prime importance. However achieving higher heat flux density in space ammonia heat pipes is a major challenge. A review of the literature reveals the current value of the heat flux density to be below $3W/Cm^2$ for majority of the space ammonia heat pipes.

Barantsevich & Shabalkin (2003) describe the design and testing aspects of ammonia axial grooved heat pipes (AGHPs) made of aluminium alloy 6063 intended for cables thermal control of the solar battery drive integrated into the international space station. The heat removal system includes four heat pipes with a diameter of 10 mm and length of 2 m. Each heat pipe shall transfer 50 W in temperature range of 0–50 °C with a maximum temperature differential of 5 °C. Heat is supplied to the middle of the AGHP and rejected from both ends, each with a length of 200–220 mm in contact with the design components on which the electronics is mounted. This corresponds to $0.8\ W/Cm^2$ heat flux density.

In Chen, Zhang, et al. (2009) study, the heat transfer capability and total thermal resistance for a heat pipe with axial "Ω"-shaped micro grooves has been optimized and the effects of the structural parameters on the heat transfer capability and total thermal resistance has been analyzed. The aluminium/ammonia heat pipe has a diameter of 12.5 mm, operates at a

temperature of 293K (20°C) and at the most optimal case shows an input heat flux of 1.46 W/Cm^2. The same authors developed a theoretical model of fluid flow and heat transfer in a heat pipe with axial "Ω"-shaped grooves (Zhang, Chen, et al., 2009) solved numerically to obtain the heat pipe performance and maximum heat transport capability. The aluminium/ammonia heat pipe sample used for optimization had a 4.5 mm diameter and 10 Cm evaporator with a maximum heat input of 47.5 W at 293K (20°C) temperature which corresponds to an input heat flux of 3.36 W/Cm^2.

Chen, Zhu, et al. (2010) also measured an input heat flux of 1.1W/Cm^2 for an aluminium/ammonia heat pipe with a diameter of 14.96 mm, 700 mm evaporator length and maximum heat input of 230W at 300K (27°C).

½ in (12.7mm) outside diameter grooved ammonia heat pipes test results aboard a sounding rocket are reported by McIntosh (1975). The pipes were 36" (0.91m) long with 12" (0.3m) evaporator length and were tested up to 1W/Cm^2 radial heat input density.

McIntosch, Ollendorf, et al. (1975) present some of the results of the international heat pipe experiment which was launched aboard a rocket that provided six minutes of near zero gravity during which a total of ten separate heat pipe experiments were performed. The experiments included two axially grooved heat pipes with 36-inches (0.91 m) length, 12-inch (0.3 m) heated length and 12-inch (0.3 m) condensers, ½-inch (12.54 mm) outside diameter, filled with ammonia. They measured a maximum input heat flux of 1.02 W/Cm^2.

The low heat flux is not limited to AGHPs but also to SS arterial heat pipes. Munzel & savage (1976) reports the life test results of ammonia aluminium and SS double artery heat pipes flight-tested aboard a sounding rocket at 0.85 W/Cm^2 heat input density at an adiabatic operating temperature of 60°C while working slightly against gravity (5 mm slope at 885 mm length). The low heat flux of the SS heat pipes is partly due to the low heat conductivity of SS comparing to aluminium. This increases the temperature drop along the length of the heat pipe considerably which consequently stimulates a reduction in the total heat input to keep the temperature drop to an acceptable level. Moreover, arterial heat pipes normally face other problems as well due to the use of different material for the mesh and container of the heat pipe. Very often this problem is the generation of non condensable gasses inside the pipe that, over the time, reduces the effective heat transfer length of the pipe. Munzel & Savage (1976) showed that only one metal heat pipes (both container and wick from the same material) reduces the non-condensable gas generation considerably.

Hoa, Demolder, et al. (2003) report higher heat flux values for current ammonia pipes in their summarization of the specifications of the current space ammonia heat pipes as below,

Diameters (mm) 9 to 25

Lengths (m) 0.25 to 4

Linear mass (g/m) for filled heat pipes 350 to 670

Heat transport capacity (Wm) 50 to 600

Maximum heat flux density (W/cm^2) 3 to 6

Operating temperature range (°C) -40 to +80

Life time (years) 15 to 20

Although the author was not able to locate any report of an actual ammonia heat pipe with higher heat fluxes than 3.36 W/Cm^2 but even the value of $6W/Cm^2$ is much lower than what is expected from a sinter-style SLM HP.

The most apparent way for increasing this heat flux is to use a sintered wick in the evaporator section of the space ammonia heat pipes. However it should be noted that there are many more parameters to consider including the higher condensate pressure drop in a sintered wick as opposed to a grooved wick which lowers the total heat handling capability of the heat pipe.

There is a large number of literature on grooved ammonia heat pipes e.g. Jiao, Ma, et al. (2007); Chen, Zhang, et al. (2009 and 2010) and Lips, Lefevre, et al. (2009) who study the structure of the grooves or Eggers, Serkiz, et al. (1971); McIntosch, Ollendorf, et al. (1975); Munzel & Savage (1976); Savage (1976); Jones (1983) and Bertoldo, Vlassov, et al. (2012) that analyze the thermal performance of a grooved ammonia heat pipes in general as well as studies like Kreeb, Groll, et al. (1973) who reports the life test results of an ammonia HP with SS 321 container, 250 Al mesh, Ø14 OD and 50mm length.

On the other hand numerous literature exist that investigate sintered porous wick structures such as Pruzan, Klingensmith, et al. (1991); Leong, Liu, et al. (1997); Wang & Peterson (2003); Carson, Lovatt, et al. (2005); Zhang & Wang (2005); Chiu, Wu, et al. (2007); Iverson, Garimella, et al. (2007); Semenic, Lin, et al. (2008); Weibel, Garimella, et al. (2010) and Vasiliev, Grakovish, et al. (2012). But the reports of any research on ammonia heat pipe with a sintered (or sintered style) wick are extremely rare (the only found cases are reported below).

The knowledge about ammonia as a working fluid is very well developed and so is the theory of heat transfer and fluid flow properties in sintered porous wick structures. It is very well known that a sintered wick provides much higher capillary force (enabling the pipe to work at higher inclination degrees against gravity) as opposed to grooved or screen mesh wicks. It is also known that a sintered wick structure has the highest heat flux density (can remove more heat from hot source per unit contact area because the coefficients of heat transfer on evaporation in thin liquid films and porous structures greatly exceed the coefficients on liquid evaporation and pool boiling (Vasiliev, Grakovish, et al. 2012) and a better circumferential fluid distribution inside the pipe comparing to other types of the wick. Therefore it is a well established fact that sintered wick increases the heat flux density considerably compared to grooves but impracticality of producing aluminium sintered wicks and the secondary problems associate with using other materials than aluminium, has limited the available options for ammonia heat pipes.

One of the few researches on sintered ammonia heat pipes has been reported by Eggers, Serkiz et al. (1971). They developed a porous grooved nickel wick which was metallurgically bonded on the inner walls of a stainless steel container, Figure 2-2. This wick design was believed to feature the combined advantages of ease of condensate return which is a characteristic of grooved wicks and high capillary pumping capability which is attributed to sintered wicks. Their test results proved that this design provides significantly higher heat transport capacity than otherwise possible with the individual wick concepts, viz., grooves. Their sample was 180 Cm long and had a 0.48 Cm outer diameter. It had eight grooves with porosity of 25% and pore radii of approximately 5μm.

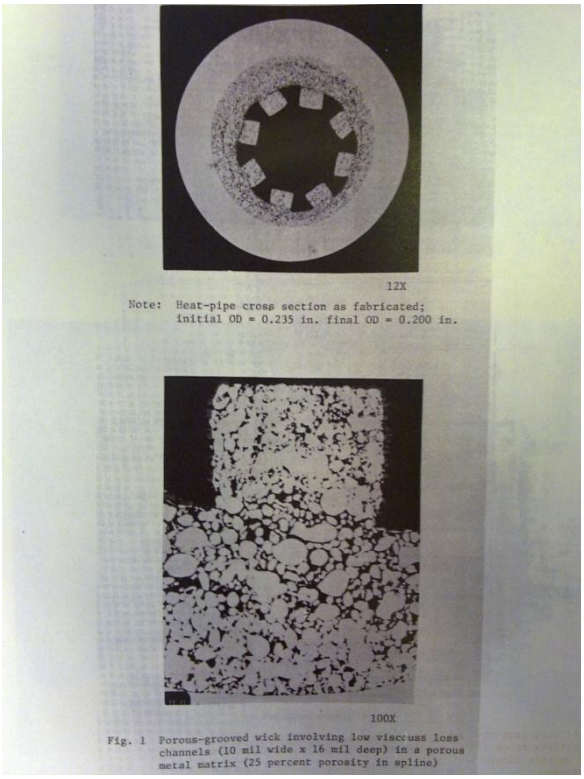

Figure 2- 2 one of the rare researches on sintered ammonia HPs. Nickel sintered grooves in a SS container (Eggers 1971)

The HP operated at radial thermal fluxes of up to 18 W/in^2 (2.8 W/Cm^2) with less than 9K (9°C) temperature difference between the evaporator and condenser in horizontal orientation. Eggers, at the time, reported the heat flux value for non-sintered heat pipes to be between 0.1 to 1 W/in^2 (0.01 to 0.15 W/Cm^2). Due to the wick contamination by oil-based residues during filling/venting (which reduces the wet-ability of ammonia on the surface) this pipe could not be operated at inclinations above approximately 30 degrees against gravity since the ammonia liquid could not be retained in the grooves. The grooves were covered by a nickel foil barrier in adiabatic region to suppress vapour-condensate interaction.

There also exist some works on the effect of deposition of a porous coating on the groove surface and how positively it affects the heat transfer coefficient. Experiments on grooved aluminium ammonia heat pipes with a 30μm-100 μm thick Al2O3 nano particles coating, 0.1 μm-2 μm pore diameter and 50% porosity testify the heat transfer enhancement of 1.3 to 1.8 times compared to heat transfer occurring on the same heat pipe with smooth grooves within the entire studied range of temperatures of -20 to 70°C (Vasiliev, Grakovish, et al. 2012).

Therefore the solution to the low heat flux limitation of the ammonia heat pipes has been well known to be the use of a sort of sintered or sinter-style normal or composite wick. The obstacle has been the impracticality of producing aluminium sintered HP wicks using the conventional methods or, in the case of using other materials such as SS or nickel, the secondary problems

associated with them including lower thermal conductivity (which leads to higher thermal resistance and higher temperature drop along the HP) and generation of non condensable gas due to the metal-metal contact.

SLM heat pipes are produced entirely in a single process with the container and wick together and from one material and some aluminium alloys, especially silicon based alloys like AlSi12, can be used in the process. This means the low heat flux shortcoming of the available space ammonia heat pipes can be resolved by the new sinter-style SLM heat pipe without any of the secondary problems associated with other approaches.

2-3) Ammonia heat pipes in terrestrial applications

In non-space (terrestrial) cases, ammonia heat pipes have been used in a relatively wide range of applications. One type of application may include many different examples with different temperature ranges and it is this working temperature that dictates the type of the required heat pipes in terms of its working fluid, material, wick structure etc. For instance in a heat pipe based heat exchangers, depending on the geographical location that it will be implemented and the temperature of the hot and cold air flows, different types of heat pipe must be used with a working fluid suitable for that temperature range. This review is limited to the applications that have instances with an operating temperature suitable for ammonia heat.

There are three major terrestrial application groups where ammonia heat pipes are currently being used or have been used in the past. In air conditioning heat recovery heat exchangers ammonia heat pipes are used to recover some of the heat from the exhaust air to pre-heat the fresh intake air. The heat pipe heat exchanger used for gas–gas heat recovery is essentially a bundle of finned heat pipes assembled like a conventional air-cooled heat exchanger. The heat pipe in the heat exchanger can be divided to three parts: evaporator, adiabatic section and condenser. Passing hot flue gases over the evaporator causes the working fluid to boil and the vapours to flow at the cold end of the tube. Cold air flowing over the condenser in counter flow direction condenses the vapours releasing latent heat that heats the air (Vasiliev, 2005). There is no doubt about the benefit of using heat pipes in heat exchangers used for these applications. According to Wan, Zhang, et al. (2007) in the usual range of 22°C–26°C indoor design temperature and 50% relative humidity, the RES (rate of energy saving) in their investigated office building was 23.5–25.7% for cooling load and 38.1–40.9% for total energy consumption by using HP- based heat exchangers.

The literature on heat pipe based heat exchangers is very rich and some examples can be seen at (Aronson, 1976); (Shao & Riffat, 1997); (Riffat & Gan, 1998); (Noie-Bagheban & Majideian, 2000); (Soylemez, 2003); (Abd El-Baky & Mohamed, 2007); (Wan, Zhang, et al., 2007); (Yau & Ahmadzadehtalatapeh, 2010); (Zhang & Lee, 2011) and (Kerrigan, O'Donnell, et al., 2012).

In cold climates with very low temperature of the fresh supply air temperature, the heat pipe operating temperature may well fall in the range of -40°C to +30°C where ammonia heat pipes have the best performance.

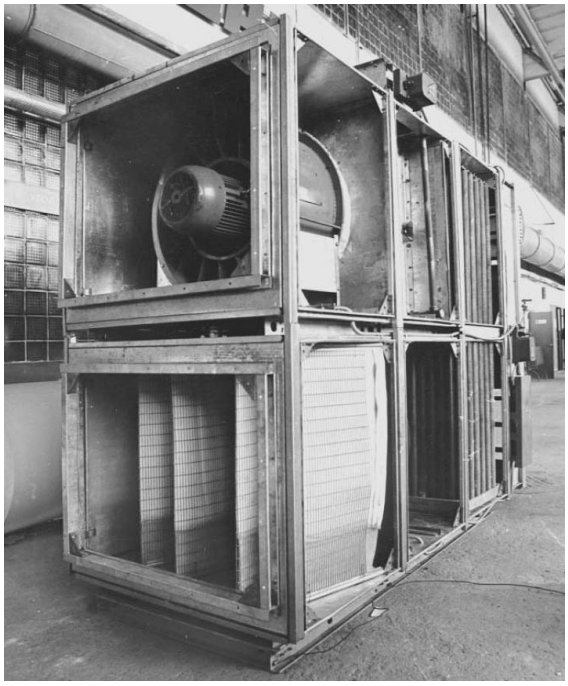

Figure 2- 3 Air conditioning system with aluminium/ammonia heat pipes (Vasiliev, 1998). Heat Pipes are at the back running top to bottom between the fresh intake and the exhaust air

Another major group of ammonia heat pipes terrestrial applications is permafrost stabilization. Stabilizing permafrost is believed to be the first application of ammonia heat pipes in a non-space application. All the structures built on permafrost depend on the permafrost, or frozen soil, staying frozen. If the permafrost melts, the structure is likely to sink and possibly sustain damage. Heat pipes are used in these cases to extract the ground residual heat during the winter (when the air temperature is colder than the soil) to lower the soil temperature and to make sure that the soil will remain frozen during summer. Depending on the specific soil type, decreasing the soil temperature from 0.1°F (0.05°C)below the freezing point to 0.5°F (0.28°C) below the freezing point increases the soil strength by 20 to 100% (Heuer, 1979). These heat pipes are often wickless and work as a thermal diode with a very limited heat flux per unit contact surface area with the soil. These heat pipes work only in winter or when the air is colder than the soil. In

summer when the air temperature is higher than the soil the working fluid condensate can not return to the top of the heat pipe which is hotter and the heat pipe ceases to work.

The first HP permafrost application was in the 70s when the 800 miles Trans-Alaska Pipeline System, the world's largest pipeline systems, was built. About 120000 heat pipes were installed along the trans-Alaska pipeline to provide additional ground cooling during the winter.

Figure 2- 4 Ammonia heat pipes used to stabilize the frozen soil under the Alaska pipeline. The finned ends of long heat pipe are seen at both sides of the pipeline at regular intervals

In Alaska pipeline, heat pipes are made of mild carbon steel and ammonia is the working fluid. They range from 8.5 m to 22 m length and 2 in. (0.05 m) outside diameter.

Hayley (1982) describes two other structures where heat pipes have been successfully used to provide thermal protection for permafrost soils supporting surface foundations. A school constructed at Ross River, Yukon Territory, in 1975, included heat pipes as an integral part of the foundation design. The heat pipe evaporator sections were installed in aluminium access tubes that extend into a gravel pad supporting a slab-on-grade foundation. Performance of the system was satisfactory over a five-year observational period (Hayley, 1982).

The second heat pipe system was installed to stabilize a tramway tower foundation also in the same area. Exposed footing foundations were experiencing settlement that could be related to thaw of the underlying permafrost gravel. Vertical heat pipes were installed adjacent to the foundation elements to arrest permafrost degradation. Ground temperature records and survey data showed that the installation had elevated the permafrost table.

In the school, the design objective was to extract sufficient heat from the foundation to freeze the gravel supporting the structure each winter. After freeze-back, the temperature of the ground must be further lowered to create a heat sink that will absorb heat during the summer months when the heat pipes are dormant. In both applications the heat pipes were made of aluminium. This technology has also been applied in the Qinghai-Tibet Railway frozen soil road bed and has successfully solved the problem of melting and sinking of ever-frozen soil along the railway in summer. This technology can be widely used to the difficult problem of melting and sinking of ever-frozen soil on which railway road bed, highway, bridge culvert, tunnel, airplane runway, oil transmission pipeline, and foundations of substation and power transmission towers are laid ("application of heat pipe", 2010). Other similar cases are reported by Aronson (1976); Chi (1976); Vasiliev, Grakovich et al. (1978); Bayasan, Korotchenko, et al. (2008) and Bayasan, Korotchenko, et al. (2008).

De-icing of the structures is another major application of ammonia heat pipes where the ground heat or other heat sources are used to de-ice the surface of the rails, roads, bridges, sea navigation buoys etc. (Larkin & dubuc, 1975, Okihara, Kanamori, et al. 1980, Vasiliev 1998).

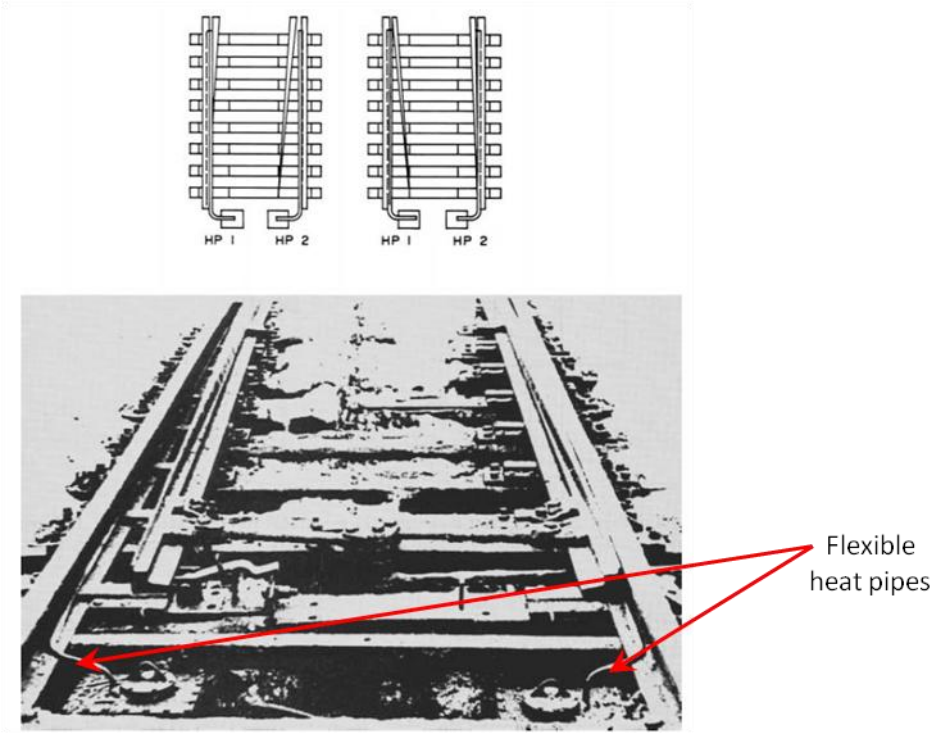

Figure 2- 5 flexible steel/ammonia heat pipes for the rail points heating in winter (Vasiliev, 1998)

Terrestrial applications, although much lower in terms of the number of the individual instances, use a wider variety of ammonia heat pipes than in the space. In space, an absolute majority of

ammonia heat pipes are aluminium AGHPs with the rest being mainly arterial heat pipes with screen mesh and, as discussed, the main attribute of an SLM HP that can benefit these applications is to provide higher heat flux densities by fabricating fully-controlled sinter-style wick structure in the evaporator section of the pipes.

In terrestrial applications possible improvement from the use of SLM HPs is obtained in different ways depending on the type of the application. Most of the ammonia heat pipes used in permafrost applications are large carbon steel wickless heat pipes (Thermosyphon). Wickless-ness in adiabatic section (middle part) is an intentional property of these pipes to enforce them to work as thermal diodes. These pipes are supposed to transfer the heat upwards from the soil to the air during winter but cease to work in the summer when the air is hotter than soil to avoid adding extra heat into the ground. However an intrinsic property of the wickless pipes is their very low surface heat flux. Moreover, due to the often large diameter of these pipes even distribution of the working fluid in the evaporator is a major problem. Ideally the pipe is expected to extract the heat from the soil evenly all across the pipe-soil contact surface area with maximized heat removal per unit of this contact surface area. Therefore an improvement in these pipes should address the low surface heat flux problem as well as the distribution of the working fluid in the evaporator. In the past, in some cases, SS or aluminium meshes have been used inside the pipes or Nickel sintered inserts have been applied inside the pipes in the evaporator section. This has improved the limits to a certain extent but often adds other secondary problems mainly due to the increased thermal resistance or non condensable gas generation caused by different metal contact. Ammonia heat pipes used in de-icing applications, closely follow the same working principal and structure as in the permafrost applications and suffer from the same limitations as well.

Vasiliev, Grakovich, et al. (1978) work contains the laboratory test results of some different types of heat pipes used for permafrost applications including a Thermosyphon and a heat pipe with two layers of SS mesh. Carbon steel pipes were both 1880 mm long with 1000 mm evaporator length, 45 mm diameter and used ammonia and operated at 90 degree with gravity at an operating temperature of 27°C. Total input power to the pipes was 180.5 W and 200 W respectively which corresponds to 1.27 and 1.41 W/Cm^2 heat input density.

Alaskan heat pipes' 4 m evaporator length, 0.05 m diameter and 5000 W/K (5000 W/°C) heat transport capability (Chi, 1976) corresponds to a heat flux density of 0.8 W/Cm^2.

Okihara, Kanamori, et al. (1980) presents the results of a laboratory experimental ammonia heat pipe for de-icing the superstructures of a vessel operating in the arctic. The pipe is 300 mm long

and 25 mm diameter with a sintered wick in the evaporator and screen covered grooves in the condenser. They measured a radial het density of 1.6 W/Cm^2 at 15°C operating temperature. The material of the container and the porous wick is not reported but is guessed to be SS and nickel.

Larkin & Dubuc (1975) present the test results of a mild steel-ammonia wickless heat pipe for self de-icing of the navigation buoys operating at a mean temperature just above 0°C. The pipe has 7.5 Cm outer diameter, 2.18 m evaporator length and 1.14 m condenser length. Test results have been presented as the heat transfer coefficient per area of the condenser and per the temperature drop along the pipe. The best measured value (by changing the ammonia filling volume) has been 3200 W/m^2.K at 0.6°C temperature difference. This corresponds to 515 W total heat input or 0.1 W/Cm^2 heat flux in the evaporator.

With regard to the working fluid distribution problem, Vasiliev, Grakovich, et al. (1978) explain that for permafrost applications Thermosyphon' great length and diameter fail to provide for the total area of the evaporator to be wetted as the returning condensate only moisten part of peripheral area of the pipe and that this can be eliminated with the aid of a thin layer of porous material laid over the evaporator surface that considerably increases the cost of the pipe therefore they suggest using a screen mesh along with a screw to push the mesh against the wall in that region. With SLM technique this issue can potentially be addressed by building the entire evaporator of the heat pipes by SLM with a sintered wick structure and then assemble it to the rest of the heat pipe by welding etc.

In the ammonia heat pipes used in heat recovery heat exchangers the nature of the limiting factor is slightly different. Although these pipes can also benefit from higher surface heat flux of an SLM sinter-style pipe, but their main issue seems to be the orientation and angles at which they can operate. Non-sintered wicked heat pipes' performance is very sensitive to the operating angle (so while some composite wick structures e.g. mesh arteries enable the pipe to work against gravity to a certain limit but the performance would be very sensitive to the angle) and existing aluminium ammonia heat pipes, as discussed, are not capable to work against gravity at all. Other types of ammonia heat pipe e.g. SS or sintered nickel ones have to compromise the overall thermal resistance and performance to achieve this capability. Gravity has less influence on sintered powder metal heat pipes than other type of the wick structure (Loh, Harris, et al. 2005).

A very important feature of the HP is the ability to transport a large amount of energy over its length with a small temperature drop by means of liquid evaporation at the HP evaporator (heat

source), vapour condensation at the condenser (heat sink) and liquid movement in the opposite direction inside a wick by capillary force. In heat exchangers it is desired to have the possibility of changing the direction of the heat flow along the HP in time to use the HPs for cooling and heating alternately (Vasiliev, 2005).

Chi (1976) explains the design process of a HVAC heat recovery heat exchanger for a hypothetical building in Washington D.C. using aluminium ammonia heat pipes. He discusses that the system can be designed for seasonal heating or cooling by ducting the intake air to pass above the exhaust air in the heating season and then switching over to the cooling season by rotating the entire heat exchanger to have the intake air passing below the exhaust air, reversing the transport direction of the heat so that higher temperature inlet air is cooled by the conditioned exhaust air. This is to keep the hot section of the heat pipe(s) below its cold section. A carefully-designed sinter-style SLM HP heat exchanger does not need to be rotated to work in different seasons but can transfer enough heat in both directions when needed.

2-4) Conclusion

Ammonia heat pipe applications have been divided into two main groups of space and terrestrial applications. In space, majority of ammonia heat pipes use aluminium container and axially grooved wick structure (AGHP). The main shortcoming of an axially grooved heat pipe (AGHP) is its low surface heat flux or the heat it can remove from the hot source per unit of the contact surface area between the source and the heat pipe. Other types of ammonia heat pipes including SS arterial HPs have also been used in space with not much improvement in their heat flux. As a matter of fact, sintered wick structure in the evaporator increases the surface heat flux well above that of a grooved wick but sintering aluminium to form sintered aluminium heat pipes is impractical due to the rapid oxidation of aluminium and low melting point of the aluminium alloys.

Use of other material for the heat pipe's container or wick or using composite wicks are all associated with secondary problems. Stainless steel low thermal conductivity increases the temperature drop along the heat pipe and, as a result, the input heat level should consequently be reduced to keep the temperature drop low. Using composite wicks e.g. SS screen mesh over the internal aluminium grooves in arterial heat pipes or sintered nickel wick inserts inside SS container increases the generation of non condensable gasses inside the pipe that shortens the effective working length of the pipe over time in addition to the increased thermal resistance of the heat passage along the pipe.

SLM technique enables production of aluminium heat pipes with a controlled sintered wick with the container and wick produced in a single process. This means much higher surface heat fluxes with a literally-completely-flexible design and no secondary problems.

In terrestrial and built environment applications ammonia heat pipes are used in more variable forms and designs than in space although the number of the individual application instances is much lower. Ammonia heat pipes used in permafrost and de-icing applications currently are without a wick (Thermosyphon) or with grooved or composite wick structure and aluminium or carbon steel container. A carefully designed controlled aluminium or steel sinter-style SLM produced wick structure improves the condensate distribution in the evaporator as well as the heat flux density and consequently the overall performance of the pipe considerably.

Likewise, for the ammonia heat pipes used in heat recovery heat pipe heat exchangers, a controlled sinter-style wick along the pipes enables the heat exchanger to work at any orientation in different seasons regardless of the relative position of the hot and cold flows with minimal sensitivity to the operating angle.

The use of selective laser melting (SLM) technique to produce heat pipes has many advantages over the conventional HP manufacturing method. The main one, which is the core of this project, is the ability to produce sinter-style aluminium heat pipes. Because these structures are produced from a CAD model there is literally full control over the property of the sinter-style structure including porosity, permeability and effective pore size as opposed to the conventional method of production of sintered structures which is by compaction and heating of a bulk of loose powder. As a result of this, and because some other materials including SS or titanium can also be used in SLM process, SLM as an alternative HP manufacturing method, can bring improvements into many other types of heat pipes as well as aluminium ammonia HPs.

3-1) Introduction

Conventional heat pipe manufacturing method has exposed some restrictions on the currently available heat pipes in terms of the shape and performance. For aluminium heat pipes the main restriction has been the impossibility of producing sintered aluminium wick structures thus non-existence of sintered aluminium heat pipes. Selective laser melting (SLM) technique is implemented in this project as a new heat pipe manufacturing method to overcome this limit.

This chapter provides a relatively comprehensive theoretical background on sintered heat pipes and their design. First, heat pipes basics are reviewed by looking at heat pipes history, material, types, operation principle and different structures as well as the conventional manufacturing method. The calculation process and mathematical formulas for design and evaluation of sintered heat pipe are described along with their use to study the feasibility of the initial SLM HP samples of this project before build.

As one of the project's objective, the described equations and HP performance governing formulas have then been linked together along with other design parameters to develop a design tool for sinter-style SLM heat pipes. The design tool takes inputs from the user about the geometry and operating conditions and using its own databases and formulas, calculates the mechanical and heat transfer characteristics of the HP. The tool is based on a Microsoft Excel workbook and has been described in this chapter.

3-2) Heat pipe definition

Heat pipe (HP) is a passive two phase system to transfer heat from one point to another. It consists of a hermetically sealed container charged with a small amount of a working fluid and a capillary structure on the inner walls called the "wick". There are a wide variety of heat pipes in terms of dimensions, material of the container and wick, working fluid type and structure of the wick.

At the designed temperature range of a heat pipe, the working fluid is always at, or very close to, its saturation pressure corresponding to the temperature of the pipe. When a section of the heat pipe is heated the working fluid evaporates inside the tube at the interface of the tube and the hot source, the vapour travels to the colder section(s) of the tube and condenses back into liquid

by rejecting the heat. The condensate is then returned back to the hotter section(s) by capillary action of the wick and/or by gravity action and the cycle repeats itself. Therefore a HP provides a passive continuous passage for heat between a hot and a cold source.

Latent heat of vaporization is considerably higher than the sensible heat, hence a much higher heat transfer capability of a heat pipe comparing to a solid tube with identical material and geometry. And the speed of the heat transfer is literally the speed of the vapour molecules (if not limited by the heat removal capacity on the colder section) so the heat is transferred with much lower temperature drop comparing to a solid bar.

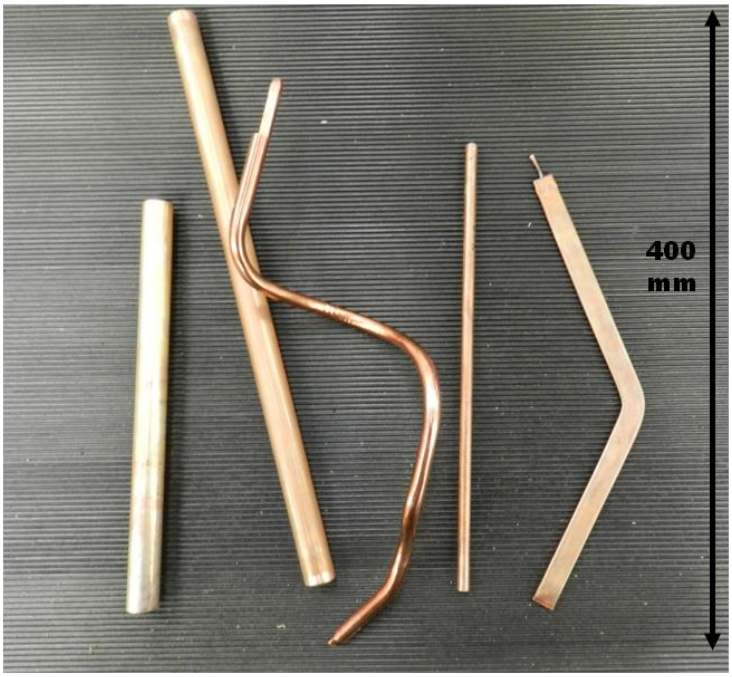

Figure 3- 1 Heat pipes in different shapes, sizes and materials

3-3) Heat Pipe History

Heat pipe history starts in mid-nineteenth century when Perkins tube was patented in England. Perkins tube is basically a form of Thermosyphon (wickless heat pipe) but they must be regarded as an essential part of the history of heat pipe. However, first Perkins tubes were working with water in single phase and high pressure and in this regard deviated from the definition of heat pipe as a two phase device (Reay & Kew, 2006). The concept of a passive two-phase heat transfer device capable of transferring large quantities of heat with a minimal temperature drop was first introduced by Gaugler in 1942 (Peterson, 1994).

The name "heat pipe" was first used in Grover's patent (Grover, G.M. Evaporation-condensation heat transfer device. US patent No. 3229759. Appl. 2 December 1963. Published 18 January 1966) to describe a device essentially identical to that in the Gaugler's patent but included a limited theoretical analysis and experimental results on stainless steel pipes incorporating a wire mesh wick and sodium as the working fluid (Reay & Kew, 2006).

Early works on heat pipes were focused on space applications. The early 1970s saw a considerable growth in the application of heat pipes to solve terrestrial heat transfer problems.

3-3-1) History of aluminium/ammonia heat pipes

The first investigations on using ammonia as a working fluid for heat pipes was done in late 60s (Cotter, 1965) and the first onboard spacecraft experiments of an ammonia heat pipe was in early 70's as reported by Harwell & Mcintosh, (1981). In space, the common working fluid is ammonia as its operational temperature is well suited for un-manned space applications (-40°C to 80 °C). Axially grooved heat pipes offer relatively simple industrial fabrication and greater reliability than other wick designs.

In early 70s ammonia heat pipes were used in terrestrial applications with aluminium or carbon steel containers. For these applications HPs have had either grooved wick or a wickless structure.

3-4) Heat Pipe operation principal

Heat pipe, in its simplest form, is a cylindrical evacuated hollow tube which is hermetically sealed. Inside the tube there is a certain volume of a fluid and the inner walls are covered with a capillary structure. Capillary structure is either an integral part of the tube or is separately applied to its inner walls.

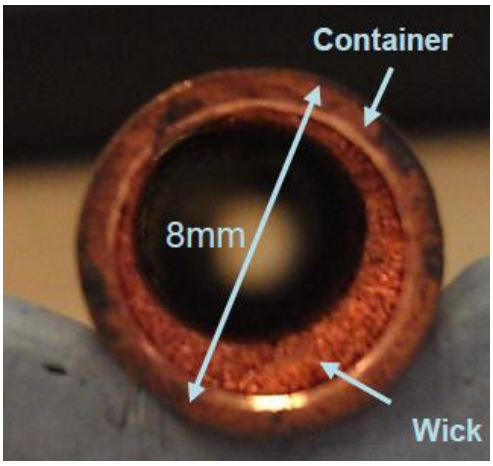

Figure 3- 2 Three main parts of a heat pipe are "Container", "wick" and the "working fluid". Working fluid is absorbed into the porous wick

In the above picture, HP is made of copper, the working fluid is water and copper powders are sintered together and to the inner wall as the wick. The volume of the working fluid is always a tiny percentage of the total internal volume of the tube and, typically, all of it is absorbed into the wick so if one cuts a heat pipe open and looks into it, the hollow duct in the centre of the tube looks empty (in fact, filled with the working fluid vapour before the tube is cut open).

Once the fluid is charged into the container and before sealing it, all the air inside the tube is evacuated. Therefore the working fluid inside the tube is always in its saturated state corresponding to the tube temperature. In a well designed heat pipe, in steady state situation condition, the wick is fully filled with the working fluid in liquid state and the hollow space in the centre of the tube is filled with the working fluid in vapour state and a pressure corresponding to the saturated pressure of the fluid at tube temperature. The hollow space in the centre of the tube is called vapour space or vapour channel.

In operation, when one end (in practice, any section) of this cylinder is heated, the heat passes through the container thickness and the wick and reaches the liquid-vapour interface roughly at the edge of the wick. To keep the saturated state at this higher temperature, more liquid vaporizes and vapour pressure is increased in that end of the tube. This heated section of the heat pipe is called "evaporator". The amount of the heat which is absorbed into the liquid is equal to the latent heat of the mass of the liquid that vaporizes.

This higher pressure at evaporator end pushes the vapour to the other end where the pipe is colder or the "condenser". When the vapour reaches that end and cools down, it condenses back into liquid and releases the heat. The heat passes through the wick and the container thickness and leaves the tube. The liquid then travels along the wick back to the evaporator either by gravity force and/or by the capillary force generated by the wick.

The main purpose of the wick is to help returning liquid back to the evaporator although it has other roles as well which will be discussed later. Gravity-aided Heat pipes (evaporator lower than the condenser and the condensate is returned to the evaporator just by gravity) sometimes are made with no wick at all. These heat pipes are called Thermosyphon.

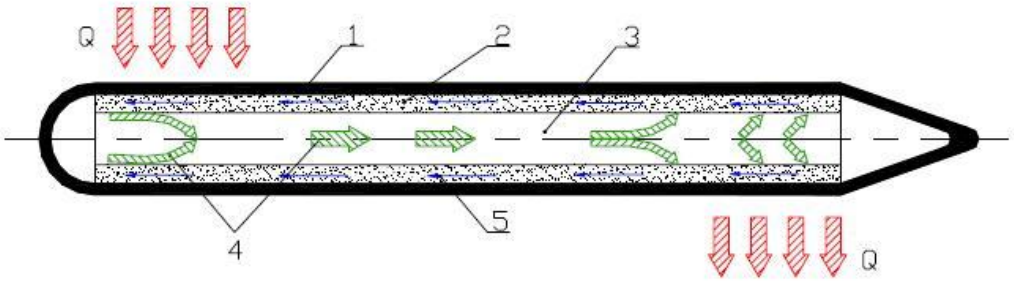

Figure 3- 3 Conventional Heat Pipe Schematic. (1) HP container, (2) wick, (3) vapour channel, (4) vapour, and (5) liquid (Vasiliev, 2005)

There are a wide variety of heat pipes based on the shape, dimensions, material and other properties of the container, type and amount of the working fluid and structure, size and material of the wick.

Also, unless specifically designed for, in a general heat pipe, evaporator and condenser are not pre-determined sections. Evaporator, condenser and adiabatic (the length of the heat pipe between evaporator and condenser) sections are defined in the real application depending on which part or parts contact the hot source and which section(s) is cooled down. For instance the middle of a cylindrical heat pipe may be attached on top of a computer chip for heat to be dissipated from the two ends. In this case the middle section is called evaporator and the two ends are known as condensers.

The working fluid is selected based on the operating temperature range of the application and the container material is chosen mainly based on the compatibility with the working fluid and thermal conductivity. The structure of the wick is determined based on the intended operating conditions including orientation of the heat pipe (relative position of the hot and cold spots to each other) and the required heat removal density (heat flux per unit surface area).

3-5) Heat Pipe components and materials

Three major components of a heat pipe, container, working fluid and the wick, are described below. All the heat pipes have the container and the working fluid but can be with or without wick.

3-5-1) Heat pipe container

The container can be made from a variety of different materials including copper, aluminium, titanium, stainless steel and tungsten. The choice firstly and mainly depends on compatibility with the working fluid. Once the compatibility with working fluid is assured, other parameters

like weight, thermal conductivity and manufacturing issues are taken into account to select between the possible options.

Normal heat pipes transfer the heat in one direction along the length of the pipe. In these heat pipes the length is much larger than the pipe cross section area. Very often the pipe is round thus the name "cylindrical heat pipe" but they can be made with different cross sections such as rectangular, triangle, etc. The length can be from a few millimetres to tens of meters and diameters from few millimetres to a few meters. Cylindrical heat pipes, in some applications, are flattened after manufacturing to provide better contact surface with hot and cold medium.

Heat pipes can also be made for two dimensional heat transfer. These heat pipes are called vapour chamber or Therma-base. Vapour chambers can have different length and widths but are typically a few millimetres thick.

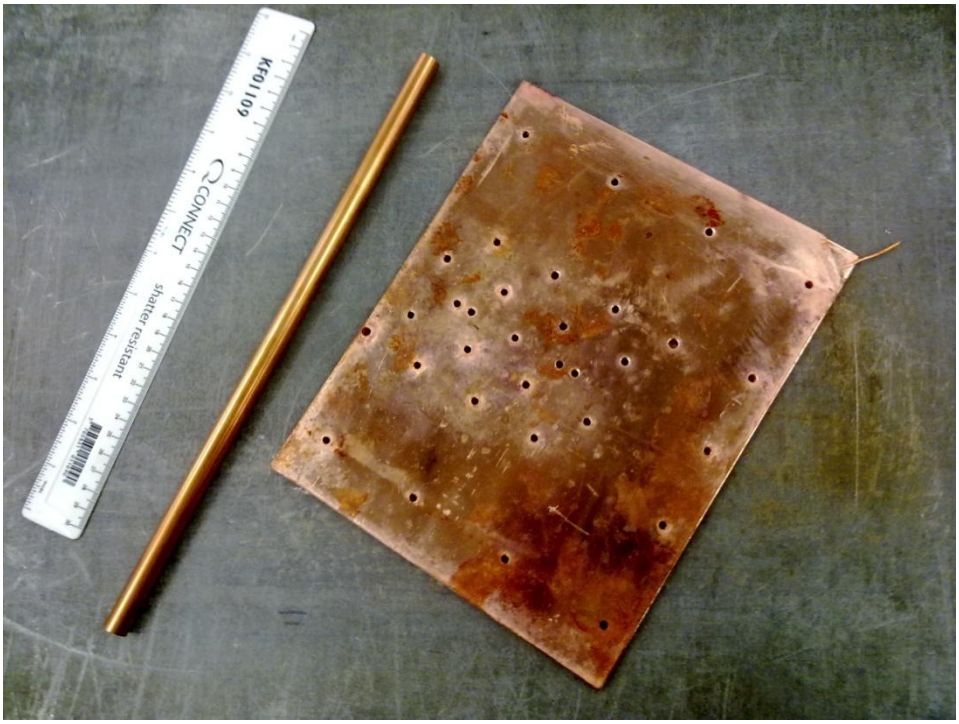

Figure 3- 4 A cylindrical heat pipe and a vapour chamber (flat, 2D Hp)

A vast majority of heat pipes are made from copper. The main reason is that copper is compatible with water which is, by far, the best working fluid for applications working in temperature range from a few degree above zero to around 250°C and most of the commercial applications in electronics, power, medical, telecommunication and military fall in this range. Copper also has a good thermal conductivity and is easy for machining.

Perhaps the second most common heat pipe material is aluminium. It has a relatively high thermal conductivity but is not compatible with water (which makes it unsuitable for many

applications) and needs protection against environment for outdoor applications. But aluminium is especially common in space applications and is compatible with ammonia, ethanol and acetone. Stainless steel is used in applications where heat pipe strength is the main design parameter. Other materials are normally used in very special applications with special working fluids like liquid metals.

3-5-2) Heat pipe working fluid

Selection of the right working fluid is the first and perhaps the most important step in designing a heat pipe. This selection mostly depends on the operating temperature range of the real application. Working fluids range from liquid helium for extremely low temperature applications (-271°C) to silver for extremely high temperatures (>2000°C). The most common heat pipe working fluid is water. Low temperature heat pipes use fluids like ammonia and nitrogen and high temperature heat pipes utilize caesium, potassium, NaK and sodium.

Table 3- 1 Common heat pipe working fluids, their operating temperature range and compatibility with container material (Thermacore, 2012)

Heat Pipe Working Fluid	**Operating Temperature Range (°C)**	**Heat Pipe Shell Material**
Low Temperature or Cryogenic Heat Pipe Working Fluids		
Carbon Dioxide	-50 to 30	Aluminum, Stainless Steel, Titanium
Helium	-271 to -269	Stainless Steel, Titanium
Hydrogen	-260 to -230	Stainless Steel
Methane	-180 to -100	Stainless Steel
Neon	-240 to -230	Stainless Steel
Nitrogen	-200 to -160	Stainless Steel
Oxygen	-210 to -130	Aluminum, Titanium
Mid Range Heat Pipe Working Fluids		
Acetone	-48 to 125	Aluminum, Stainless Steel
Ammonia	-75 to 125	Aluminum, Stainless Steel

Table 3- 1 Common heat pipe working fluids, their operating temperature range and compatibility with container material (Thermacore, 2012)		
Heat Pipe Working Fluid	**Operating Temperature Range (°C)**	**Heat Pipe Shell Material**
Ethane	-150 to 25	Aluminum
Methanol	-75 to 120	Copper, Stainless Steel
Methylamine	-90 to 125	Aluminum
Pentane	-125 to 125	Aluminum, Stainless Steel
Propylene	-150 to 60	Aluminum, Stainless Steel
Water	1 to 325	Copper, Monel, Nickel, Titanium
High Temperature Heat Pipe Fluids		
Caesium	350 to 925	Stainless Steel, Inconel, Haynes
NaK	425 to 825	Stainless Steel, Inconel, Haynes
Potassium	400 to 1,025	Stainless Steel, Inconel, Haynes
Sodium	500 to 1,225	Stainless Steel, Inconel, Haynes
Lithium	925 to 1,825	Tungsten, Niobium
Silver	1,625 to 2,025	Tungsten, Molybdenum

For successful operation of a heat pipe its working fluid must have a melting point temperature below and a critical point temperature above the pipe operating temperature. Because of overlapping of this melting point-critical point temperature range for different working fluids, different fluids can often be used for a given operating temperature. The relative merits of different overlapping fluids in any specific range can be measured by considering some general tips in addition to some more formulated methods. The general tips are;

- In a specific temperature range, working fluids with an average vapour pressure are desirable. Very high vapour pressures cause concerns about the strength of the

pipe container and the wick and very low vapour pressures help the production of non-condensable gases inside the pipe (Reay & Kew, 2006).

- It has been observed for most fluids, that properties relevant to heat pipe performance are maximum in the vicinity of the fluid's normal boiling points (Chi, 1976).

Also, with some simplifications, it is shown by Chi (1976) that for a pipe of fixed wick structure and dimensions its heat transport is directly proportional to a combination of liquid properties which is called "Merit Number". Merit Number is a mean for ranking working fluids with higher values being more desirable.

$$M = \frac{\rho_l \sigma \lambda}{\mu_l} \qquad \text{(Eq. 3-1)}$$

Where;

M: Merit Number, W/m^2

ϱ_l : Liquid density, Kg/m^3

σ : Surface tension, N/m

λ: (also denoted as " L" in this project): Latent heat, J/Kg

μ_l : Liquid viscosity, Pa.s (Kg/m.s)

Figure 3-5 demonstrate the advantage of ammonia, NH3, in the range of -40°C to about 80°C. It should be noted that merit number is not the only criteria when selecting the working fluid for instance while water seems to be good at temperatures well above 250°C, at above 250°C its vapour pressure gets too high.

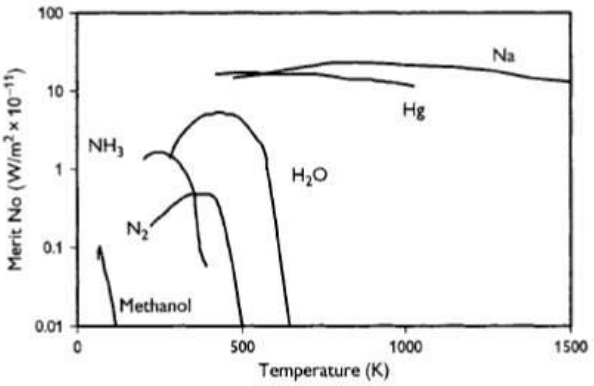

Figure 3- 5 Merit number of selected working fluids

In this project only ammonia (and acetone) is considered. Ammonia has the best properties from tens of degree below zero to about zero and very good properties until tens of degree above zero. At below -40°C and above around 30°C it again loses its advantage due to very low or very high vapour pressure although ammonia has been used in these extreme ranges in the past for special applications where its use has been justified by other considerations.

All the experiments of this project have been done using acetone and ammonia. Figure 3-6 demonstrate their Merit Numbers over the working temperature.

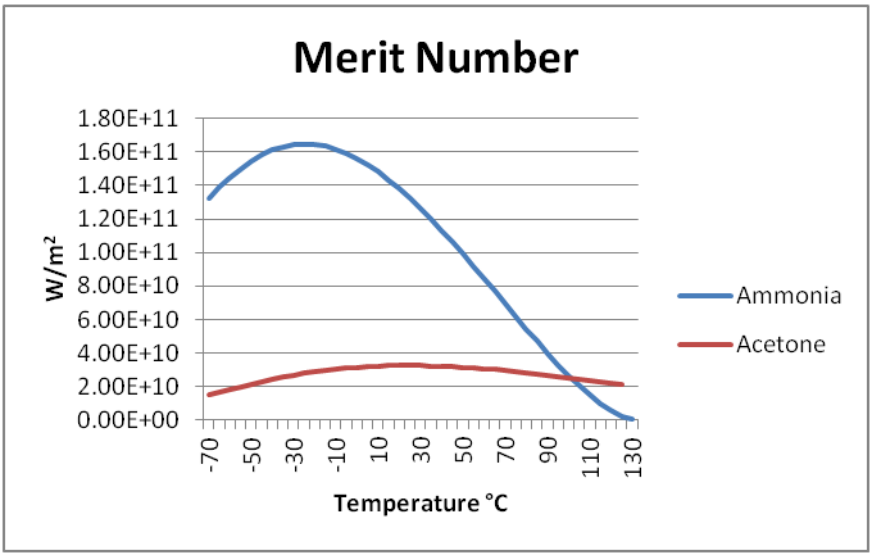

Figure 3- 6 Merit Number - Ammonia versus acetone

3-5-3) Heat pipe's wick structure

Capillary structure, or wick, is an optional feature on the internal wall of a heat pipe that exerts a capillary pressure on the liquid phase of the working fluid. The term capillary, with relation to heat pipes, is defined as the flow of a liquid under the influence of its own surface and interfacial

forces (Faghri, 1995). The purpose of the wick is to generate capillary pressure to return the working fluid back to the evaporator, to distribute the liquid circumferentially in the evaporator where the heat is applied to the pipe and to enhance the heat pipe heat transfer. The latter is the reason that some sorts of capillary structure are used even in gravity assisted heat pipes, where evaporator is lower than the condenser and the condensed fluid can return to evaporator by gravity (Reay & Kew, 2006).

Wick transfers the liquid by capillary action. Capillary action is the result of adhesion of the liquid molecules to the solid wick molecules. The best known example of capillary action is the rise of water level inside a straw in a glass of water. There are three major types of the wick structures, screen mesh, sintered wick and grooved wick and a wide variety of composite wicks in practice which are generated by combining these together with different properties for instance, arteries, bi-dispersed sintered powder and composite wick structures (Faghri, 1995).

Screen mesh and grooved wick heat pipes are only used if the hot spot is below the cold section as they are not able (or are limited) to pump the working fluid against gravity. Sintered wick heat pipes can work in any orientation and handle higher surface heat fluxes however their overall heat transfer capability is lower due to a reduced mass flow rate of condensate through the wick back to the evaporator. Currently ammonia heat pipes with aluminium containers are mainly manufactured with grooved wick.

Wick structures are constructed from various materials and methods. The selection of the wick mostly depends on the heat pipe length and the working fluid properties (compatibility and wet-ability) although the orientation, power density, total power, cost and manufacturing complications also effect this selection. As a thumb rule, screen mesh wicks are an easy option but can cause excessive temperature gradients as opposed to sintered wicks.

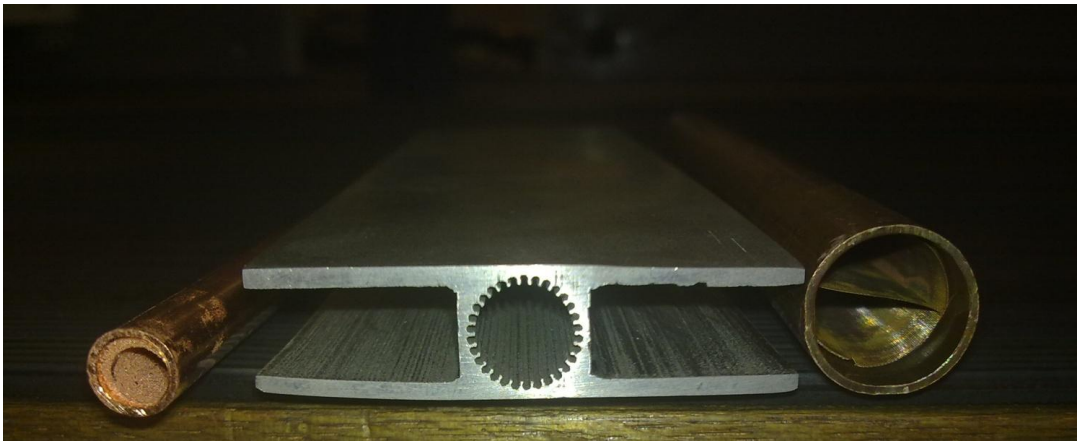

Figure 3- 7 Three major wick types. Left is a copper heat pipe with sintered wick, an aluminium heat pipe with grooved wick is shown in the middle and a copper screen mesh pipe at the right

Screen mesh wicks are sheets of woven metallic wires. Woven meshes are manufactured in a range of pore sizes and materials including stainless steel, nickel, copper and aluminium. Screen mesh size is usually specified in mesh number, which is defined as the number of meshes per linear inch measured in a direction perpendicular to the wire. Mesh numbers from 50 to 300 are the most commonly used wicks in practice. The higher the number is, the smaller the spaces between the wires or the pores are. To use as a heat pipe wick, one or few layers of these sheets are rolled and inserted into the pipe after cutting to the right length. They normally stick to the wall under their own tension.

Grooved wick is the name for the grooves formed on the inner walls of a heat pipe. These can be part of the tube profile generated during the tube extrusion or can be fabricated by different machining technique inside the pipe.

Sintered wick is a name generally given to metal structures with some voids in them. It comes from the fact that most of these wicks are generated by compacting metal powders together and rising the temperature to right below the powder particles melting temperature for the powders to get soft, deform at their contact point by the adjacent particles and finally sinter together and to the HP inner wall. Sintering is not the only method to produce these porous structures but often the same name used in literature. In addition to high capillary force, sintered heat pipes can remove more heat from the hot source per unit contact surface area between the pipe and the source due to improved evaporation heat transfer.

3-6) Heat pipe conventional manufacturing process

Manufacturing process of heat pipes is diverse due to the wide range of materials used in heat pipes and also the variety of the heat pipe structures and final applications.

For most common heat pipes which are copper-water heat pipes operating at normal temperature ranges, manufacturing process is relatively simple. A copper tube with the right thickness is cut to the right length. The tube goes through a delicate cleaning process including different chemical solutions. One end of the tube is then sealed by welding an end cap (there are other techniques as well). Care is taken in terms of the compatibility of the welding agent with the tube material and working fluid.

If the wick is of screen mesh type, it is rolled around a mandrel, inserted into the pipe and the mandrel is taken out leaving the mesh inside. If sintered wick is to be used, a mandrel is inserted inside the tube with a diameter smaller than the inner diameter of the tube leaving a donut-shape

gap as wide as the desired thickness for the wick. This gap is filled with copper powder while the assembly is on a shaking bed to compress the copper powders together.

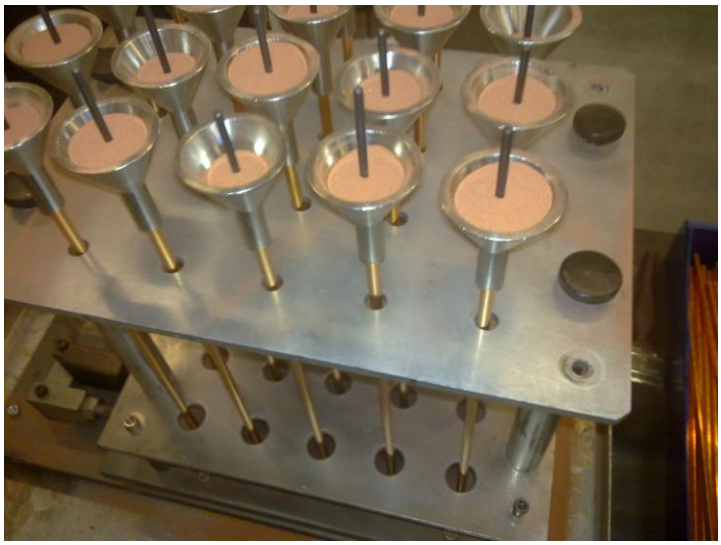

Figure 3- 8 Copper powder is being filled into the gap between the mandrels and the copper tubes on a vibrating table

Then the entire assembly is put into a sintering oven and heated to a specific temperature slightly below the copper melting point and remains there for a period of time for the copper particles to sinter together and to the tube inner wall. Mandrel is removed after sintering as it is of a material that does not stick to copper powders.

The required amount of the working fluid is then calculated and measured inside a syringe. The other end of the tube is closed leaving only a small passage for injecting the working fluid.

Figure 3- 9 A flattened heat pipe with the fill tube at the end. Fill tube is used to inject the working fluid into the pipe

The heat pipe is then placed on a hot base with the fill tube facing up and heated to a temperature above the boiling temperature of its working fluid at atmospheric pressure. The liquid is injected into the pipe and the fill tube is temporarily closed by a pin for the liquid vapour pressure to build up inside the pipe. Then the pin is quickly removed so that the liquid vapour can push all the air inside the pipe out. Once the liquid vapour starts to eject from the pipe the fill tube is closed and permanently sealed using solder or weld. The final stage is testing the built heat pipe for any possible leak and then for its thermal performance. This process is considerably more complicated for many of the other working fluids including liquid metals or low temperature heat pipes. Also, guarantying the long term consistent performance of a heat pipe closely depends on the technical details of the manufacturing process including cleaning and leak testing which hugely affects the manufacturing cost.

3-7) Sintered heat pipes' characteristics

The main contribution of this project to knowledge has been to develop the first sintered aluminium heat pipe. This heat pipe is not produced with the conventional heat pipe manufacturing method but by an additive layer manufacturing technique.

Although in this new heat pipe the wick structure has the shape of a conventional sintered wick (as seen in figure 3-10 below) but it is not produced by sintering therefore it has been called sinter-style throughout this document. The same operating principle and equations that govern the conventional sintered heat pipes are closely applicable to this new SLM sinter-style heat pipes. These governing rules and equations are reviewed below and have formed the core of the designing tool which has been developed during the project.

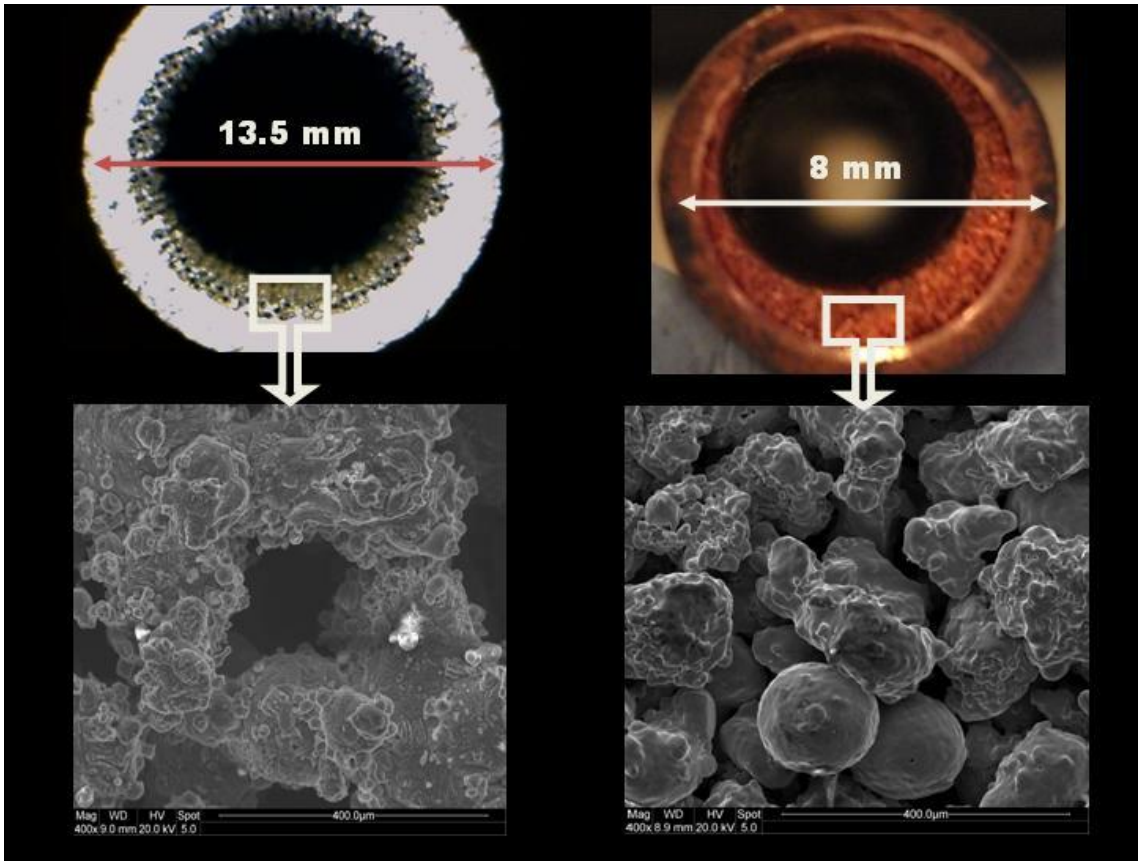

Figure 3- 10 A sintered conventional HP is shown at the right next to a sinter-style SLM HP. The wick structures are shown below at a 400X magnification and on a 400 µm scale

Sintered metallic powder compacts are used as wicks in heat pipes for maintaining a closed circulation of the working fluid and thus facilitating heat transport. Sintered metal powders or particles provide a higher thermal conductivity as opposed to traditional evaporative surfaces/wick structures used in the design of heat pipes, while still facilitating the thin film evaporating heat transfer (Hanlon and Ma, 2003).

When heat is applied to the evaporating region of a sintered heat pipe, the heat travels through the thickness of the wall of the solid container to reach the working fluid. The heat is transferred through the sintered particles filled with the working fluid, reaching the top surface where the liquid-vapour-solid interface exists (provided that the fluid level is not above the top surface of the wick). There by utilizing the thin film evaporation, the heat is removed.

The topology and geometry of sintered wick microstructures play a crucial role in determining their heat transfer performance in passive cooling devices such as heat pipes. It is therefore important to characterize microstructures based on their wicking performance, the thermal conduction resistance of the liquid filling the microstructure, and the thin-film characteristics of the liquid meniscus. The most important parameters which affect evaporation heat transfer in a wicking microstructure, are the conduction resistance offered by the filling liquid, the total

exposed free surface area for evaporation, and the extent of the liquid meniscus that is in the thin film region (Ranjan, Murthy, et al. 2009). Here we only focus on the physical characteristics of the sintered wick as the other parameters including the shape and behaviour of the meniscuses do not depend on the manufacturing method of the porous structure.

There are three main physical characteristics of a sintered wick structure; pore size, porosity and permeability. Pore size is an indicator of the size of the voids in the wick. Depending on the wick type, pore size is defined differently. For instance for a sintered wick which is powder particles sintered together, pore size is defined as the radius of the spaces left between the powder particles.

Porosity is the percentage of the volumetric ratio of the empty spaces or voids in the wick to the total volume of the wick and permeability is a measure of how easily a liquid can move through the wick.

Optimizing these three characteristics of a wick is a critical and tricky task in heat pipe design process. The main task of the wick, transporting the liquid by capillary action, stimulates small voids and small pore size but this means more resistance to the liquid flow and lower permeability. Lower permeability means less liquid can be transferred through the wick at a time thus lowers the overall heat transfer capability of the heat pipe. Increasing the pore size increases the permeability but reduces the capillary pumping force of the wick instead.

Usually high performance wicks have large values for porosity and small pore radius values. However, other considerations such as self-priming, boiling susceptibility, static rising height of the liquid in the wick and cost of wick fabrication must also be considered in the selection of wick structures. In addition, the effects of wick structure on the pipe temperature gradient may also be important (Chi, 1976).

For sintered heat pipes analysing the sintered capillary wick structure inside heat pipes to determine the effects of the thin film evaporation on the heat transfer behaviour of the wick structure, whether an optimum wick structure exists, how the value for maximum heat removal for a wick structure is determined (Hanlon & Ma, 2003) and the other relevant parameters of the wick such as particle dimensions, porosity and permeability, material etc. is an essential step to take in order to characterize existing heat pipes or to develop new heat pipes and heat pie applications.

3-7-1) Porosity, Permeability and pore size in sintered capillary structures

Porosity or void fraction is a measure of the void spaces in a material, and is a fraction of the volume of voids over the total volume. Its value is between 0–1, or as a percentage between 0%–100 %. Porosity is a function of the particle size distribution, with a tighter distribution tending towards higher porosities (Bear 2013). Following equation is used for calculating the degree of porosity of the powder compacts:

$$\text{Porosity}, \% = \left(1 - \frac{\text{Apparent density of porous material}}{\text{Density of non} - \text{porous material}}\right) \times 100 \quad \text{(Eq. 3-2)}$$

Permeability is the capacity of a porous medium to transmit fluids. It is related to measurable properties of the pore geometry such as porosity, pore size distribution, and internal surface area. A high permeability value leads to low flow resistance in the wick and thus to higher heat transfer rates. For powder compacts used as wicks in heat pipes, the permeability can be calculated from the following equation (ESDU 1979):

$$k = \frac{d^2\varepsilon^2}{150(1-\varepsilon)^2} \quad \text{(Eq. 3-3)}$$

with K being the permeability in m2, d the diameter of the powder particles in meters and ε the porosity.

Pore size is the trickiest property of a porous structure to measure or to even define. One definition for the pore size is that the pore size at any point in a porous structure is "the diameter of the largest sphere that contains that point while still remaining entirely within the pore space". The radius of this sphere is called the pore radii or capillary radius. As normally there are different size pores in a porous structure, most literature talk about effective pore radius.

In general, to achieve a high heat transfer rate in a heat pipe, the wick structure should exhibit high permeability, k, and low capillary radius, r. A high permeability results in a low flow resistance in a wick while a low capillary radius leads to a high capillary pressure. Designing an optimum porous wick for a heat pipe is to find a trade-off between these three main parameters to achieve a high heat transfer and capillary force at the same time. This has been the subject of numerous works done on sintered porous structures.

3-7-2) Sintered heat pipes' heat transfer and fluid flow theory and heat transfer limitations

In order for a heat pipe to work, regardless of its type, the working fluid must circulate between evaporator and condenser to transfer the heat.

Using this fundamental rule, the governing equations for the heat pipe performance and its limitations can be extracted. In the rest of this section all the formulas are taken from the main heat pipe reference books already cited in this project e.g. Reay & Kew (2006), Chi (1976) and Faghri (1995).

In order for the working fluid to circulate, the wick capillary action must overcome all the other opposing forces on the liquid. There are three opposing forces, the liquid pressure drop due to friction inside the wick, the pressure gradient of the vapour which causes the vapour to flow to the condenser and finally the gravitational forced (if the liquid should travel inside the wick against the gravity. In gravity assisted pipes this force will help the capillary action). Therefore;

$$\Delta Pc, max \geq \Delta P_l + \Delta Pv + \Delta Pg \qquad \text{(Eq. 3-4)}$$

Where

ΔP_c, max : Maximum capillary pumping pressure of the wick, Pa

ΔP_l : The pressure drop required to return the liquid from the condenser to the evaporator, Pa

ΔP_v : The required pressure drop to cause the vapour to flow from the evaporator to the condenser, Pa

ΔP_g : The pressure due to the gravitational head which may be zero, positive or negative, depending on the inclination of the heat pipe, Pa

The maximum heat flux for which the above equation holds is referred to as the capillary limit (denoted as circulation limit in figure 3-11). Typically, the capillary limit will determine the maximum heat flux over much of the operating range. But there are other limits as well that constrain the heat pipe performance at special conditions. These include;

Viscous limit: normally happens at start up when vapour pressure gradient along the pipe is not enough to overcome the viscous

Sonic limit: mainly during start up when the vapour velocity approaches sonic and causes the vapour flow to chock

Entrainment limit: normally at high heat fluxes when vapour velocity is high enough to entrain the liquid, that flows inside the wick in the opposite direction into the vapour duct and back to the condenser

Boiling limit: This happens when the heat input density to the pipe gets so high that a vapour blanket covers the inner wall and works as an insulator.

These limits are shown in the following graph. A heat pipe designer should make sure that the heat pipe operation point will always fall into the hashed area over its expected operating range.

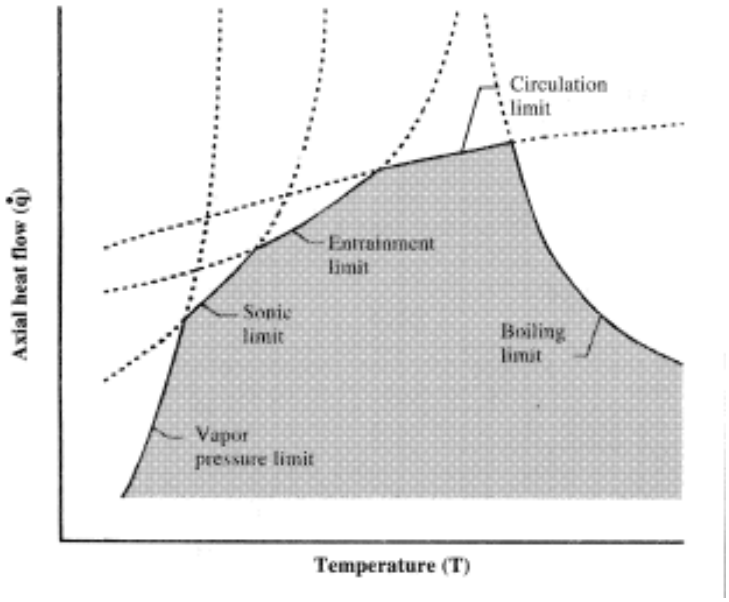

Figure 3- 11 Heat pipe heat transfer limitations. Heat pipe can only work if its operating point falls in the hashed area

There are many different scenarios that for each one, the pressure drop terms in above equation is calculated differently. But with some simplifications;

$$\Delta P_{c,max} = 2\sigma_l \frac{\cos\theta}{r_c} \quad \text{(Eq. 3-5)}$$

Where;

rc : Effective pore radius, m

θ_c : Liquid solid contact angle

σl : Surface tension of the liquid, N/m

Assuming a laminar liquid flow inside the wick, a constant rate of vaporization and condensation per unit length and a homogenous wick (including screen mesh and sintered);

$$\Delta P_l = \frac{8\mu_l \dot{Q} L_{eff}}{\pi({r_w}^2 - {r_v}^2)\varepsilon {r_c}^2 \rho_l L} \quad \text{(Eq. 3-6)}$$

Where;

Effective length, $L_{eff} = \frac{1}{2}(L_e + L_c) + L_a$, m (Eq. 3-7)

L_e : Evaporator section length, m

L_c : Condenser section length, m

L_a : Adiabatic section length, m (total length of the HP minus the lengths of the evaporator and condenser)

μ_l: Dynamic viscosity of the liquid , Pa.s

$\dot{Q}$: heat flux , W

ρ_l: Liquid density, Kg/m^3

L : Latent heat of vaporization (also denoted as λ in this document), J/Kg

ε : Porosity

r_w : Radius of the internal wall of the container, m

r_v : radius of the vapour channel, m

The above formula is for a cylindrical tube. It is modified for porous structure by replacing "8" by a constant value between 8 to 20 to include a correction for tortuosity.

When r_c, ε and the constant value are difficult to measure, the following formula is used;

$$\Delta P_l = \frac{\mu_l l_{eff} \dot{m}}{\rho_l K A_w} \quad \text{(Eq. 3-8)}$$

Where;

Mass flow rate of the working fluid : $\dot{m} = \frac{\dot{Q}}{\lambda\,(or\ L)}$, Kg/s (Eq. 3-9)

K : Permeability of the porous wick, m^2

A_w : Cross sectional area of the porous wick, m^2

For the vapour pressure drop, in steady state condition, the mass flow rate of vapour is equal to the mass flow rate of liquid in the same axial position however because of low density of the vapour in comparison to that of the liquid its pressure drop can be due to frictional drag as well as dynamic effects. So the vapour flow can either be laminar or turbulent (as opposed to the liquid flow inside the wick which is almost always laminar). Compressibility may also become important. Assuming an incompressible flow of vapour (or in other terms, a low vapour pressure gradient compare to its average pressure in the pipe, which is not necessarily correct during heat pipe start up), a 0.405 evaporator pressure gradient recovery in the condenser (some theories assume that the vapour pressure increase in the evaporator is equal to the vapour pressure decrease in condenser. They refer only to inertia term and not the viscous pressure drop) and a fully developed laminar flow of the vapour;

$$\Delta P_v = \left(1 - \frac{4}{\pi^2}\right)\frac{\dot{m}^2}{8\rho_v {r_v}^4} + \frac{8\mu_v \dot{m} L_a}{\pi \rho_v {r_v}^4} \quad \text{(Eq. 3-10)}$$

Where;

ρ_v: Vapour density , Kg/m3

μ_v: Dynamic viscosity of the vapour , Pa.s

And finally the pressure drop due to gravitational head;

$$\Delta P_g = \rho_l g l \sin\varphi \quad \text{(Eq. 3-11)}$$

g: $Acceleration\ due\ to\ gravity = 9.81\ \frac{m}{s^2}$

l: $heat\ pipe\ total\ length$, m

φ: The angle between the heat pipe and the horizontal. It is positive when condenser is lower than evaporator

All the above formulas are for incompressible one dimensional flow. Incompressible assumption is very often a right assumption. The exceptions are during the start-up and for liquid metal heat pipes. One-dimensional flow assumes that the temperature and pressure are

constant across the cross sectional area. This is also correct for |Rer|<10 (Reay & Kew, 2006), where;

$$Re_r = \frac{\rho_v v_r r_v}{\mu_v} \quad \text{(Eq. 3-12)}$$

v_r : Radial velocity component at the wick surface where r = r_v, m/s

Now that the capillary limit is explained which is the main heat transfer limit over the majority of the heat pipe's performance range, a brief description is given about the overall heat transfer phenomena inside the pipe and then the other limits are described.

At the start up, when heat is applied to the evaporator, it conducts through the thickness of the container (heat pipe wall) and then travels through the liquid-filled wick mainly by conduction through the solid and liquid and partly by convection through the liquid and reaches the surface of the liquid which is the vapour-liquid-solid interface. That is where evaporation happens.

By increasing the heat gradually, the same process happens but more heat is transferred by convection. After a while bubbles start to form on the heat pipe wall. At first bubbles easily leave the wall and travel to the surface which increases the convection. By increasing the heat even more, at one point bubbles cover the entire surface of the heat pipe inner wall in the evaporator and block further heat transfer into the pipe. This point is called burn-out. The evaporator temperature suddenly jumps up and no more heat is transferred by the pipe.

Therefore it is important to know the effective thermal conductivity of a porous wick structure. To calculate this, there are two models in the literature; one model assumes that the liquid and solid passages in the wick are effectively in parallel;

$$K_w = (1 - \varepsilon)K_s + \varepsilon K_l \quad \text{(Eq. 3-13)}$$

Where;

K_w : Wick effective thermal conductivity, W/m.K (= W/m.°C)

K_l : Thermal conductivity of the working fluid, W/m.K

K_s : Thermal conductivity of the wick material, W/m.K

Another model assumes the fluid and solid bits of the wick are in series;

$$K_w = \frac{1}{\frac{(1-\varepsilon)}{K_s} + \frac{\varepsilon}{K_l}} \quad \text{(Eq. 3-14)}$$

Knowing the exact heat transfer passage through a porous wick, hence its effective thermal conductivity is impossible but the real value is always between the values calculated by two above methods. Some correlations have been experimentally developed for special types of a porous wick. Thermal conductivity for liquid saturated wick of packed spheres has been correlated by the following equation;

$$K_w = \frac{K_l[(2K_l + K_s) - 2(1-\varepsilon)(K_l - K_s)]}{[(2K_l + K_s) + (1-\varepsilon)(K_l - K_w)]} \quad \text{(Eq. 3-15)}$$

This equation can also be used to approximate the effective conductivity of liquid saturated porous metal wick but it should be noted that the accuracy decreases as the radius of contact among adjacent particles, rc in following picture, increases.

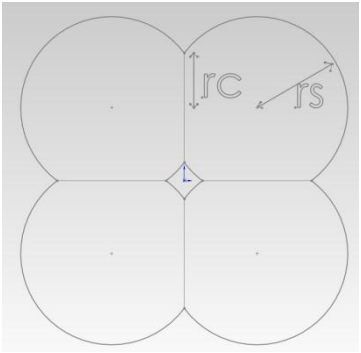

Figure 3- 12 In sintered wicks, particles are deformed at the contact point and this should be noted when applying an ideal packed sphere's formulas to them

For a sintered metal wick with a large contact radius, Kw is calculated by the equation;

$$K_w = \frac{\pi}{8}\left(\frac{r_c}{r_s}\right)^2 K_s + \left[1 - \frac{\pi}{8}\left(\frac{r_c}{r_s}\right)^2\right]\left[\frac{K_l K_s}{\varepsilon' K_s + K_l(1-\varepsilon')}\right] \quad \text{(Eq. 3-16)}$$

Where;

$$\varepsilon' = \frac{\varepsilon}{1 - \frac{\pi}{8}\left(\frac{r_c}{r_s}\right)^2} \quad \text{(Eq. 3-17)}$$

In the absence of data for the contact radius, rc can be estimated by means of a material balance for the idealized geometry as per following equation (Chi, 1976);

$$\varepsilon = \frac{\pi}{6\left[1-\left(\frac{r_c}{r_s}\right)^2\right]^{2/3}}\left\{1-\left(\frac{r_c}{r_s}\right)^2\left[2-\sqrt{1-\left(\frac{r_c}{r_s}\right)^2}\right]\right\} \quad \text{(Eq. 3-18)}$$

Capillary limit is the main heat transfer limit over the majority of the heat pipe's performance range but there are other limits to the heat transfer capability of a heat pipe. Most of these limits occur under special circumstances and normally heat pipe operation can be restarted after hitting one of these limits just by changing the operating conditions.

Viscous Limit;

$$\dot{q}_{Viscous} = \frac{{r_v}^2 L \rho_v P_v}{16 \mu_v l_{eff}} \quad \text{(Eq. 3-19)}$$

Where;

$\dot{q}_{viscous}$: Maximum heat transfer due to viscous limit per unit vapour channel area, W/m^2

P_v : vapour pressure, Pa

Sonic Limit:

$$\dot{q}_{sonic} = 0.474 L (\rho_v P_v)^{0.5} \quad \text{(Eq. 3-20)}$$

$\dot{q}_{sonic}$: Maximum heat transfer due to sonic limit per unit vapour channel area, W/m^2

Entrainment Limit:

$$\dot{q}_{entrainment} = L.\sqrt{\frac{\rho_v \sigma}{x}} \quad \text{(Eq. 3-21)}$$

$\dot{q}_{entrainment}$: Maximum heat transfer due to entrainment limit per unit vapour channel area, W/m^2

x is a number depending on the wick type and size. For a typical sintered wick it is roughly $2r_c$ according to Faghri (1995).

Capillary Limit:

$$\dot{Q}_{capillary} = \dot{m}_{max} L = \left[\frac{\rho_l \sigma L}{\mu_l}\right]\left[\frac{K A_w}{l_{eff}}\right]\left[\frac{2}{r_c} - \frac{\rho_l g l_{eff}}{\sigma} sin\,\varphi\right] \quad \text{(Eq. 3-22)}$$

Where;

$\dot{Q}_{capillary}$: Maximum total heat transfer due to capillary limit, W

l_{eff} : Effective length of the heat pipe, m

Boiling Limit according to Faghri (1995):

$$\dot{Q}_{boiling} = \frac{2\pi L_e K_{eff} \Delta T_{crit}}{\ln(r_w/r_v)} \quad \text{(Eq. 3-23)}$$

$$\Delta T_{crit} = \frac{2\sigma T_v}{L\rho_v}\left(\frac{1}{R_b} - \frac{1}{R_{men}}\right) \quad \text{(Eq. 3-24)}$$

$\dot{Q}_{boiling}$: Maximum total heat transfer due to boiling limit, W

R_{men} : $r_{c,\,m}$

$R_b = 10^{-7}$m for conventional heat pipes

$K_{eff} = K_w$: Effective thermal conductivity of the wick, W/m.K

T_v : vapour temperature, K

For medium temperature working fluids like water and ammonia and common non-composite wicks heat pipes that work outside of their extreme operating temperatures, capillary limit is the main and perhaps the only limit as discussed before. For other heat pipes, other limits get more important and especially the start-up period is of prime concern. Heat pipe start-up is a function primarily of the sink temperature (where the heat is being dumped) and the interface thermal resistance at the condenser.

Generally speaking, the start-up of a heat pipe from high vapour pressure does not present a special problem as it means low vapour pressure drop and velocity. However, the start-up of a heat pipe from initial low vapour pressure and low interface thermal resistance at the condenser normally involves high vapour velocities that can cause the performance to hit the sonic and eventually the entrainment limit.

As in case of ammonia heat pipe, because ammonia vapour pressure is relatively high and very often the pipe starts-up with some of the working fluid in liquid state, the start-up should not be a problem unless the temperature is so high that all the working fluid is expected to be in vapour state. In that case the pipe is better to be started by cooling the condenser to condense some of the working fluid until the wick is filled with liquid working fluid and then apply the heat to the evaporator gradually.

3-8) Heat pipe's container design

The container details are specified using the mechanical design rules. Heat pipe is treated as a pressure vessel and it is designed so that the maximum stress at any temperature to be one-quarter of the material's ultimate tensile strength at that temperature. For round tubes the maximum pressure stress is approximated according to the following tabled formulas (Chi, 1976);

Vessel type	Maximum pressure stress f_{max}	
Round tube in which the wall thickness is less than 10% of the diameter	$f_{max} = \frac{P d_0}{2t}$	(Eq. 3-25)
Thick wall cylinder subject to normal pressure	$f_{max} = \frac{P\left({d_0}^2 + {d_i}^2\right)}{{d_0}^2 - {d_i}^2}$	(Eq. 3-26)
Thick wall hemispherical end cap	$f_{max} = \frac{P\left({d_0}^3 + 2{d_i}^3\right)}{2\left({d_0}^3 - {d_i}^3\right)}$	(Eq. 3-27)
Hemispherical end cap with wall thickness less than 10% of its diameter	$f_{max} = \frac{P d_0}{4t}$	(Eq. 3-28)
Flat circular end cap	$f_{max} = \frac{P {d_0}^2}{8t^2}$	(Eq. 3-29)

Where

f_{max} : Maximum hoop stress in the wall, Pa

P : Pressure differential across the wall or end cap, Pa

d_0 : Tube outside diameter or end cap diameter, m

t : Tube wall thickness or end cap thickness, m

d_i : Tube inside diameter, m

Normally the internal pressure is the saturated vapour pressure of the working fluid at its operating temperature. The pressure differential is equal to vapour pressure minus the ambient pressure. Knowing the pipe outside diameter, these equations can be used to calculate the wall thickness of the pipe and the end caps.

3-9) SLM heat pipes' thermal resistance – Temperature drop along the pipe

The heat transfer process in a heat pipe is associated with a temperature drop which can be represented by thermal resistances as shown below;

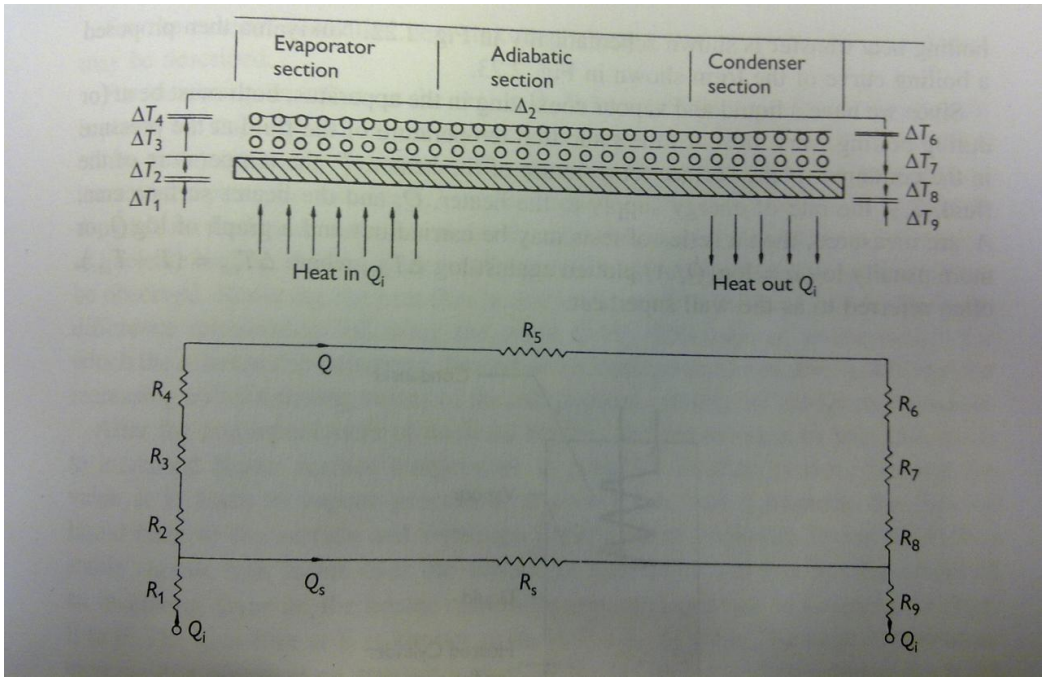

Figure 3- 13 Temperature drops and equivalent thermal resistance in a heat pipe (Reay & Kew; 2006)

As explained in details by Reay & Kew (2006), R_1 and R_9 are the thermal resistances between the hot and cold sources and the heat pipes, R_2 and R_8 are the thermal resistance of the heat pipe wall. R_3 and R_7 are the thermal resistance of the week in evaporator and condenser regions. In normal operating conditions, these are the sum of the thermal resistance of the liquid filling the wick and the conduction through the solid parts of the wick which can be calculated as explained before. But if boiling happens in the evaporator or if there is excess liquid in the condenser, their estimation gets more difficult.

R_4 and R_6 are the resistance along the vapour-liquid interface and can generally be neglected. R_5 is due to the temperature drop along the vapour column and can usually be neglected. R_s is the resistance in the thickness of the container along the structure of the heat pipe and can normally be neglected.

$$R_1 = \frac{t}{A_e * K_{TIM}} \quad \text{(Eq. 3-30)}$$

$$R_9 = \frac{t}{A_c * K_{TIM}} \quad \text{(Eq. 3-31)}$$

Where;

t : Thickness of the thermal interface in the evaporator and condenser regions, m

K_{TIM} : Thermal conductivity of the thermal interface material, m

Ae : Evaporator surface area (Contact surface area between the hot source and the heat pipe), m^2

Ac : condenser surface area (Contact surface area between the cold source and the heat pipe), m^2

$$R_2 \; and \; R_8 = r_o \frac{\ln \frac{r_o}{r_w}}{K_s A_{e \; or \; c}} \quad \text{(Eq. 3-32)}$$

Where;

r_o : Outer radius of the heat pipe container, m

r_w : Inner radius of the heat pipe wall, m

K_s = Conductivity of the heat pipe container material, W/m.K

$$R_3 \; and \; R_7 = r_w \frac{\ln \frac{r_w}{r_v}}{K_w A_{e \; or \; c}} \quad \text{(Eq. 3-33)}$$

Where;

$r_{w \text{ and }} r_v$: Outer and inner wick radius, m

K_w : Effective conductivity of the wick, W/m.K

$$R_s = \frac{l_e + l_c + l_a}{A_s K_s + A_w K_w} \quad \text{(Eq. 3-34)}$$

Where;

A_s : Cross sectional area of the heat pipe wall, m^2

A_w : Cross sectional area of the wick structure, m^2

It is clear from figure 3-13 that R_2 till R_8 are in series and altogether in parallel with R_s. We assume the total carried power is divided between these two parallel resistances in accordance to their ratio.

$$Rseries = R2+R3+R7+R8 \quad \text{(Eq. 3-35)}$$

For a certain total input power P, the total temperature drop ΔT along the pipe will be;

$$\Delta T = P\left[(R_1 + R_9) + \frac{1}{\frac{R_s + R_{series}}{R_s R_{series}}}\right]°C \quad \text{(Eq. 3-36)}$$

Obviously this is purely theoretical and does not consider any superheat between the wall and the vapour or extra fluid in the condenser but it provides a rough idea of the value of different resistances and highlights the importance of each one of them.

3-10) Design tool for SLM sinter-style heat pipes

During the course of this project a design tool has been developed in the form of a Microsoft Office Excel workbook. The core of the tool and its background calculations are what is explained above. The design tool is meant to be a user friendly tool for the use of engineers for evaluating or designing a sinter-style SLM heat pipes without getting involved with the complications of the calculation process and individual formulas and to avoid possible errors including mistakes in unit conversions.

The specialty of this tool is not the used formulas and not even the calculation process. These can be found in heat pipe reference books and some heat pipe manufacturing companies already have similar tools to design sintered heat pipes but firstly, almost all these tools are proprietary assets of the companies and are not available to individual researchers. Secondly, there is not a general agreement in the literature about the HP performance governing equations. This is a

reflection of the fact that the real performance of a heat pipe is a complicated multi-dimensional two-phase phenomena that is also subjected to some unknown and immeasurable parameters including the possible extra added volume of the fill tube, more or less volume of the working fluid inside the tube than the theoretically calculated value, generation of non condensable gasses in the short and long term that alters the effective working length, contaminations during manufacturing process, external profile of the heat pipes and many other parameters. Some of these may be the nature of a specific manufacturing process thus unavoidable and obviously could not have been considered by others when developing the governing equations. For instance, many HP manufacturers use a fill tube to vent, fill and seal a heat pipe. This adds a dead volume to the internal space of the pipe that for smaller HPs can be considerable and affects the performance in some working orientations. The effect of this excess volume has to be considered in the theoretical design tool through the validation process and by applying necessary correction factors.

Therefore the available formulas are all based on some simplifications, use some experimentally process-dependent values and naturally, could not have taken some other process-dependant parameters into account at all. During the development process of this tool, it was proved that using different suggested formulas leads to different results which can be considerably different. It is believed that each HP manufacturing company has validated/modified their own design tools (if any) against their own products and in a certain range.

Likewise, in this tool, a full set of required formulas and equations have been gathered from different references and the calculation results have been validated in a specific range where the actual experiments on the real samples had been conducted. Also, this tool takes the special shape of the built SLM HPs into account to calculate the heated and cooled surface areas and heat fluxes.

The tool can be implemented in two ways; either to check the viability of a set of design parameters to ensure the required performance is achievable or to optimize an individual parameter based on the known values of the others.

An example of the former is given later in this chapter where these calculations were used before producing the first batch of the SLM prototypes to check the feasibility of them achieving the required thermal performance. The design tool validation data/process is presented in the next chapters.

Followings are a few screen shots of the design workbook along with a brief description about how it works. The final tool will be equipped to an encrypted input interface to block the access of the user to the formulas to avoid any possible unwanted changes to the equations and data.

For the specific working fluid, the tool has a data base of its different physical and thermal properties at different temperatures in the entire range between its melting and critical points in 5 degree increments. Currently these data are for acetone but can be replaced with the data for any other fluid.

Working Fluid: **ACETONE**

Temperature	Pressure	Liquid Density	Vapor Density	Heat of Vapor.	Liquid Therm. Cond.	Vapor Therm. Cond.	Liquid Viscosity	Vapor Viscosity	Surf. Tension
(°C)	(MPa)	(kg/m³)	(kg/m³)	(kJ/kg)	(mW/m-K)	(mW/m-K)	(μPa-s)	(μPa-s)	(mN/m)
-90	4.4241E-06	908.12	0.00016875	644.54	193.6350971	4.34392467	2526.685721	4.457264682	39.856
-85	0.000008482	902.71	0.00031495	639.66	192.3141739	4.58589924	2116.707786	4.589482665	39.085
-80	0.00001565	897.33	0.00056611	634.81	190.9875901	4.83321281	1796.953272	4.721672181	38.317
-75	0.000027876	891.98	0.00098298	629.99	189.6551893	5.08586538	1544.064071	4.853833228	37.552
-70	0.000048062	886.64	0.00165330	625.19	188.3168083	5.34385695	1341.477913	4.985965807	36.79
-65	0.000080413	881.32	0.00270020	620.41	186.972277	5.60718752	1177.26143	5.118069918	36.032
-60	0.00013085	876	0.00429170	615.66	185.6214179	5.87585709	1042.687716	5.250145561	35.276
-55	0.00020751	870.7	0.00665190	610.92	184.2640454	6.14986566	931.2860331	5.382192736	34.525
-50	0.0003213	865.41	0.01007300	606.2	182.8999658	6.42921323	838.1964676	5.514211444	33.776
-45	0.00048656	860.11	0.01492600	601.49	181.5289763	6.7138998	759.7249135	5.646201683	33.031
-40	0.00072172	854.82	0.02167700	596.79	180.1508646	7.00392537	693.0317953	5.778163454	32.29
-35	0.0010501	849.52	0.03089900	592.09	178.7654085	7.29928994	635.9113993	5.910096757	31.551

Figure 3- 14 Snapshot of the working fluid database of the design tool

Required wall and end caps' thickness can be checked in another sheet based on the pipe material, geometry and maximum working temperature. The samples for this project were all produced from aluminium alloy AlSi12 but if in future SLM heat pipes are built from other materials or aluminium alloys their mechanical properties can be simply inserted into the tool.

Wall and end cap's thickness

Yield tensile strength for ALSi12 = 238 (150-230)MPa and maximum stress inside the pipe must be a quater of that - d0 is the outside diameter of SLM samples, 12.7mm

Temperati (°C)	Pressure (MPa)	Min wall thickness t >.. mm	Min thickness of the flatcircular end cap mm	Min thickness of the hemispherical end cap mm
-90	4.9E-06	0.01081315	0.18528832	0.005406577
-85	9.3E-06	0.01081269	0.185284313	0.005406343
-80	1.7E-05	0.01081187	0.185277312	0.005405934
-75	3E-05	0.01081049	0.185265487	0.005405244
-70	5.1E-05	0.01080823	0.185246132	0.005404115
-65	8.5E-05	0.01080464	0.185215352	0.005402319
-60	0.00014	0.01079908	0.185167687	0.005399539
-55	0.00022	0.01079068	0.185095667	0.00539534
-50	0.00033	0.01077828	0.184989291	0.00538914
-45	0.0005	0.01076036	0.184835435	0.005380179
-40	0.00074	0.01073496	0.184617184	0.005367481
-35	0.00107	0.01069963	0.184313088	0.005349813
-30	0.00152	0.0106513	0.183896336	0.005325648
-25	0.00213	0.01058623	0.183333824	0.005293117
-20	0.00294	0.01049994	0.182585102	0.005249972
-15	0.004	0.01038708	0.181601142	0.005193539
-10	0.00536	0.01024136	0.180322857	0.005120682
-5	0.0071	0.01005552	0.178679247	0.00502776
0	0.0093	0.00982118	0.176584974	0.004910591
5	0.01204	0.00952885	0.173937066	0.004764426

Wall thickness= 1.09mm

As a result of these calculation, 1.09mm wall thickness of the existing samples theoretically should be enough for temperatures way higher than 125C

And the one end which is 5 mm thick should be good enough for temperatures well above 125C

Vesseltype	Maximum pressure stress f_{max}
Round tube in which the wall thickness is less than 10% of the diameter	$f_{max} = \frac{Pd_0}{2t}$
Thick wall cylinder subject to normal pressure	$f_{max} = \frac{P(d_0^2 + d_i^2)}{d_0^2 - d_i^2}$
Thick wall hemispherical end cap	$f_{max} = \frac{P(d_0^3 + 2d_i^3)}{2(d_0^3 - d_i^3)}$
Hemispherical end cap with wall thickness less than 10% of its diameter	$f_{max} = \frac{Pd_0}{4t}$
Flat circular end cap	$f_{max} = \frac{Pd_0^2}{8t^2}$

Where

45

f_{max} = maximum hoop stress in the wall
P = pressure differential across the wall or end cap
d_0 = Tube outside diameter or end cap diameter
t = Tube wall thickness or end cap thickness
d_i = Tube inside diameter

Figure 3- 15 Snapshot of the pipe thickness calculation sheet of the design tool

Some inputs are asked from the user as shown in figure 3-16 and then the capillary and other limits of the HP are calculated over the required temperature range using the set of formulas presented above along with the pipe temperature drop.

	A	B	C	D	E	F	G	H
1								
2	Working fluid	Acetone						
3	Working Temperature (C)	30						
4	Ltot (m)	0.0595	HP total length					
5	Le (m)	0.012	HP evaporator length					
6	Lc (m)	0.0215	HP condenser length					
7	Ro (m)	0.00635	Outer radius of the HP wall					
8	Ri (m)	0.00526	Inner radius of the HP wall					
9	Riw (m)	0.00381	Inner radius of the wick					
10	t (m)	0.00109	Wall thickness					
11	K (W/m.K)	180	HP container material conductivity					
12	HP material yield tensile strength (MPa)	238						
13	Kw (W/m.K)	40	wick effective conductivity					
14	rc (m)	0.000115	Pore radius					
15	permeability (m2)	1.00E-10		2.80E-10	5.60E-10			
16	Porosity	0.58						
17	Contact angle (degree)	19.4	Acetone/aluminium contact angle					
18	Working angle (degree)	-90	HP orientation					
19	Power (W)	15	Total HP input power					
20								
21	La (m)	0.026	Adiabatic Length					
22	Leff (m)	0.04275	HP effective length					
23	Aw (m2)	4.13167E-05	Wick cross section area					
24								
25	Pressure MPa	0.037809663						
26	Liquid Density Kg/m3	779.7558032						

Figure 3- 16 Snapshot of the input data of the design tool

For every set of inputs general diagrams can be produced by varying all the other free parameters for optimization purposes. An exemplary curve is shown in figure 3-17.

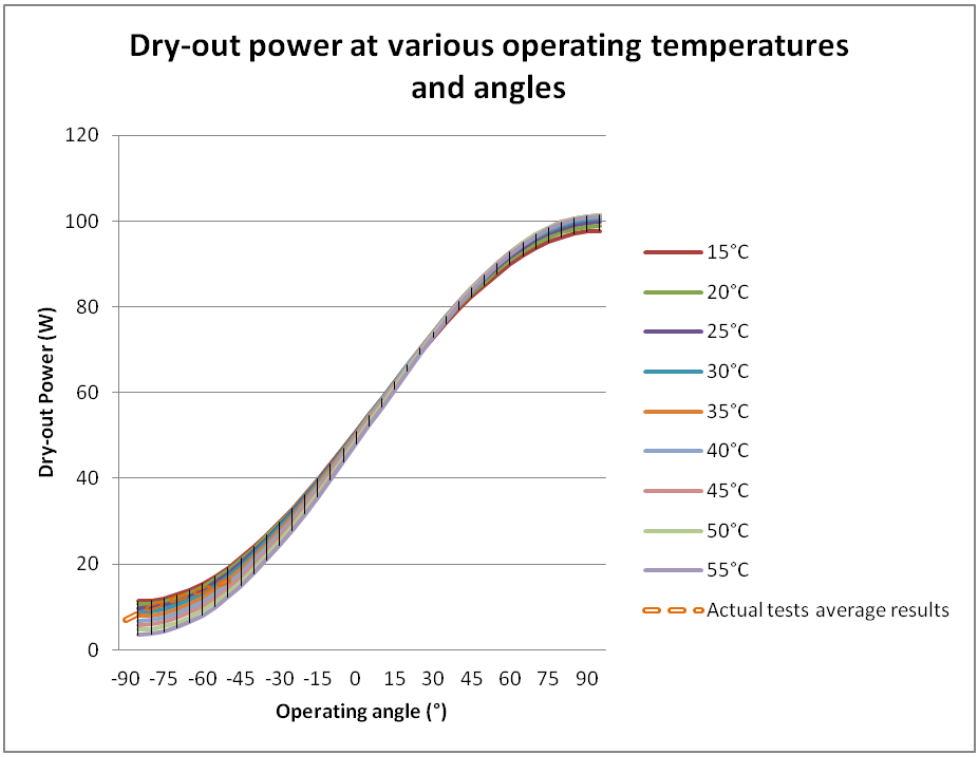

Figure 3- 17 An exemplary general diagram developed by the design tool for optimization/validation purpose

3-11) Theoretical design/evaluation of the initial SLM heat pipe samples

The ultimate aim of this project is to produce SLM heat pipes with an external profile identical to that of the existing extruded axially grooved heat pipes (AGHPs) to enable a direct comparison. This plus some of the other restrictions known at the time (before start building the first samples) in terms of the SLM machine capability, had provided a rough idea of the final shape and structure of the SLM HP samples.

Following calculations were done at that time with those assumptions to check the feasibility of the SLM HPs to hit the required performance. Many of these assumptions were proved to be roughly correct but some others changed later. Following comments and calculations are brought here exactly as they were done at the time to demonstrate the use of the above calculation process to check the feasibility of a design. This section should be read in conjunction with the next chapter for all the used terms and phrases (especially about SLM process) to make sense. Those assumptions that subsequently changed are mentioned in brackets and in italic font.

Initial SLM aluminium porous samples are to be fabricated using SLM100 machine. SM100 has a maximum working envelop of Ø125x80mm. Out of possible 80mm sample height, 60mm is believed to be a reasonable height to aim for the first samples.
AL6061 powder with a particle size of 25-40 microns will be used (*This was later changed to AlSi12*). Deposited layers have 50-100 microns thickness. A porosity of 60% and minimum pore radii of 100 microns are thought to be achievable. (*This was later changed to 58% and 115 microns*)
The plan is to initially produce some simple cubic samples to work out the minimum achievable pore radii and maximum possible porosity and then use an existing extruded grooved aluminium tube, as shown below, and produce a similar structure using the SLM machine by just replacing the solid fins of the grooved tube with SLM produced porous fins. (*The overall shape of the HP was later changed slightly*)

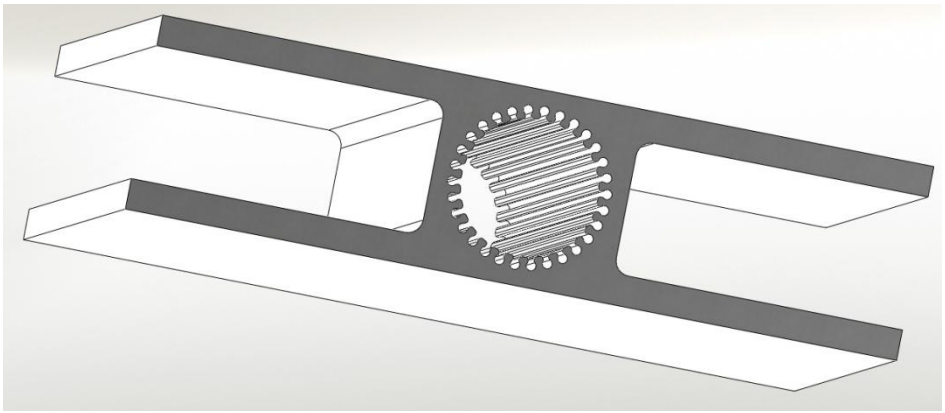

Theoretical performance of the to-be-produced sample, once converted into functional heat pipes, is predicted as follows;

Assumptions

Heat pipe length $= 60\ mm$

Working fluid: Ammonia (*This was later changed to acetone for main body of the experiments although some ammonia experiments were also conducted*)

Operating Temperature: -20ºC (*This was later changed to a range between 20°C to 40°C*)

Evaporator Length $L_e = 10\ mm$ (*This was later changed to 12mm*)

Condenser length $L_c = 20\ mm$ (*This was later changed to 21.5mm*)

Adiabatic Length $L_a = 30\ mm$ (*This was later changed to 26mm*)

Power (Heat flow): $\dot{Q} = 10\ W = 0.01\ KW$

Ammonia properties at -20ºC:

Temperature (°C)	Pressure (MPa)	Liquid Density (kg/m³)	Vapor Density (kg/m³)	Heat of Vapor. (kJ/kg)	Liquid Therm. Cond. (mW/m-K)	Vapor Therm. Cond. (mW/m-K)	Liquid Viscosity (µPa-s)	Vapor Viscosity (µPa-s)	Surf. Tension (mN/m)
-20.000	0.19008	665.14	1.6033	1329.1	621.96	21.768	214.41	8.4495	39.879

Porosity $\varepsilon = 60\%$

Pore radii $r_c = 100\ microns$

Pipe internal radius $r_w = \frac{10.7}{2} = 0.00535\ m$ (This is the internal radius of the tube from the centre to the solid wall)

Vapour space radius $r_v = \frac{8.9}{2} = 0.00445\ m$ (This is internal radius of the tube from the centre to the tip of the fins. To simplify the calculations, it is assumed that the porous structure will be full circular shape and not grooved as it will be in reality)

Effective length of the heat pipe $L_{eff} = \frac{1}{2}(L_e + L_c) + L_a = 45\ mm$

Maximum capillary pressure:

$$\Delta P_{cmax} = \frac{2\sigma \cos\theta}{r_c}$$

$$\Delta P_{cmax} = \frac{2 \times 0.039879 \times \cos 0}{0.0001} = 797.58\ Pa$$

Where σ is the liquid ammonia surface tension and θ is the contact angle which is taken to be zero meaning full wet-ability of ammonia on aluminium. (*Contact angle here has been assumed to be zero but later it was changed to 19.4° which is the right contact angle between acetone and AlSi12*)

On the other hand for correct operation of a heat pipe;

$$\Delta Pcmax \geq \Delta Pl + \Delta Pv + \Delta Pg$$

If this condition is not met, the wick will dry out in the evaporator region and the heat pipe will not operate.

$$\Delta P_l = \frac{8\mu_l \dot{Q} L_{eff}}{\pi(r_w{}^2 - r_v{}^2)\varepsilon r_c{}^2 \rho_l L}$$

$$\Delta P_l = \frac{8 \times 0.000214 \times 10 \times 0.045}{3.14 \times (0.00535^2 - 0.00445^2) \times 0.6 \times 0.0001^2 \times 665.14 \times 1329.1 \times 1000} = 5.2\ Pa$$

And

$$\Delta P_v = \left(1 - \frac{4}{\pi^2}\right)\frac{\dot{m}^2}{8\rho_v {r_v}^4} + \frac{8\mu_v \dot{m} L_a}{\pi \rho_v {r_v}^4}$$

Knowing that $\dot{m} = \frac{\dot{Q}}{L}$

$$\Delta P_v = \left(1 - \frac{4}{3.14^2}\right) \times \frac{0.01^2}{8 \times 1.6033 \times 0.00445^4 \times 1329.1^2} + \frac{8 \times 0.0000084495 \times 0.01 \times 0.03}{3.14 \times 1.6033 \times 0.00445^4 \times 1329.1} = 0.014\ Pa$$

Therefore;

$$797.58 \geq 5.2 + 0.014 + \Delta P_g$$

Thus $\Delta P_g \leq 792.4$

And since $\Delta P_g = \rho_l g l \sin\varphi$

$g = Acceleration\ due\ to\ gravity = 9.81\ \frac{m}{s^2}$

$l = heat\ pipe\ length$

$\varphi =$ The angle between the heat pipe and the horizontal

And this means an SLM porous structure made and tested with the above mentioned characteristics can be used in a heat pipe with a maximum length of 121mm working at -90° against gravity.

Temperature drop

(*The external profile of the produced SLM HP samples was slightly modified between batch one and two of the samples and it is seen below that the temperature drop calculations were done for this modified profile)*

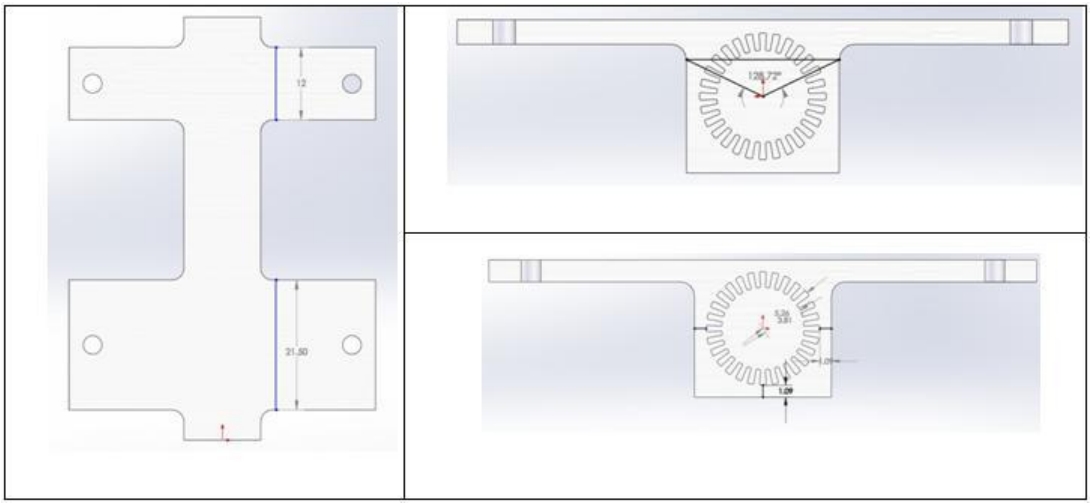

Figure 3- 18 Dimensions of the modified profile for use in temperature drop calculations

t : Thickness of the thermal interface in the evaporator and condenser regions = 0.0001m

K_{TIM} : Thermal conductivity of the thermal interface material = 3 W/m.K

Le: evaporator length = 0.012m

lc= condenser length = 0.0215m

0.05m = the width of the H-section pipes

A_e : Contact surface area between the hot source and the heat pipe = 3.14*0.0127*0.012*128.72/360= $1.711x10^{-4}$ m^2

A_c : Contact surface area between the cold source and the heat pipe = 3.14*0.0127*0.0215*128.72/360= $3.065x10^{-4}$ m^2

r_o : Outer radius of the heat pipe container = 0.0127/2 =0.00635 m

r_w : Inner radius of the heat pipe wall =0.00526 m

K_s : Conductivity of the heat pipe container material =180 W/m.K

$r_{w\ and}$ r_v : Outer and inner wick radius =0.00526 m and 0.00381 m

K_w : Effective conductivity of the wick = 40W/m.K

A_s : Cross sectional area of the heat pipe wall=3.14*(0.00635^2-0.00526^2)=$3.97x10^{-5}$ m^2

A_w : Cross sectional area of the wick structure=3.14*(0.00526^2-0.00381^2)=$4.13x10^{-5}$ m^2

According to Eq. 3-30 to Eq. 3-36; (Note that A_e and A_c in this HP profile are different for R_1 and R_9 than the rest of formulas because the contact area between the heat pipe and the thermal interface, TIM, is different from the heat input area into the pipe)

$$R_s = \frac{0.0595}{3.97 \times 10^{-5} \times 180 + 4.13 \times 10^{-5} \times 40} = 6.76 \frac{°C}{W}$$

$$R_1 = \frac{0.0001}{3 \times 0.012 * 0.05} = 0.056$$

$$R_9 = \frac{0.0001}{3 \times 0.0215 * 0.05} = 0.031$$

$$R_2 = 0.00635 \frac{\ln \frac{0.00635}{0.00526}}{180 \times 1.711 \times 10^{-4}} = 0.039$$

$$R_8 = 0.00635 \frac{\ln \frac{0.00635}{0.00526}}{180 \times 3.065 \times 10^{-4}} = 0.022$$

$$R_3 = 0.00526 \frac{\ln \frac{0.00526}{0.00381}}{40 \times 1.711 \times 10^{-4}} = 0.248$$

$$R_7 = 0.00526 \frac{\ln \frac{0.00526}{0.00381}}{40 \times 3.065 \times 10^{-4}} = 0.138$$

Rseries = R2+R3+R7+R8=0.447

For a certain total input power P, the total temperature drop ΔT along the pipe will be;

$$\Delta T = P \left[(R_1 + R_9) + \frac{1}{\frac{R_s + R_{series}}{R_s R_{series}}} \right] = P[0.0.087 + 0.419]°C$$

Therefore for a 5W power transfer a theoretical temperature drop of 2.5°C is expected and it can be seen that the effect of Rs is almost negligible as expected. The importance of the thermal interface in evaporator and condenser regions can be seen.

3-12) Conclusion

A theoretical background is given in this chapter which is essential to understand heat pipes in general and the basis of all the experiments explained in next chapters in particular. The calculation process and mathematical formulas that govern the performance of a sintered heat pipe are described. It is shown how they have been used at different stages of the project to evaluate or measure certain parameters before producing the actual samples.

There is also a brief description of a design tool which has been developed to encapsulate all the formulas in a user friendly easy-to-use environment. Not all the theoretical aspects of the project are included in this chapter. Some cases like the study of the SLM sintered structure or ammonia properties are given in next chapters to keep the flow of the text to avoid incoherency between the materials.

4-1) Introduction

This chapter is a relatively detailed description of the process and methodology of building the prototypes, hardware and the test rigs and the measurements on the critical parameters. It illustrates the entire process up to the point that the final SLM HP prototypes were ready for experiments which is the subject of the following chapter along with their experimental results. Some of the activities involved in this process have been moved to appendices at the end of this document to keep the flow of the material.

This chapter can be quickly reviewed before reading the following chapters and only be referred to again when it is needed but confusions will occur if the test results and conclusions are read before it.

Since a novel manufacturing process has being developed, several specifically-designed and fabricated test rigs, accessories and hardware had to be developed. Hardware e.g. welding fixtures were essential for the completion of the build process as were some of the test rigs e.g. permeability measurement rig while evaluation of some other parameters e.g. density or hardness were needed in order to provide an overall image of the process and identify the challenging issues for the future works or for the use in theoretical evaluations.

There have been numerous parameters involved and full characterization of the process with regard to each one of them is the subject of a full PhD project but critical parameters have been analyzed to the extent that the time and resources of the project allowed.

Summed up briefly, the experiments setup and the final HP tests preparation process has been as follows;

a) Built parameters definition/determination

b) Production of the initial SLM HP prototypes

c) Conversion of the initial samples into functional heat pipes and the initial tests to prove the feasibility of the SLM HP concept

d) Build parameters optimization – Built samples characterization

e) Production of the final SLM HP prototypes and extruded AGHPs benchmark samples

f) Further built samples characterization – Preparations for the final experiments

g) Development of the ammonia filling rig

h) Conversion of the final samples into functional heat pipes and final experiments

Items (c) and (h) are subject of the next chapter. Many of these steps have been comprised of several activities including building test rigs, developing hardware and accessories and conducting measurements.

Many different resources needed during the project with limited availability that actions had to be planned and completed around their availability including the SLM machine, SLM machine operator, raw materials, scanning electronic microscope (SEM), auxiliary hardware design and provision from sub suppliers, machining facilities, test rigs, vibration machine, etc. Therefore the organization of this chapter does not follow the chronological order that the activities were completed.

Also, the followings should be noticed when reading this chapter;

- Design and fabrication of the ammonia filling rig, described in Appendix A, has been a long task continuing almost through the entire project. The rig was completed towards the very end of the project therefore the experiments have been performed using acetone. This change of the test fluid from ammonia to acetone, as explained before, does not affect the concluded results in no way.

- Some of the measurements/experiments described here were to determine the value of the parameters needed for the theoretical design tool described in the previous chapter e.g. wet-ability of the working fluid, yield strength and the hardness of the material. All these are moved to Appendix A.

- Some other measurements/experiments were to identify the challenging issues for further investigation or to provide a better overall image of the process and the produced samples' properties e.g. the morphology of the produced structures and vibration resistance of the samples. The latter is explained in Appendix A.

- And the third group of measurements/experiments were to specify or to optimize the value of the settings for the SLM machine to produce the prototypes e.g. SLM porous structures' pore size, porosity, permeability, SLM solid structures' density, remaining pores in the solid structures and elemental composition of the material.

- There were auxiliary hardware needed at different stages including the permeability and porosity measurement test rigs, welding jig and thermal test rig. These are discussed here as well.

- The ultimate goal and outcome of this process has been two batches of SLM heat pipes with different external profile as shown in figure 4-1 and 4-2. The former, also called the "initial prototypes", was used to prove the feasibility of the SLM HP concept. The latter, called the "final prototypes", was used for performance comparison against extruded grooved AGHPs.

- Full characterization of SLM heat pipes stimulates measurement of many more parameters e.g. the thermal conductivity of the structures built by SLM from AlSi12 powder, life time compatibility between ammonia or acetone and AlSi12 and so on which is far beyond the scope of this project.

Figure 4- 1 Round cross section SLM HP

Figure 4- 2 H cross section SLM HP

4-2) Build parameters definition/determination

The first critical step was to determine the parameters that were needed in order to be able to produce the initial SLM HP samples for investigation of the feasibility of the idea e.g. machine

settings. Had the idea of implementing SLM to produce heat pipes been proved unfeasible during this stage, the entire project direction needed to be changed.

Because, it was the first time that SLM was being used to produce heat pipes, there were a series of parameters that their value (or at least some estimation of their value) was needed before being able to produce the initial prototypes. They were mostly the build parameters of the SLM machine and the process including the required laser power, laser scanning parameters, material, etc.

4-2-1) Specifying the structure of the SLM HPs' sinter-style wick

As it is described below, in SLM, sinter-style porous structures are generated by building an array of interconnected octahedral geometries. The resulting porous structure's properties closely depend on the laser beam settings. In the next sections it is explained how four different settings were selected and characterized and then the best one was chosen for the use in building the SLM HPs sinter-style wicks.

4-2-1-1) Selective Laser Melting (SLM)

Selective Laser Sintering/Melting (SLS/SLM) manufacturing process utilizes a laser beam to locally melt a thin layer of metal powder. By applying additional powder layers and using 3D CAD & custom beam control software to melt a pattern across each layer, complex 3D components that are not able to be manufactured using conventional machining are produced (Almeida, 2004). SLM process begins with a completely defined CAD model of the part to be made. Divided into cross-sections by special software, the model is then directly involved in the process. The essential operation is the laser beam scanning over the surface of a thin powder layer previously deposited on a substrate. The forming process goes along the scanning direction of the laser beam. Each cross-section (layer) of the part is sequentially filled with elongated lines (vectors) of molten powder (Yadroitsev, Bertrand, et al. 2007).

Nowadays, SLS/SLM technologies are widely used in various industries including medicine and research offering a range of advantages compared to conventional manufacturing techniques including shorter time to market, use of inexpensive materials, higher production rate, versatility, high part accuracy, ability to produce more functionality in the parts with unique design and intrinsic engineered features (Yadroitsev, Bertrand, et al. 2007). Different aspects of the laser treated surfaces have been studied in literature e.g. corrosion (Liu, Chong, et al. 2006), optimum value of the process parameters (Yadroitsev, Bertrand, et al. 2007) and residual stresses (Mercelis & Kruth 2006).

The samples for this project were manufactured by MCP Realizer 100 (MTT Tooling Technologies, UK) SLM machine. The ytterbium fibre laser with maximum laser output of 200 W having continuous wavelength (CW), λ=1.071µm and nominal beam diameter of 50µm was employed in the machine. The optical system controls the movement of the focused laser beam on the build substrate having accuracy of +/- 5µm. The SLM100 machine and the schematic diagram of the machine components are shown in figure 4-3 and 4-4;

Figure 4-3 SLM 100 machine used for producing the SLM HP prototypes

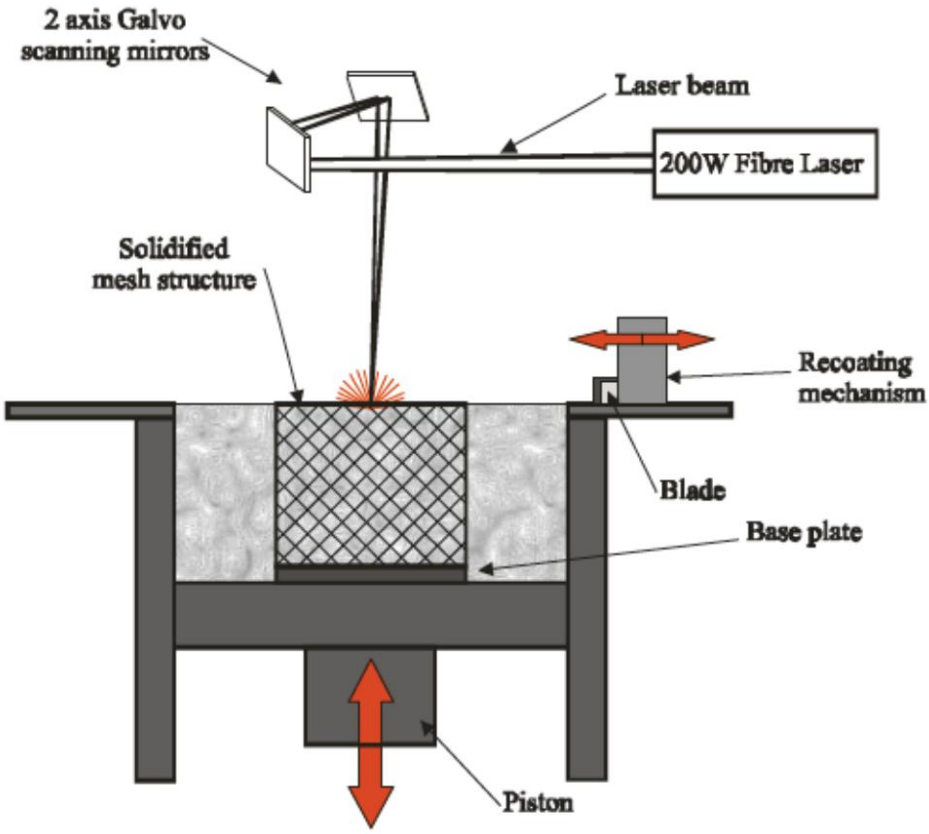

Figure 4-4 Schematic arrangement of various components in SLM build chamber

The processing chamber operates in a positive argon pressure of 14 mbar with oxygen levels kept between 0.1% - 0.2%. The atmosphere within the chamber is circulated and filtered to remove processed bi- products such as particles formed from condensed metal vapour, from the recycled gas. The specimens are manufactured layer by layer on an aluminium substrate plate secured on an elevator plate that moves vertically downwards allowing the controlled deposition of powder layers at 50μm intervals. The power and exposure time of the laser during each layer projected in spots is set from defined process window. These parameters control the degree of melting at each laser contact spot and the melt pool, which in turn controls the strut diameter of the porous structures and consequently their porosity and strength. Porous structures are generated by formation of octahedral units, repeated in a constrained boundary representing structural geometry. The build substrate plate is removed from the build chamber after completion of build and un-fused powder is removed by applying a vibratory action to the up-turned plate. Test pieces are then cut from the substrate plates using a wire erosion process to avoid excessive smearing of the pores. Figure 4-5 shows a substrate with some random geometry fabricated on it. An imaginary cylinder, its dicretized version in SLM CAD software and a unit cell are seen in figure 4-6;

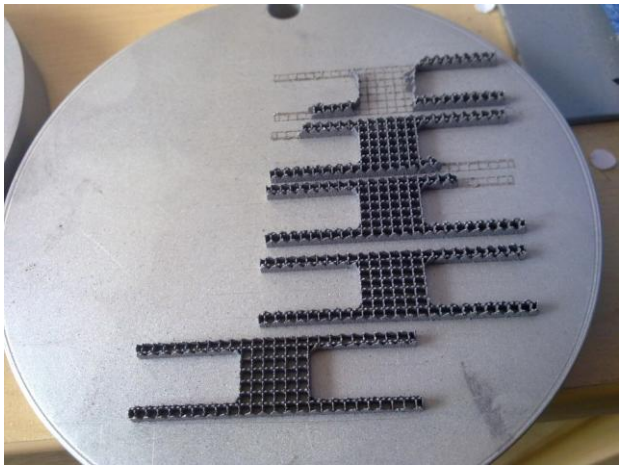

Figure 4-5 A substrate disc with some random geometry fabricated on it.

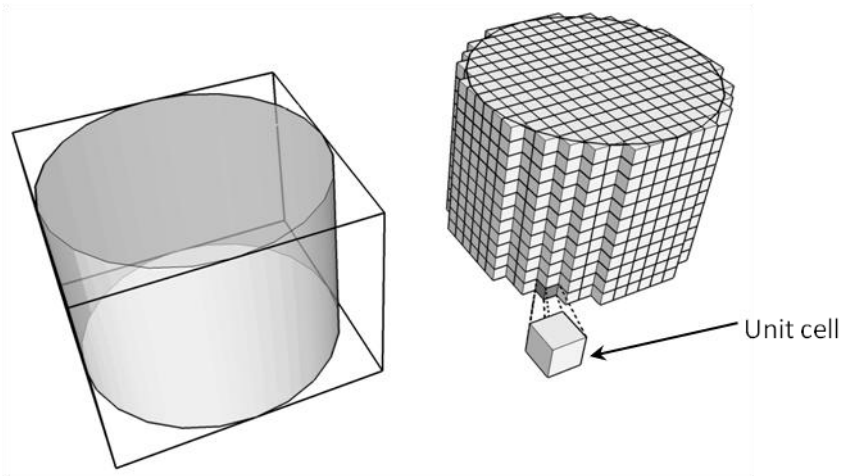

Figure 4- 6 An imaginary cylinder, its discretized version in SLM CAD software and a unit cell

Heat pipes are built up from the end cap upwards, with the end cap, wick and wall being made together in a single process (Figure 4-7).

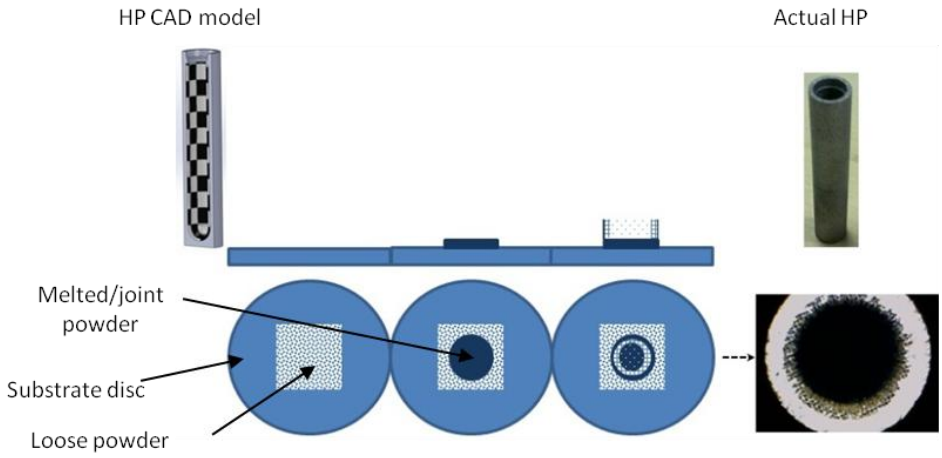

Figure 4- 7 HP build process in SLM. Objects are built on top of a substrate disk

CAD model preparation in SLM machine

SLM machine uses specific CAD software that converts normal CAD models to a layered geometry as it is fabricated in the machine. This conversion process is as follows;

1. Selecting the appropriate cylinder CAD geometry, contained in a bounding box enclosing the entire CAD geometry.

2. Populating the bounding box with cuboids of a defined unit cell size.

3. Populating the cuboids individually with 3-D octahedral geometry for porous structures (figure 4-8).

4. Trimming this repeated unit cell geometry to the candidate CAD cylinder dimensions.

5. Slicing the final geometry at appropriate layer thickness and create the appropriate machine format.

6. Applying specific commands to change the Cartesian coordinates of the octahedral structure's centre point if randomising of the structures is required (to obtain porous structures with a mix of pore radii's as opposed to homogeneous porous structure).

7. Building individual identification into the structures by the SLM process using standard software.

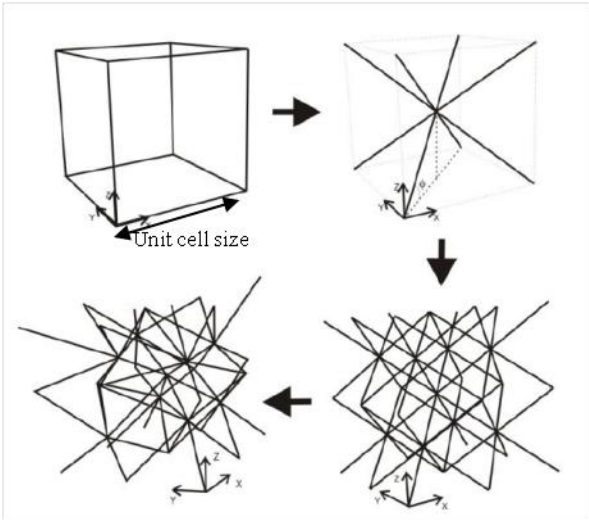

Figure 4-8 Transformation of the unit cell into a regular or randomised porous structure

To produce a porous structure the porous region is filled with small unit cells (dicretized) and each unit cell will contain an octahedral structure. This does not have to be necessarily octahedral to form a porous structure and can have many other shapes but in this project only octahedral have been used. Some of the other possible forms which have been used in SLM process to produce porous structures for other applications are shown in figure 4-9.

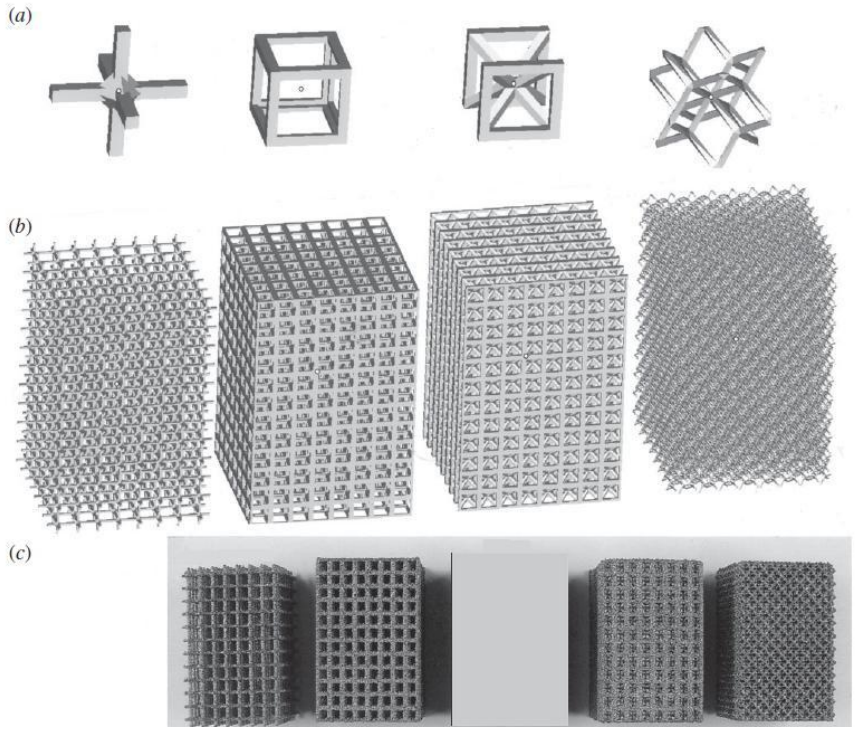

Figure 4- 9 (a) four different forms of the SLM cell filling structures to generate a porous object (b) CAD models and (c) real SLM fabricated blocks (Murr, Gaytan, et al., 2010)

In Figure 4-8, each one of the lines that connect the centre of a unit cell to one corner is called a strut. Strut diameter is dictated by the laser beam power and exposure time (the higher the exposure time the thicker the strut). If the centre of the octahedral geometry that fills each unit cell remains at the centre in all the unit cells, geometry is called a regular geometry and if it changes from the centre point to another point inside the unit cell from cell to cell, it is called a randomised geometry. A regular and a randomised porous geometry are shown in figure 4-10;

Figure 4-10 Randomised and regular (in inset) SLM porous structures

Some other terms and phrases used in SLM are as follows;

Point Distance: Each hatch is generated by a series of equidistant points where laser beam stays for a period of time equivalent to exposure time.

Hatch Distance: It's the distance between two adjacent paths scanned by laser.

Scanning Strategy: This includes the priority in scanning, scanning route and direction, hatch direction and the number of exposures per layer.

Exposure Time: Time for which laser stays at a point at each scan.

SLM has previously been used for making porous structures e.g. porous finned heat sinks or medical implants but only during the course of this project it has been used, for the first time, to

make porous structures which meant to work as a heat pipe capillary wick. Therefore there were a wide range of parameters that their values needed to be set both for the optimal performance of the SLM machine and also for the built samples to work efficiently as a heat pipe for instance the best aluminium alloy for the SLM process, powder size distribution and laser beam power.

Also, a heat pipe consists of a solid wall, which is desired to be completely solid to avoid any leakage into the heat pipe, and a porous wick structure which is characterized by its porosity, permeability and pore radii. SLM machine settings need to be separately optimized for each of these two solid and porous structures.

Following is a list of these parameters and their set values for this project;

A. Unit cell size: For the SLM process, an object CAD model is discretized into small cubic sections called "unit cell" by the machine special CAD software. Then the octahedral structures are built into each unit cell (for porous structures) as shown in figure 4-8. Obviously, for the same laser beam parameters, larger unit cells mean bigger empty spaces between the struts, or in porous structure terms, higher porosity and lower capillary force and vice versa. Previous experiences with SLM technique had used unit cell sizes down to about 300μm. For this project to get a reasonable and sensible difference between the samples for characterization purposes, prototypes were built with three unit cell sizes of 300, 500 and 700 μm.

B. Powder material: Al6061 and Al6063 are the most popular aluminium alloys for AGHPs and in thermal engineering as they are standard extrusion alloys and easily available worldwide. There is not much data available for the use of Al6000 series in SLM process as opposed to aluminium silicon alloys like AlSi12 which is a relatively established SLM material. During this project some sample were produced from Al6061 but soon it was shifted to AlSi12 to have a better control on the build parameters. Chemical composition of the used Al6061 and AlSi12 powder are shown below;

Table 4- 1 Al6061 powder chemical composition

Si	Fe	Cu	Mn	Mg	Cr	Zn	Ti	Al
0.4%-0.8%	0.0%-0.7%,	0.15%-0.40%	0.0% - 0.15%	0.8% - 1.2%	0.04%-0.35%	0.0% - 0.25%	0.0% - 0.15%	95.85%-98.56%

Table 4- 2 AlSi12 powder chemical composition

Si	Fe	Cu	Mn	Mg	Zn	Be	Al
11%-13%	0.06%	0.05%	0.15%	0.05%	0.2%	0.0008%	86.49 -88.49%

C. Powder size distribution: Both of the aluminium alloys which were used to make the prototypes had a particle size range of 25 to 40μm with particle size distributions as per figures 4-11 and 4-12;

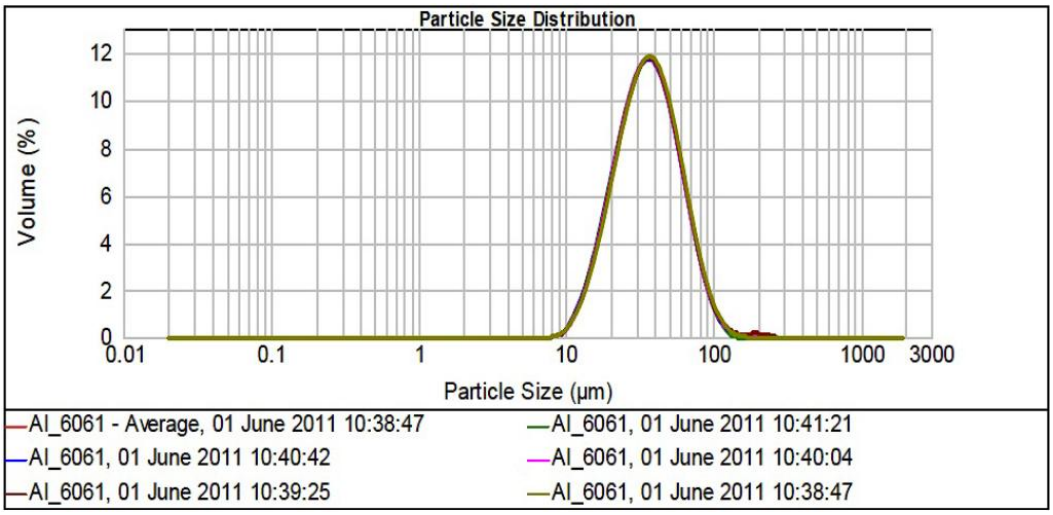

Figure 4-11 Powder particle size distribution for Al6061

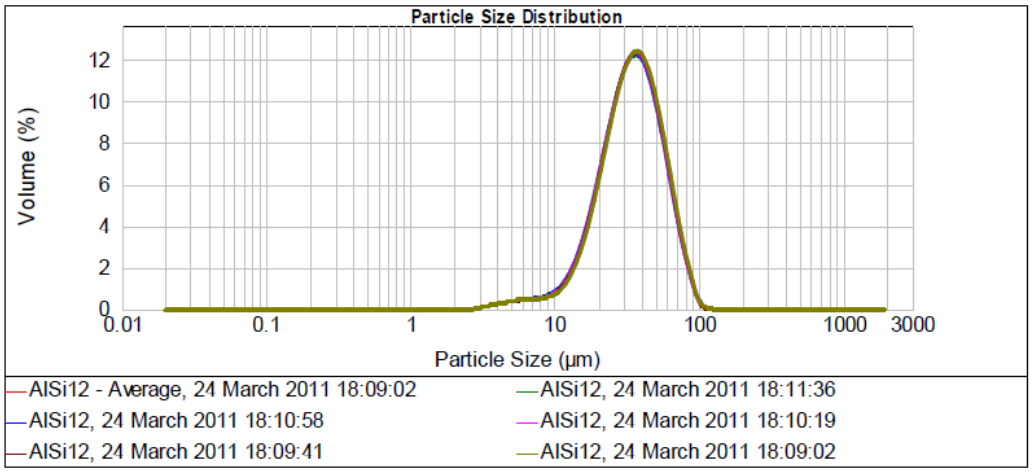

Figure 4- 12 Powder particle size distribution for AlSi12

These powders were the available powders at the time. Other particle sizes can be obtained once/if it is required to improve the samples' performance. Theoretically, powders with wider particle size distribution, once used for making porous structures, result in lower porosity and higher capillary force. The more similar the particles are, the bigger the remaining voids between them would be. AlSi12 powder particle are shown in figure 4-13 under an electronic microscope;

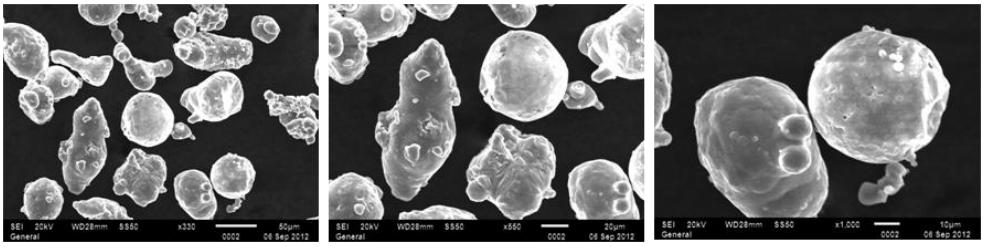

Figure 4- 13 AlSi12 powder particles; 330X, 550X and 1000X magnifications

D. Exposure time: Laser exposure times of 10 to 200ms were used. Following diagram shows the relation between the exposure time and the strut diameter;

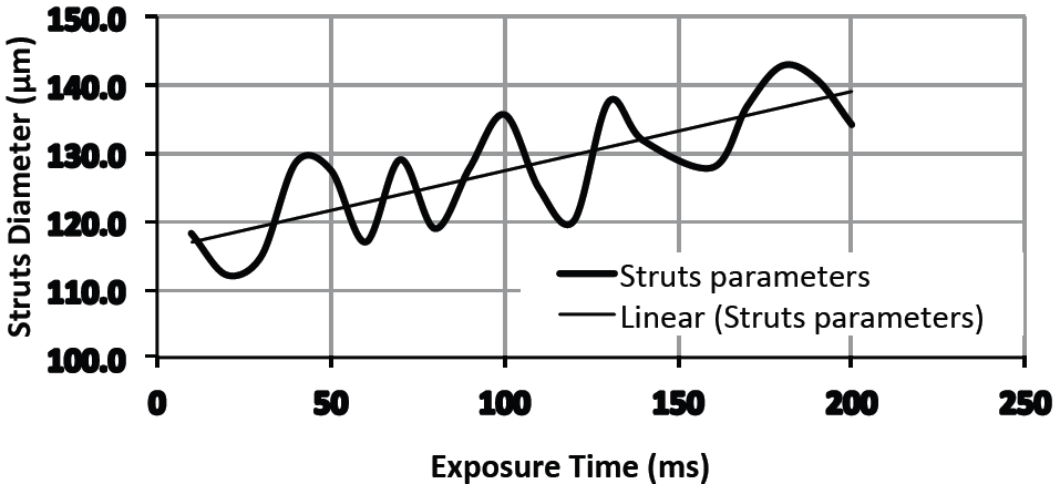

Figure 4-14 Average strut diameters for various laser exposure times

Obviously for a certain laser power, the longer the exposure time is the thicker the struts would be. First samples were produced with an exposure time of 60ms. This selection was based on a trade-off between the build time, porosity and structure rigidity.

E. Solid Structures: SLM solid structures are defined by the laser point distance, hatch distance and exposure time. A series of thin walls were made to understand the relation between these parameters as shown in figures 4-15 and 4-16 below;

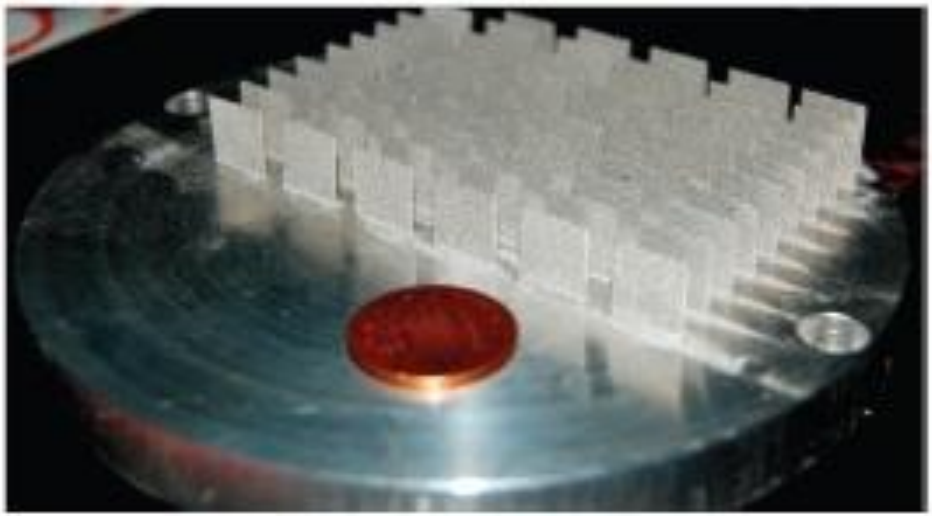

Figure 4-15 Al6061 thin walls made by SLM by varying the exposure time and point distance

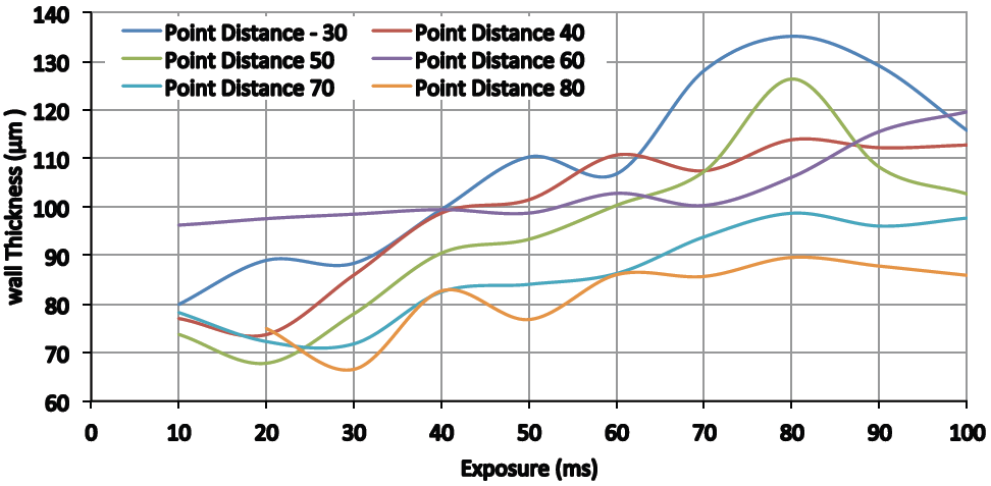

Figure 4-16 Average wall thickness measured for various exposure time and point distance

The "Points" are the locations that the laser beam stops for a time equal to the exposure time and then moves to the next point. Obviously the longer a specific exposure time and the closer the points are together, the denser the resulting structure would be.

Then a series of solid blocks were fabricated using a point distance of 0.01mm with various exposure times and hatch distances as shown below;

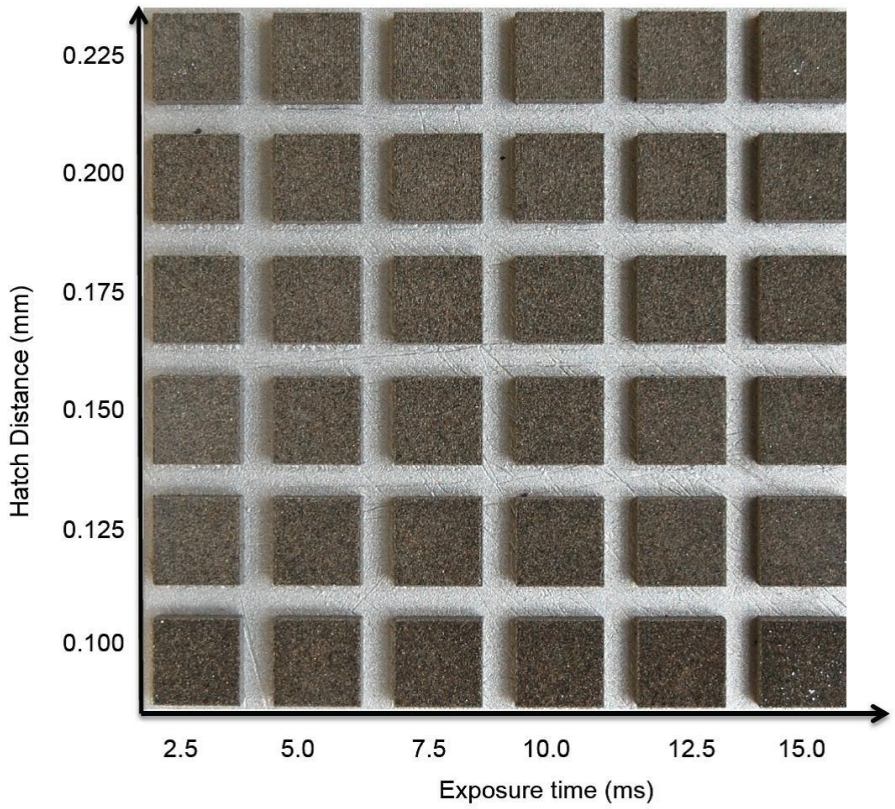

Figure 4-17 Al6061 solid blocks fabricated with different exposure times and hatch distances

Hatch distance is the distance between two adjacent scanning lines of the laser. Obviously lower hatch distance and higher exposure time leads to a more dense structure with less remaining voids. However the optimum value of these parameters is a trade-off between the required density and the production time. Smaller hatch distance and point distance and larger exposure times, increase the overall production time considerably.

F. Porous Structures: Initially, regular porous structures of 15x15x15 mm block of 300, 500 and 700µm octahedral unit cell sizes were manufactured at 30ms exposure time. The porous structures with 500µm and 700µm unit cell sizes were brittle, requiring higher energy for melting. This was achieved by manufacturing them at an exposure time of 60ms. Figure 4-18 shows regular and 30% randomised porous structures manufactured at 60ms exposure time from Al6061;

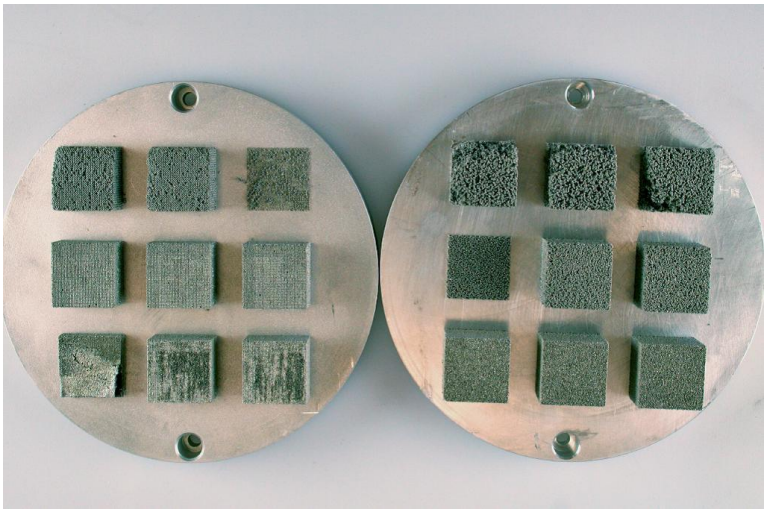

Figure 4-18 Al6061 regular (left) and 30% randomised (right) blocks fabricated with 60ms exposure time and 300, 500 and 700µm unit cell sizes from bottom row to the top row respectively

A set of porous samples were also manufactured for permeability testing. These specimens were manufactured in Ø13 mm porous structures surrounded by thin solid wall of 0.2 mm, figure 4-19. Therefore during permeability test, water will flow through top and bottom surfaces of the porous specimen, but there is no leakage along its length and through the side walls.

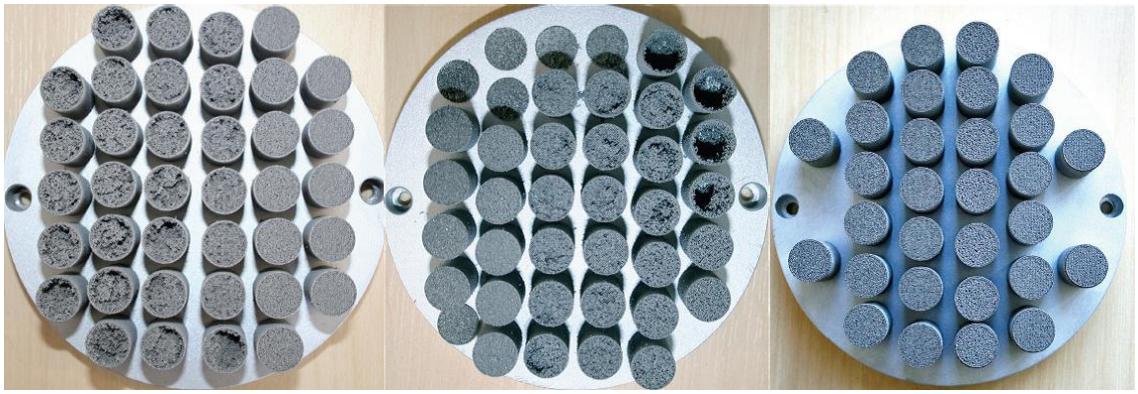

Figure 4-19 Porous samples made for permeability measurements. Different tries improved the quality as shown above from first build at the left to the 3rd build at the right

The method for cutting the samples off the substrate tuned out to be very critical. Analysing surfaces of porous structures shows closure of most of the pores due to higher smearing while wire cutting in 300µm unit cell samples. This causes problem when measuring permeability as it blocks the fluid flow through the sample. Also 700µm unit cell porous structures were breaking while wire cutting which again causes problems for permeability measurements as the samples has to have a regular shape and geometry with a measurable total volume. Both these issues can be addressed by reducing the speed of wire cutting.

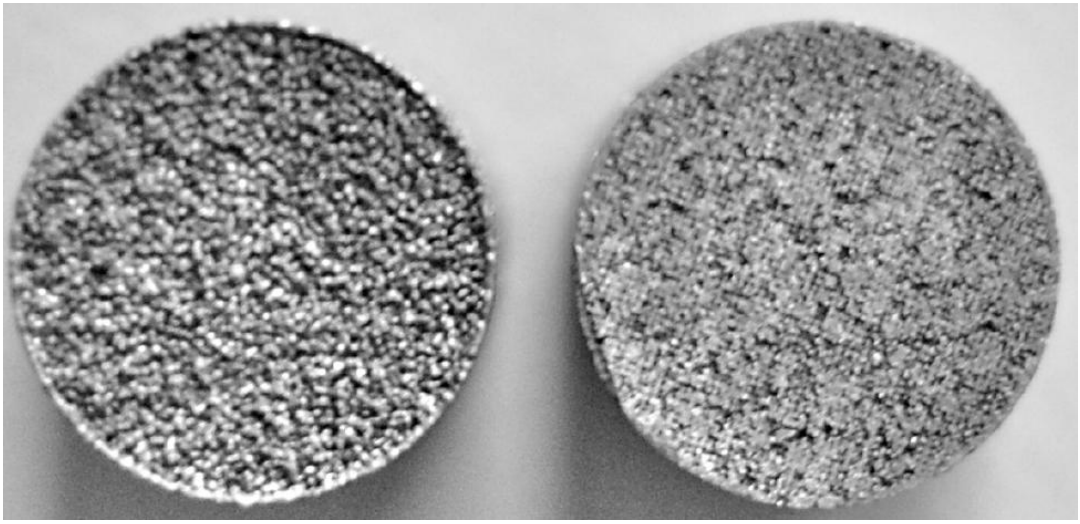

Figure 4-20 Top unprocessed face (left) and bottom (wire-cut) face. Wire cutting, if not done properly, clogs the voids

Due to the very large pores in 700μm samples, they were not considered for further analysis and further measurements and tests were focused on the following four porous structures;

1. 300μm random unit cell size
2. 300μm regular unit cell size
3. 500μm random unit cell size
4. 500μm regular unit cell size

These are shown below at the actual size and magnified. There is also a picture of a typical copper sintered wick for comparison purposes.

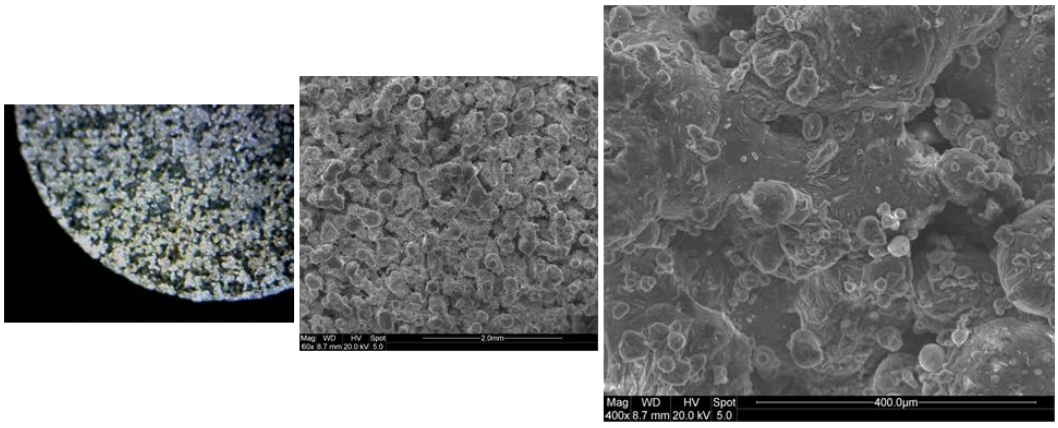

Figure 4- 21 300micron random SLM porous structure. Actual size, 60X and 400X magnified

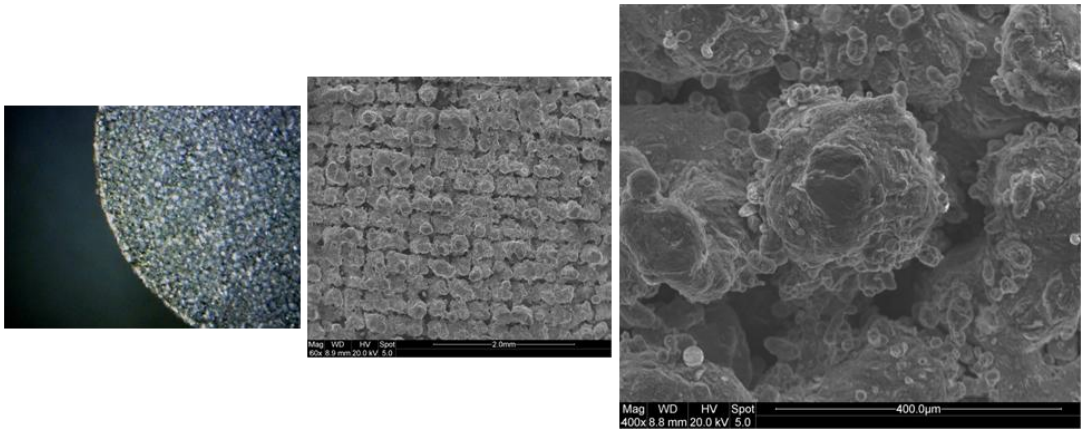

Figure 4- 22 300micron regular SLM porous structure. Actual size, 60X and 400X magnified

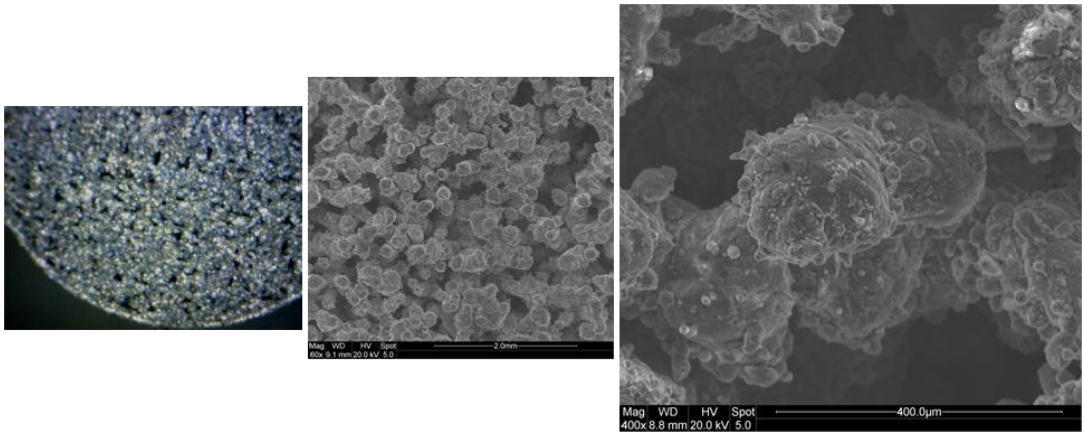

Figure 4- 23 500micron random SLM porous structure. Actual size, 60X and 400X magnified

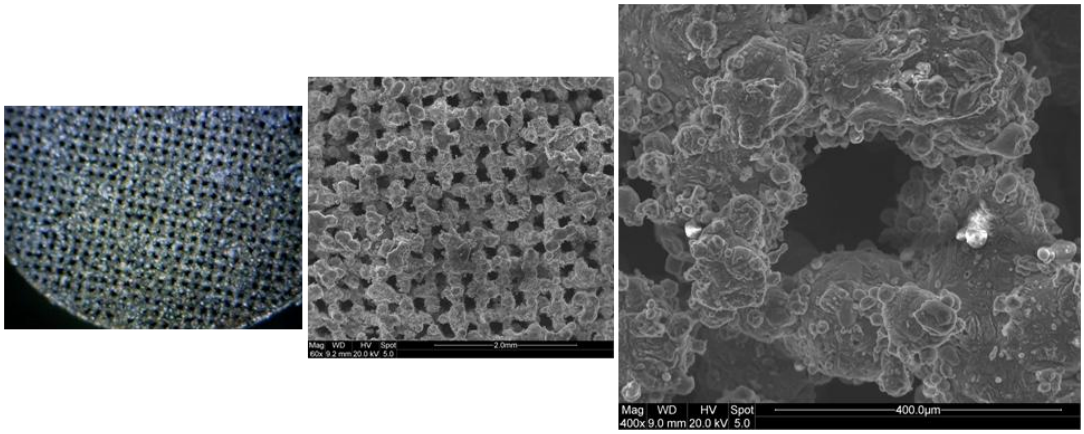

Figure 4- 24 500micron regular SLM porous structure. Actual size, 60X and 400X magnified

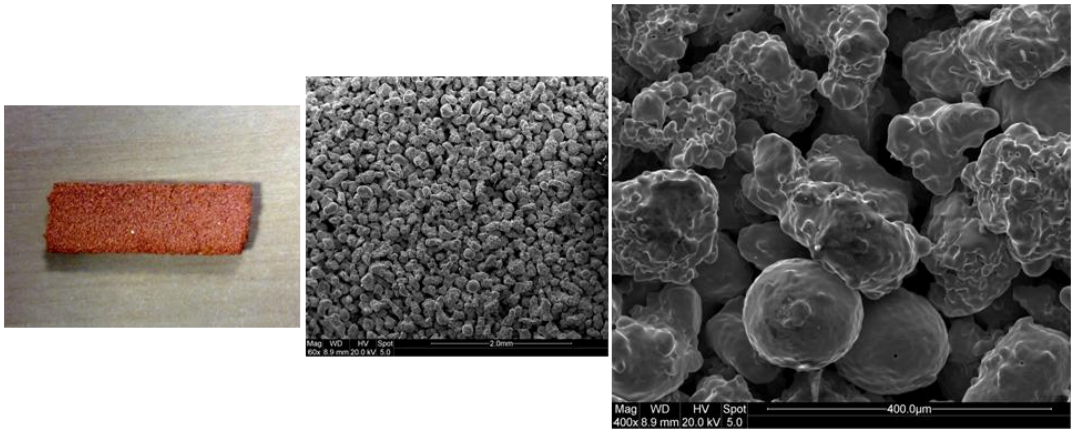

Figure 4- 25 Typical HP sintered copper structure. Actual size, 60X and 400X magnified

The next step was to determine which one of these four SLM porous structures had the most suitable combination of permeability, porosity and pore radii to be used for producing the wick structure of the SLM HPs. Following sections explain how these parameters were measured for several samples of each one of these four structures.

4-2-1-2) Permeability

Permeability is the capacity of a porous medium to transmit fluids. It is related to measurable properties of the pore geometry such as porosity, pore size distribution, and internal surface area.

Measuring permeability practically is easy as well. By pumping a fluid through the porous sample and measuring flow rate and pressure drop along the sample and the viscosity of the fluid, Darcy's law can be used to calculate the bulk permeability;

$$V = \frac{Q}{A} = \frac{K}{\mu}\left(\frac{dh}{dL}\right) \quad \text{(Eq. 4-1)}$$

Or for our purpose for sufficiently slow, unidirectional, steady flow (Dullien, 1991);

$$V = \frac{Q}{A} = \frac{K}{\mu}\left(\frac{\Delta P}{l}\right) \quad \text{(Eq. 4-2)}$$

Where;

V : Fluid velocity, m/s

Q : Fluid volume flow rate, m^3/s

A : Cross sectional area of the porous sample, m^2

K : Bulk permeability, m^2

l : Porous sample length, m

ΔP : Hydrostatic pressure drop of the liquid along the length, l, of the sample, Pa

μ : Fluid dynamic viscosity, Pa.s (kg/m.s)

A test rig was designed and fabricated in order to measure the permeability of the four candidate SLM porous structures. It is shown in figure 4-26;

Figure 4- 26 Permeability measurement test rig

The samples shown in figure 4-19 and 4-20 are inserted into the plastic hose which is connected by a valve to the bottom of a large water-filled glass tube.

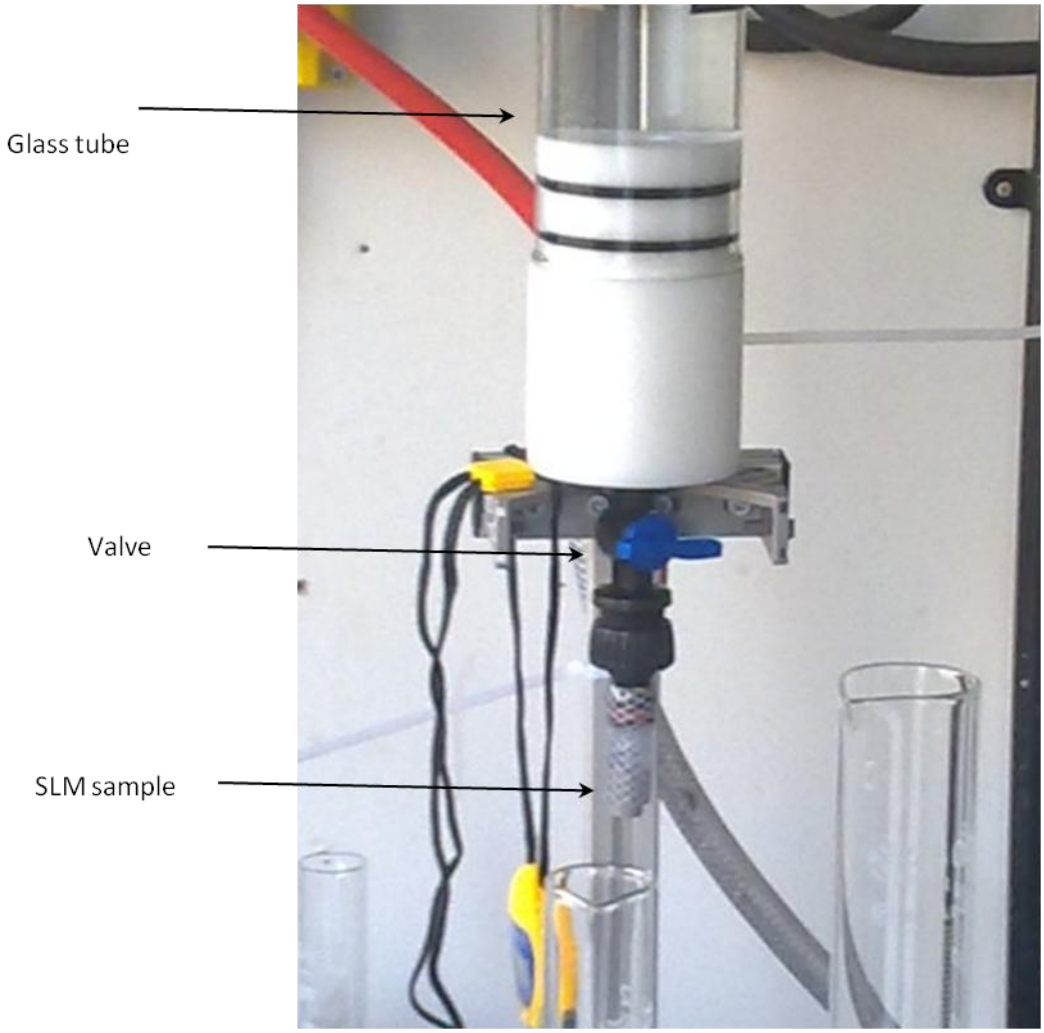

Figure 4- 27 Permeability measurement test rig- Sample close up

Once the valve opens the water flows through the sample. At the same time the tap water is let to flow into the glass tube from the top end and its flow is adjusted to keep the water level in the tube constant. This means a constant back pressure. By measuring the flow rate through the sample and knowing the pressure on both sides of the sample, cross sectional area of the sample and its length and assuming a unidirectional and steady flow, Darcy's law is used to calculate the bulk permeability. For our samples, permeability of the samples was measured using this test rig. Where;

Porous samples diameter = 13 mm

Porous samples length = 20 mm

So A = Cross sectional area of the porous sample = 1.327×10^{-4} m^2

μ = 1.307 x 10-3 Pa.s, Dynamic viscosity of water at 10°C (temperature of the water when the tests were being done)

For the first sample which was a 500 micron, random SLM porous structure, the height of the water column above the sample was kept constant at 602mm so; (considering that the pressure at the bottom end of the sample or the outlet is atmosphere pressure, the pressure difference between both end of the sample is equal to the weight of the water column above the sample)

$$\Delta P = \varrho g h \qquad \text{(Eq. 4-3)}$$

where;

ϱ : Liquid density, Kg/m^3

g : Acceleration due to gravity, m/s^2

h : Height of the water column above the sample, m

Therefore;

$\Delta P = 1000 * 9.81 * 0.602 = 5905.62$ Pa, $(Kg/m.s^2)$

The water flow rate through the sample was 84 ml at 25 seconds, therefore,

Q = 0.084/1000/25 = 3.36 X 10-6 m^3/s

And permeability K according to formula 4-2 would be;

$$K = \frac{Q.\mu.l}{A.\Delta P} = \frac{3.36 \times 10^{-6} \times 1.307 \times 10^{-3} \times 0.02}{1.327 \times 10^{-4} \times 5905.62} = 1.12 \times 10^{-10}\ m^2$$

For each of the four candidate porous structures several samples were built and their permeability was measured as per table 4-3;

Table 4- 3 Measured permeability of the SLM produced porous samples

Sample	Description	Permeability, m^2	Sample	Description	permeability
1	500µm, Random	1.12 x 10^{-10}	11	300µm, Regular	2.22 x 10^{-13}
2	500µm, Random	1.47 x 10^{-10}	12	300µm, Regular	3.31x 10^{-13}
3	500µm, Random	2.06 x 10^{-10}	13	300µm, Regular	3.23 x 10^{-13}
4	500µm, Random	1.93 x 10^{-10}	14	300µm, Regular	2.70 x 10^{-13}
5	500µm, Random	1.53 x 10^{-10}	15	300µm, Random	2.95 x 10^{-13}
6	500µm, Regular	2.74 x 10^{-10}	16	300µm, Random	3.80 x 10^{-13}

Table 4- 3 Measured permeability of the SLM produced porous samples					
Sample	**Description**	**Permeability, m²**	**Sample**	**Description**	**permeability**
7	500µm, Regular	$2.85x\ 10^{-10}$	17	300µm, Random	$7.80\ x\ 10^{-13}$
8	500µm, Regular	$2.86\ x\ 10^{-10}$	18	300µm, Random	$4.70\ x\ 10^{-13}$
9	500µm, Regular	$2.86\ x\ 10^{-10}$	19	300µm, Random	$2.85\ x\ 10^{-13}$
10	500µm, Regular	$2.52\ x\ 10^{-10}$	20	300µm, Random	$1.65\ x\ 10^{-13}$

In table 4-3;

- In the samples' description, the number is the size of the unit cells which are used in the SLM machine's CAD software to discretize the model. For this project, samples with unit sizes of 300, 500 and 700 microns were built. 700 micron samples failed the visual tests due to their very large pores (which do not generate much capillary force) and thus were not considered for further tests/measurements. SLM porous structures can be made as a regular or randomised structure as explained before
- In SLM machine, samples are built on a base plate and need to be cut off the base plate once they are made. These samples were cut off using wire-cut. This process was found to be tricky. In 700 micron samples due to very large pores the strength of the structure was minimal and wire-cutting was distorting the regular shape of the sample by taking large pieces off the sample. In 300 micron samples, wire-cutting blocks the very small pores by smearing the particles and this blocks the fluid flow through the sample. This may explain the larger variation between the 300 micron samples' permeability measurement results. This is more clear in figure 4-20.

Final SLM HP prototypes were produced with a 500µm regular porous structure for the reasons explained later.

4-2-1-3) Porosity

Porosity, ε, is the fraction of the bulk volume of the porous sample that is occupied by pore or void space. (Dullien, 1991). There are two types of pores inside a porous structure, interconnected and isolated. Isolated pores do not contribute to transport of matter along the porous medium. Total porosity is the porosity considering all the pores, interconnected and isolated. Effective porosity only considers the interconnected pores.

$$Total\ Porosity\ = 100\% \,.\left(1 - \frac{\rho_b}{\rho_s}\right) \qquad \text{(Eq. 4-4)}$$

Where:

ρ_b : Bulk density of the sample, Kg/m^3

ρ_s : Density of the solid material, Kg/m^3

And effective porosity,

$$Effective\ Porosity\ = 100\% . \left(\frac{V_{pores}}{V_b} \right) \quad \text{(Eq. 4-5)}$$

Where:

$$V_{pores}\ = \frac{m_l - m_a}{\rho_l} \quad \text{(Eq. 4-6)}$$

With

V_{pores} : Volume of the pores, m^3

m_a : Mass of the dry sample, Kg

m_l : Mass of the wet sample with liquid filling all the pores, Kg

ρ_l : Density of the liquid, Kg/m^3

V_b : Bulk volume of the sample, m^3

There are different methods to measure porosity. The method used in this project is imbibition method. In this method a sample is immersed in a preferentially wetting fluid under vacuum for a sufficiently long time to let the fluid to imbibe into all the pores. The sample is weighed before and after imbibition. Using these two weights, coupled with the density of the liquid the pores volume is calculated. By knowing the sample's bulk volume and pores volume the porosity can then be directly calculated.

The samples were kept inside oven at 125ºC for several hours to make sure that they were completely dry and then weighed. Then each sample was immersed in water inside a vacuum chamber for 5 minutes and was weighed again.

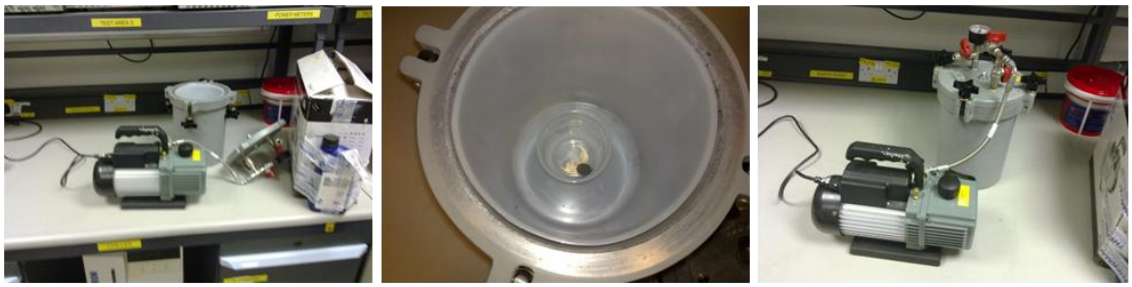

Vaccuum pump/chamber | SLM porous sample inside water in the vaccum chamber | Vaccum chamber/pump- in operating

Figure 4- 28 Porosity measurement process

The porosity measurement results for several samples of each one of the four SLM porous structure candidates are shown below;

Table 4- 4 Measured porosity of the SLM produced porous samples

Sample	Description	Bulk Volume, V_b, m^3	Dry Weight, m_a, g	Wet Weight, m_l, g	Liquid density, Kg/m^3 (Water @22°C)	V_{pores}, Volume of the pores, m^3	Effective Porosity, %
1	500µm, Random	2.65 x 10^{-6}	3.44	4.81	997.78	1.37305E-06	51.8
2	500µm, Random	2.65 x 10^{-6}	3.51	4.83	997.78	1.32294E-06	49.9
3	500µm, Random	2.65 x 10^{-6}	3.43	4.79	997.78	1.36303E-06	51.4
4	500µm, Random	2.65 x 10^{-6}	3.47	4.80	997.78	1.33296E-06	50.3
5	500µm, Random	2.65 x 10^{-6}	3.40	4.77	997.78	1.37305E-06	51.8
6	500µm, Regular	2.65 x 10^{-6}	3.08	4.61	997.78	1.5334E-06	57.9
7	500µm, Regular	2.65 x 10^{-6}	3.10	4.62	997.78	1.52338E-06	57.5
8	500µm, Regular	2.65 x 10^{-6}	2.99	4.53	997.78	1.54343E-06	58.2
9	500µm, Regular	2.65 x 10^{-6}	3.09	4.59	997.78	1.50334E-06	56.7
10	500µm, Regular	2.65 x 10^{-6}	3.08	4.69	997.78	1.61358E-06	60.9
11	300µm,	2.65 x 10^{-6}	6.11	6.58	997.78	4.71046E-07	17.8

Table 4- 4 Measured porosity of the SLM produced porous samples							
Sample	**Description**	**Bulk Volume, V_b, m^3**	**Dry Weight, m_a, g**	**Wet Weight, m_l, g**	**Liquid density, Kg/m^3 (Water @22°C)**	**V_{pores}, Volume of the pores, m^3**	**Effective Porosity, %**
	Regular						
12	300µm, Regular	2.65 x 10^{-6}	5.99	6.48	997.78	4.9109E-07	18.5
13	300µm, Regular	2.65 x 10^{-6}	6.19	6.60	997.78	4.10912E-07	15.5
14	300µm, Regular	2.65 x 10^{-6}	6.15	6.58	997.78	4.30957E-07	16.3
15	300µm, Random	2.65 x 10^{-6}	5.72	6.32	997.78	6.01335E-07	22.7
16	300µm, Random	2.65 x 10^{-6}	5.87	6.42	997.78	5.51224E-07	20.8
17	300µm, Random	2.65 x 10^{-6}	5.84	6.43	997.78	5.91313E-07	22.3
18	300µm, Random	2.65 x 10^{-6}	5.90	6.44	997.78	5.41201E-07	20.4
19	300µm, Random	2.65 x 10^{-6}	5.91	6.41	997.78	5.01112E-07	18.9
20	300µm, Random	2.65 x 10^{-6}	5.73	6.31	997.78	5.8129E-07	21.9

Because SLM porous structures are generated from a CAD model, porosity can also be calculated theoretically. Following pictures depicts a 500microns unit cell size porous geometry as it is made in a SLM machine (strut diameter of 125 microns).

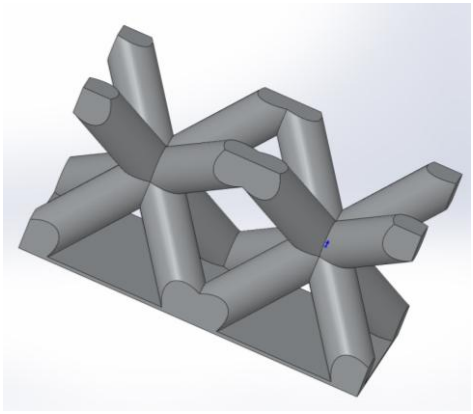

Figure 4- 29 500microns unit cell size regular porous structure with 130 microns strut diameter

The picture shows two adjacent units with the inscribed octahedral structures. This obviously is repeated in every direction to fill the entire geometry where the porous structure is meant to be. Using the CAD software, the exact empty space of this geometry can be calculated and in this case it is 64% empty space or porosity. According to the previous table, in actual test this value has been measured from 56.7% to 60.9% for different samples. In practice, the struts are not as neat as in the CAD model. Nearby powder particles are pulled into the melt pool which causes variation of the strut diameter along its length. Moreover when the loose powder is shaken out of the object at the end of the process, some of it remains trapped in the pores and clog them thus lower porosity in actual test results.

The CAD model for 300 microns regular porous structure suggests a porosity of 24% while the actual test results measure between 15.5% to 18.5% for different samples. As the pores are smaller in this case, more of them are expected to be clogged by the loose powder thus the bigger difference between the theoretical and actual porosity. This method can not be used for random structures for obvious reasons.

4-2-1-4) Pore radius

Detailed description of the pore space is impossible especially for random porous structures. One way to define a pore size is by defining the pore radius at a point within the pore space of a porous medium as the diameter of the largest sphere that contains this point while still remaining entirely within the pore space. Thus by attaching a pore radius to each point of the pore space, a pore size distribution may be defined by determining what fraction of the total pore volume has a pore radius in a certain range. (Bear, 2013)

Again using a CAD model this pore radius can be calculated theoretically. Following picture shows a two adjacent 500microns regular SLM unit cells and an imaginary sphere that fills a pore.

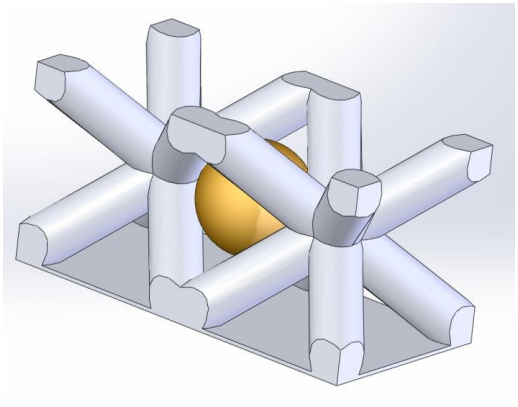

Figure 4- 30 500microns regular SLM porous structure with an imaginary sphere filling a pore.

Therefore, theoretically the pore radius of this structure is the radius of this sphere or around 140microns. In regular structures, there is only one pore radius everywhere across the geometry (ignoring the pores clogged by the loose powder) but in random SLM porous structures there are numerous different pore radiuses due to the random movement of the octahedral structure centre point inside the unit cell. With the same definition, the CAD model for a 300 microns regular SLM porous structure with 130 microns strut diameter suggest a pore radius of around 60 microns.

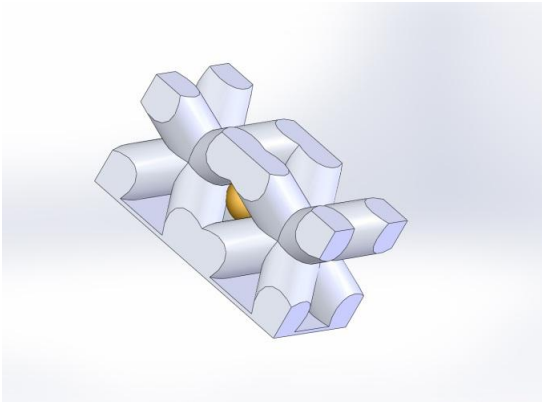

Figure 4- 31 300 micron regular SLM porous structure with an imaginary sphere filling a pore

The results of the measurements on the porosity, permeability and pore radii of four different SLM structures are summarized below and compared against an existing sintered porous copper wick structure.

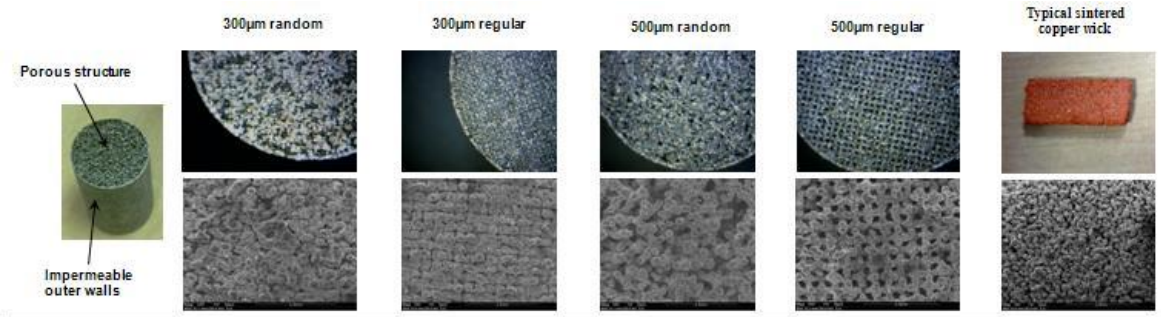

Porosity %	20	17	50	58	40-52
Permeability m^2	10^{-13}	10^{-13}	10^{-10}	10^{-10}	10^{-11}-10^{-12}
Pore radii µm		60		140	23-60

Figure 4- 32 Properties of different SLM porous structures compared against sintered copper wick structure properties

4-2-1-5) Selected SLM porous structure for the use to build the SLM HPs sinter-style wick

If the SLM is to be used for producing heat pipes, designers have to be able to interpret SLM language and phrases to meaningful terms in heat pipe language. For instance a heat pipe sintered wick is defined by its three main characteristics, porosity, permeability and pore size while for producing a sinter-style structure by SLM, assuming that the unit cell filling structure (in this case octahedral) and laser properties are specified, the operator needs to know the unit cell size and the regular or random shape of it.

The measurements explained in three previous sections enable this interpretation for 300 and 500 micron regular and random structures. For instance according to the above measurements, now it is known that a laser power of 200W, 60ms exposure time at 30µm point distance and 0.2mm hatch distance to build regular octahedral based porous structures with 500µm unit cells results in 58% porosity, 10^{-12} m^2 water permeability and a rough pore size of 140µm. Rough estimations can be made for other values by interpolating/extrapolating of these values.

500 micron regular structure was selected for building the wick structure of the SLM HP prototypes. The reasons behind this selection were as follows;

a) Because this is the first time that heat pipes are produced by SLM, regular structure helps the characterization and theoretical designing process by reducing the number of variables (in this case the variance in the pore size and effective pore radii). Although there are experimental methods for measuring the effective pore radii of a random porous structure e.g. mercury intrusion porosimetry, firstly, there was no access to this

resource during this project and secondly, interpolate or extrapolating of these measurements are tricky while for a regular structure, the pore size can roughly be measured theoretically as explained in section 4-2-1-4.

b) 500µm structures seem to possess a closer combination of porosity, permeability and pore size to those of an existing copper sintered wick. Also, measurement of the water static rise height of the samples under their capillary force influence showed a minimum rise height of 60mm for these samples that was sufficient for the intended SLM heat pipes. Porosity of the 300µm structures is too low.

4-3) Production of the initial SLM HP prototypes

Available axially grooved heat pipes (AGHPs) are produced with different external profiles. Because an H cross section extruded AGHP (Figure 4-2) was available for this project to be used as a benchmark, the ultimate goal was to produce the SLM heat pipes with the same external profile to facilitate a direct comparison. For this reason the very first trials on the SLM machine was to produce a similar profile but then the initial SLM HP prototypes were produced with a round cross section (Figure 4-1) as it was identified to be easier for initial tests and to prove the feasibility of the concept. This process is explained below.

At the beginning of the project various designs were proposed for the to-be-built SLM HPs. In order to check the feasibility of the proposed designs and specifically axial grooved heat pipe (AGHP), a preliminary 20 mm section of heat pipe was built from titanium as titanium powder was loaded into the machine funnel at the time. It is shown in Figure 4-32.

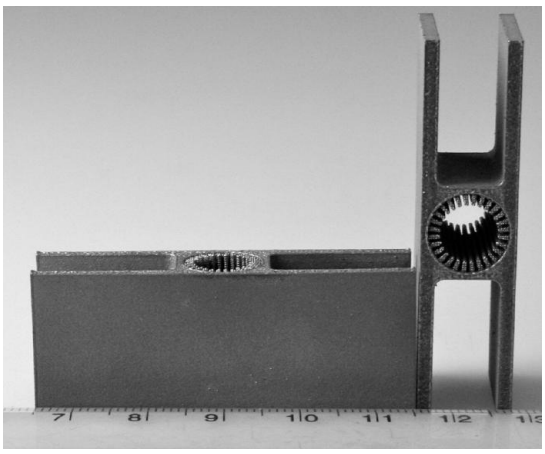

Figure 4- 33 First axially grooved heat pipe made by SLM from titanium

Then the same geometry was produced from AL6061 and with 60mm length, Figure 4-34;

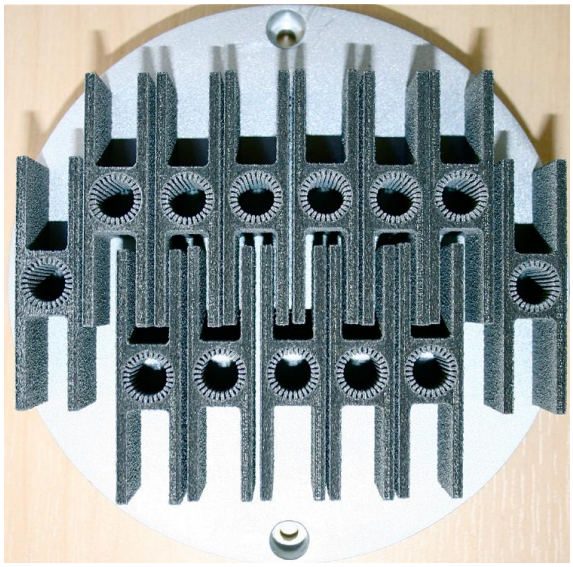

Figure 4- 34 thirteen axially grooved AL6061 heat pipes on a substrate plate made by SLM

As explained before, Al6061 was being used in SLM for the first time and its required build parameters (laser beam power and movement specs) were unknown and this lead to the samples to have a very porous look and badly formed fins. On the other hand Alsi12 aluminium alloy is a relatively established material for the use in SLM process so from this point on all the other samples were made from AlSi12.

4-3-1) Proof of the SLM flexibility and ability to produce complicated wick structures

SLM is introduced in this project as a novel HP manufacturing method. One of the main advantages of this method over the conventional methods is its incredible flexibility to produce very complex wick structures. Conventional sintered wick structures are limited in terms of their form and shape to the extent that sintering process allows while a sinter-style wick structure generated by SLM can literally have any form or shape at any region of a heat pipes. An SLM sinter-style heat pipe can have graded (various pore sizes radially) wick with different thickness along its length.

Several samples were produced to prove the ability of the SLM in manufacturing complicated wick structures. In total three different wick structures were manufactured, axial grooved wick with porous fins, annular wick and arterial wick (small ducts fabricated into an annular porous wick to facilitate the return of the working fluid condensate). The first one is shown in figure 4-33 and the other two types in figures 4-35 to 4-37 below.

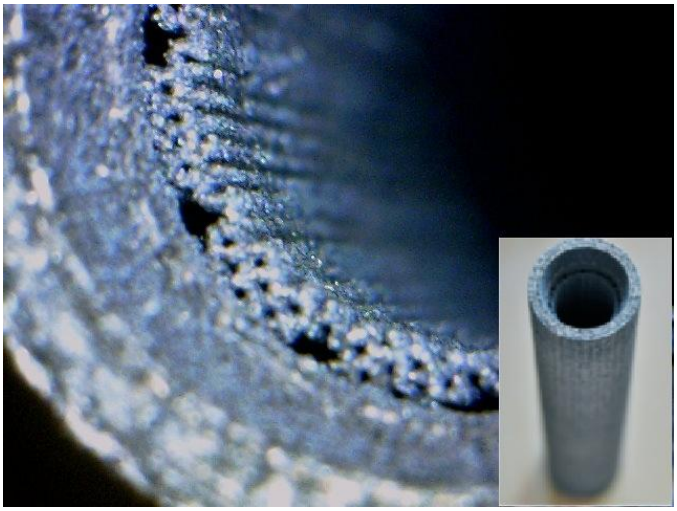

Figure 4- 35 Arterial wick SLM heat pipe made from AlSi12

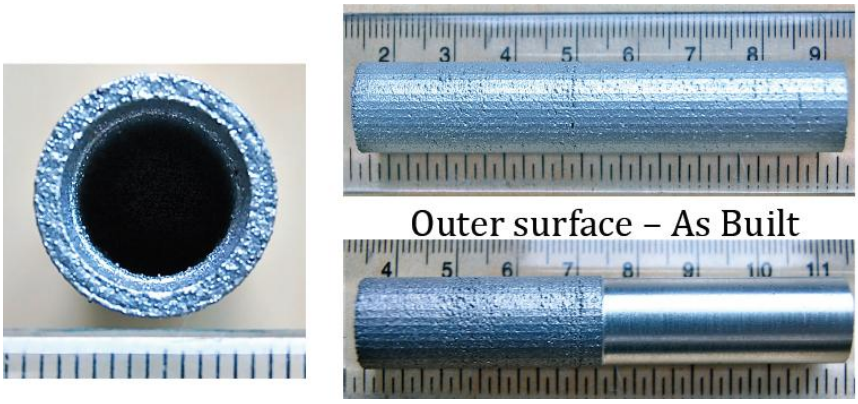

Figure 4- 36 Annular wick SLM heat pipe from AlSi12. Right top shows the outer surface of the pipe as built and right bottom after getting machined partially

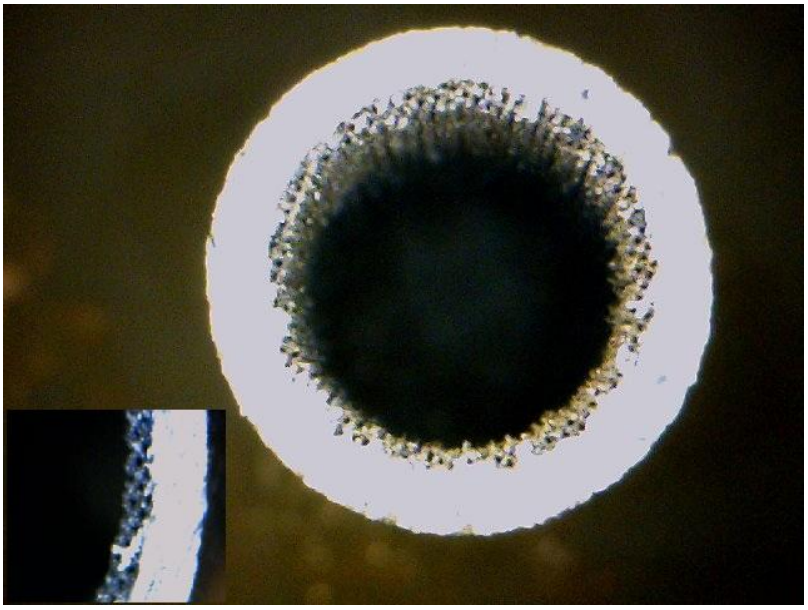

Figure 4- 37 A cross sectional cut of the annular wick SLM heat pipe sample. Solid walls and porous wick (magnified in the inset) can be seen

One end of these heat pipes is already sealed and the whole heat pipe including the bottom cap, solid walls and porous wick is built in a single process. Obviously the top cap and fill tube can also be made as integrated parts of the heat pipe.

The pipe shown in figure 4-36 was then used for the concept proof and SLM HP feasibility study. This is one of the four main objectives of the project and it is explained in the next chapter along with its experimental results.

4-4) Build parameters optimization – Built samples characterization

After testing the initial SLM HP prototypes and prove the feasibility of the concept (results presented in the next chapter) the next step was to optimize the specified parameters' values and to get a better understanding of the properties of the SLM produced heat pipes. This included the density of the solid structures, hardness, mechanical yield strength, morphology of the SLM solid structures, etc.

4-4-1) Density of the SLM solid structures

Heat pipe walls ideally should be solid or hundred percent dense for the sake of the rigidity of the heat pipe and to avoid any possible leakage through the walls. In SLM process, solid structures are generated by melting and fusing the powders together that intrinsically, is associated with some remaining pores inside the structure. This is shown in figure 4-38.

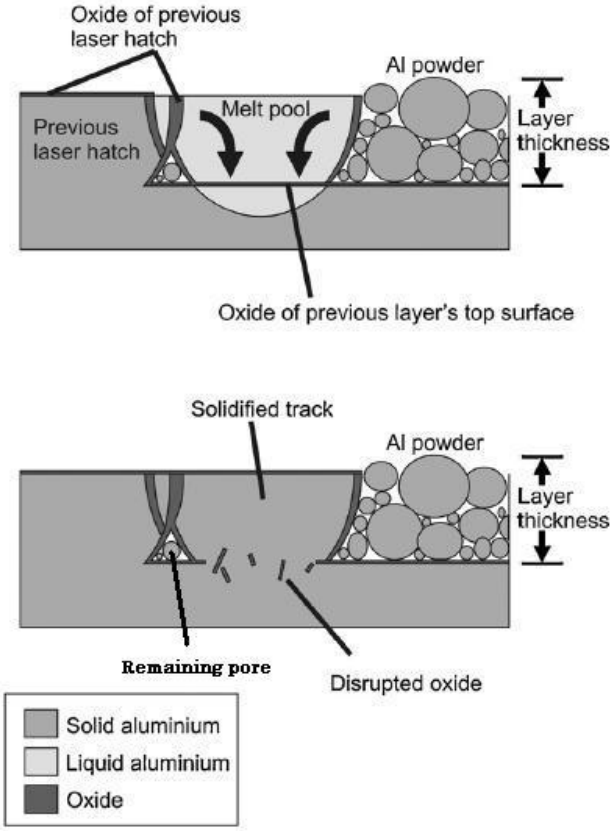

Figure 4- 38 Remaining pores and oxide layers in an aluminium SLM built structure (Louvis, Fox, et al., 2011)

The percentage of the pores directly relates to the laser parameters. Higher laser power and exposure time and smaller point and hatch distances result in powders having more time to melt in a bigger melt pool and less number of the remaining pores.

Assuming that the surface and volume porosity are equal, the density of the produced solid structures was measured by skinning the rough surface of the samples and measuring the ratio of the surface area of the pore to the total area, Figure 4-39. This value was from 86% to about 88% for initial ALSi12 samples.

The main worry at this point was that the remaining pores might lead to a leakage through the heat pipe wall. As explained in the next chapter initial SLM HP prototypes (with a round cross section and wall density of 86% to 88%) actually passed the leak test. However following samples that were produced with the same SLM machine parameters but with H-cross section almost all failed the leak test.

It is believed that the failure of those samples were due to the build-up direction and strategy inside the SLM machine (that could have led to excess remaining stress inside the parts and creating micro-cracks in the wall at the time of cutting them off the substrate) and not the remaining pores in the walls. However improving the density of the SLM solid structures was

identified as a major goal for further studies. During the project and before producing the final prototypes, further optimization was conducted on the laser parameters which led to an increase in the density of the final prototypes solid structures to around 98%.

Figure 4- 39 Remaining pores in the initial SLM HP prototypes

4-4-2) Hardness of the SLM solid structures

Hardness of the SLM solid structures was measured on four pieces with two different densities. Explanation and results are given in Appendix A. SLM AlSi12 structures show a higher hardness than the conventional Al6063 AGHPs.

4-4-3) Yield strength/yield point of the SLM solid structures

Yield strength and yield point of the SLM samples was measured on different samples and the results are given in Appendix A. SLM structures proved to be very brittle but with a yield point high enough for the purpose.

4-5) Production of the final SLM HP prototypes and extruded AGHPs benchmark samples

Once the initial experiments were conducted using acetone and the SLM HP concept was proved to be feasible and after some parametric studies on the SLM produced structures as explained above, a second set of SLM HP samples were produced with an H cross section identical to the available extruded AGHPs to enable a direct performance comparison.

As stated before, these samples all failed the leak test. The failure was believed to be more due to micro-cracks occurred during their building inside the SLM machine and cutting off the substrate rather than the remaining pores in their structure. In SLM process, the build direction

and strategy are critical parameters. This batch of SLM HPs were built vertically (as in the initial round shape samples) but with a thicker base and some supports to avoid deformation of the external fins during the build. It is believed that these extra supports resulted in concentration of excess heat and stress in their contact point to the HP which caused micro cracks when the supports were being cut at the end of the process.

This experience revealed another challenge in producing SLM HPs which we call "the build strategy".

Therefore a subsequent batch of H cross section HPs were produced using improved build parameters (that led to an increase in density to around 98%) and a different build strategy to avoid extra stress and micro cracks (Figure 4-40).

Figure 4- 40 Final SLM HP prototypes

These samples were used to conduct the detailed characterizing experiments that are explained in the next chapter. From the available extruded AGHP profile (which was identical to these SLM HPs) some samples were also provided with the same length and processed to be converted into functional heat pipes and were tested alongside these prototypes for a direct comparison. Again the results are presented in the next chapter.

4-6) Further built samples characterization – preparations for the final experiments

Once the final prototypes were produced and while they were being prepared for the final experiments, further characterization tests and measurements were conducted as well as developing a thermal test rig for testing the final prototypes as described below.

4-6-1) Heat pipe tilting/thermal performance measurement test rig

Another test rig was fabricated to perform the thermal tests on the H shape heat pipe samples. After the fill tube welding and filling/venting process (explained in the next chapter) and during the thermal tests two aluminium blocks are attached to the two ends of the pipe. In one block heater cartridge(s) is inserted to apply heat to one end of the pipe and chilled water flows though the other block to cool down that end and take the heat away from the pipe. These two blocks are called evaporator and condenser block respectively.

The rig lets heat pipe to be oriented in any required angle and its performance (temperature gradient versus power and all other relevant measurements) to be measured in different orientations.

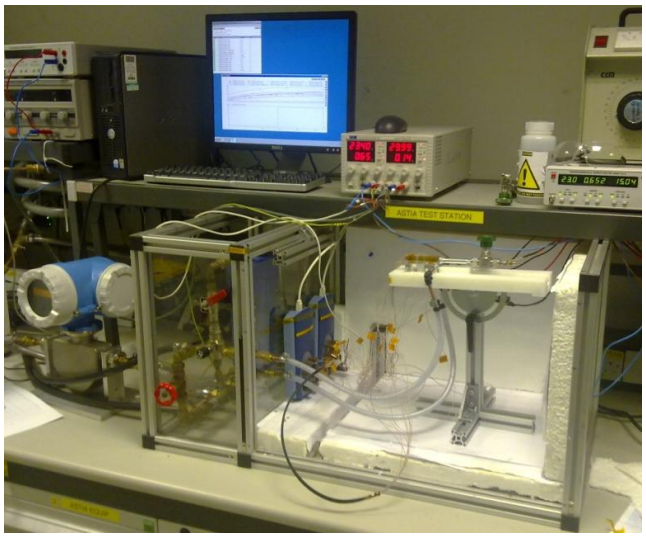

Figure 4- 41 SLM HPs thermal test rig

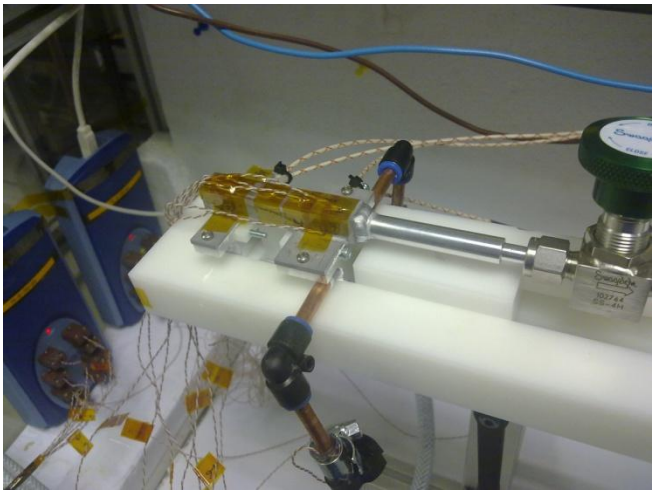

Figure 4- 42 machined SLM HP attached to the evaporator and condenser blocks – during the thermal test

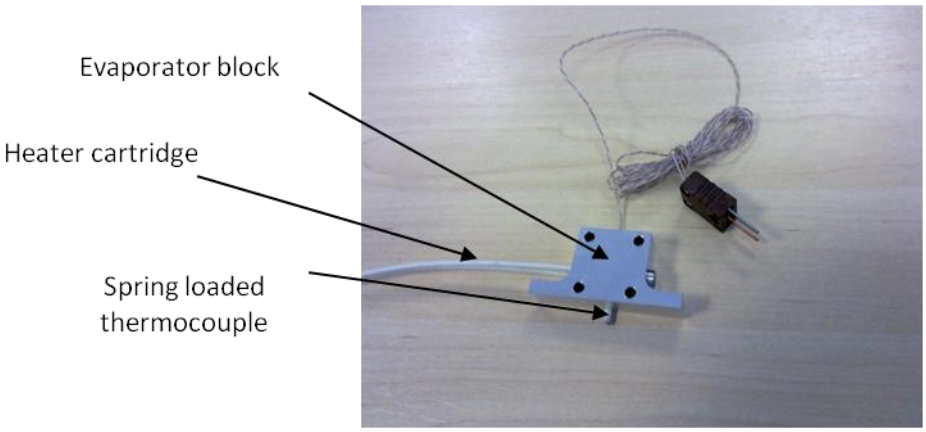

Figure 4- 43 Evaporator block with heater cartridge and spring loaded thermocouple

4-6-2) Welding fixture

A special welding jig was designed and manufactured for welding fill tubes to the machined SLM heat pipes and is described in Appendix A.

4-6-3) Shock and vibration fixtures and experiments

Shock and vibration testing are used to simulate the extreme conditions that a product may face during operation and determine the ruggedness of a product. By the experiment conducted in this project it was proved that SLM heat pipes have enough rigidity in vibrating environments encountered in most of applications although testing to the high space standard requirements was not possible. Details are given in Appendix A.

4-6-4) SEM (Scanning Electron Microscopy) of the SLM structures

The scanning electron microscope (SEM) functions by projecting a beam of electrons through magnetic focusing lenses at a specimen and recording secondary electrons excited by the primary beam. The amount of secondary electron emission portrays the topography of the specimen because more secondary electrons are emitted from high points than from low points (Weinbrandt & Fatt, 1969). Depending on the detector mounted on the SEM, a variety of other reflected energies from electron-solid interaction, and consequently other characteristics, can be analysed. Secondary electrons are detected for imaging purposes, backscattered electrons for contrasts in composition, diffracted backscattered electrons for crystalline structure and orientation and photons or X-ray for chemical composition analysis. In addition to these, some of the energy is reflected as visible light or heat.

Throughout this project SEM was used at different stages. The first instance was to have a closer look at the SLM porous structures as shown in figures 4-21 to 4-25 earlier in this chapter. Then it was used to study the surface of the SLM HP. The final prototypes are believed to have a density of up to 98% as stated before but SEM images of the SLM heat pipe solid walls did not reveal any pores in them as seen in Figure 4-44.

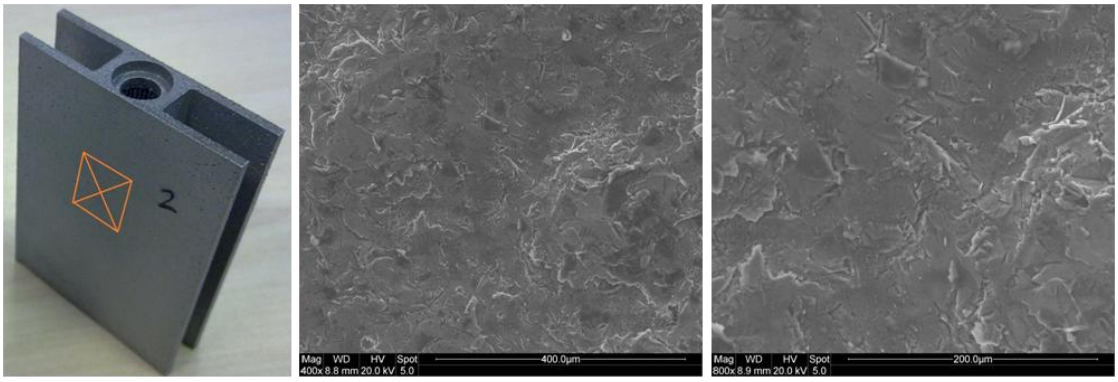

SLM heat pipe sample used for analysis of the SLM solid structures' density using SEM. Scanned area indicated

Solid surface under microscope – 400X magnified – no pore can be seen

Solid surface under microscope – 800X magnified – no pore can be seen

Figure 4- 44 Study of the SLM HP solid wall by scanning electron microscope

SEM was also used to analyze the elemental composition of the SLM heat pipe samples made from AlSi12. Composition analysis was done on the same indicated area as per Figure 4-44.

The surface was first polished and then analyzed. The polish surface, under the SEM looks like below;

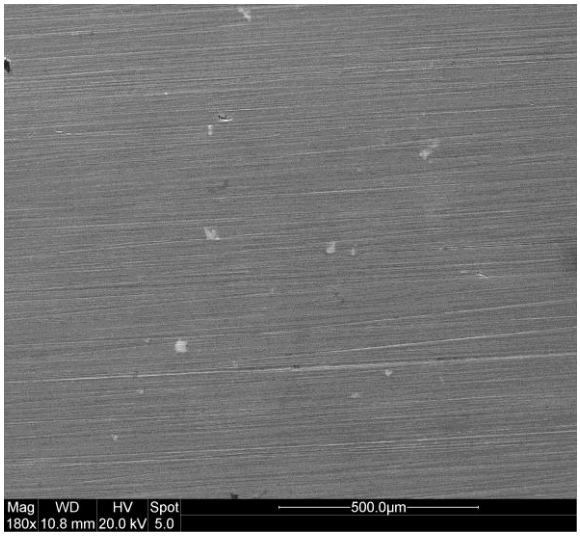

Figure 4- 45 SLM HP polished solid surface under SEM

Apart from oxygen which was expected to be seen on the surface due to oxidization, some white spots were also observed which in composition analysis were proved to be titanium. Titanium traces in the samples are believed to be due to the residual titanium powder in the SLM lab environment and in the SLM machine's funnel from previous builds. A closer picture of these white spots and the composition analysis results on three points on the surface away from the white spots and two points right on the white spots are shown below;

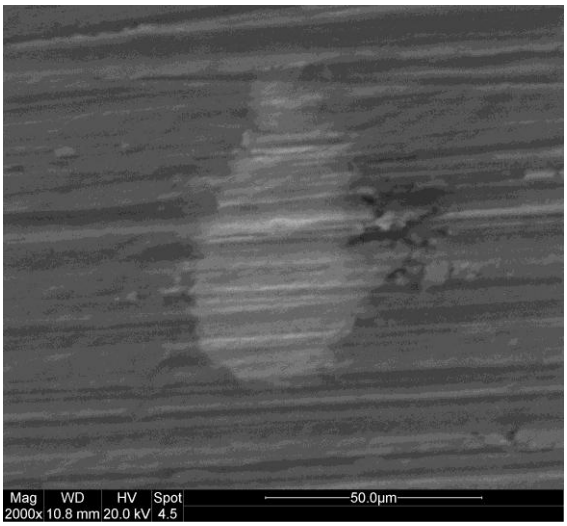

Figure 4- 46 2000X magnified picture of one of the white spots on the surface of the SLM HP

Table 4- 5 Element analysis results - base a, b and c are three random points on the surface away from the white spots. and two analysis of the actual white particles which are identified to be titanium

Processing option : All elements analysed (Normalised)

Spectrum	In stats.	O	Al	Si	Ti	Total
Al Si 12 Base a	Yes	5.04	81.65	13.32		100.00
Al Si 12 Base b	Yes	3.19	83.58	12.35	0.89	100.00
Al Si 12 White Paricle a	Yes	10.80	11.23	2.51	75.47	100.00
Al Si 12 Base c	Yes	3.87	83.18	12.94		100.00
Al Si 12 White Paricle b	Yes	5.94	11.81	1.85	80.40	100.00
Max.		10.80	83.58	13.32	80.40	
Min.		3.19	11.23	1.85	0.89	

All results in weight%

Composition analysis of the samples revealed another major challenge in using SLM for producing aluminium heat pipes. Aluminium ammonia heat pipes are extremely susceptible to non condensable gasses (NCGs). NCGs are generated in the pipe by reaction of the working fluid with the impurities of the heat pipe material. For this reason cleaning process and almost zero water content of the ammonia are extremely critical parameters as any water content will

react with aluminium and the resulted NCG will collect at one of the pipe and reduces its effective length over time.

Composition analysis revealed that the samples were contaminated by the tiny traces of titanium remained in the environment from previous usage of the SLM machine. These unnoticed contaminations could have disastrous consequences especially in sensitive applications.

4-6-5) Contact Angle – Wettability

Capillary pressure is the main driving force in a heat pipe that transports the condensed working liquid through the wick to the evaporator. Capillary pressure is generated by the difference between the curvature radius of the working fluid menisci inside the pores in the evaporator and condenser regions of a heat pipe. The curvature radius in turn is dictated by the contact angle between the liquid and solid surface. For the use in the theoretical calculations, the contact angle of acetone on the SLM HP samples material was measured and the results are given in Appendix A.

4-7) Development of the ammonia filling rig

One of the major activities during almost the entire project was to develop an ammonia filling rig in a specially designed ammonia laboratory in Thermacore. The rig was completed towards the very end of the project hence all the experiments were conducted using acetone. A description of this rig is given in Appendix A.

5-1) Introduction

This chapter describes the final preparation steps and experimental results of the SLM HP prototypes. Previous chapter explained the course of the actions to produce and characterize two sets of prototypes up to the point that the raw SLM HP samples were ready. This chapter picks up that discussion and illustrates how the raw samples were converted into functional heat pipes along with the testing process and the experimental results. The experiments were specifically planned to meet the following project objectives;

1. To prove that functional heat pipes, in general, can be produced by SLM

2. To prove that functional sinter-style aluminium/ammonia heat pipes can be produced by SLM and to prove that they possess the main characteristics attributed to the conventional sintered heat pipes including the ability to work at inclination angles against gravity and high surface heat flux.

The accuracy and reliability of the results are also discussed along with the validation of the numerical design tool by comparing its predictions against the actual experimental results.

To prove the first point, SLM HP samples have been tested in two "charged" and "uncharged" states at the same conditions. It is shown that when the samples are processed and charged with acetone, they transfer the heat with much lower temperature gradient exactly as expected from a heat pipe.

To meet the second objective, performance of the aluminium SLM HP samples with a sinter-style wick has been compared against identical extruded aluminium axially grooved heat pipes (AGHP). The test results illustrate that SLM samples have a consistent performance at all inclination angles with any relative position of the hot and cold medium while AGHP cease to work when the hot source is above the cold section or when they work against gravity. SLM HPs behave exactly as any other conventional sintered heat pipe.

Although the project objectives have been precisely met, the data can not be used for characterization purposes due to the limited number and the very short length of the samples.

Only two successful functional SLM HP samples were available for the experiments due to inevitable mistakes and failures at different stages. Several samples were rejected in the leak test due to the micro-cracks that supposedly, had been generated during the SLM build process due to the wrong build strategy. Nevertheless rough error margin of the results has been investigated by repeated experiments on the available samples.

Also, all the experiments have been conducted using acetone as the required ammonia filling rig was not completed until the very end of the project. The change of the working fluid does not affect the concluded results in no way since all the experiments have had a comparative nature.

A list of the instruments used during the experiments is given in Appendix B for future references.

5-2) Experiments to prove that functional heat pipes, in general, can be produced by SLM

The "initial prototypes" were converted into functional heat pipes and were tested to prove the feasibility of the SLM HP concept. SLM HP prototypes with a round cross section and an annular sinter-style wick, as shown in figure 5-1, were used for these experiments.

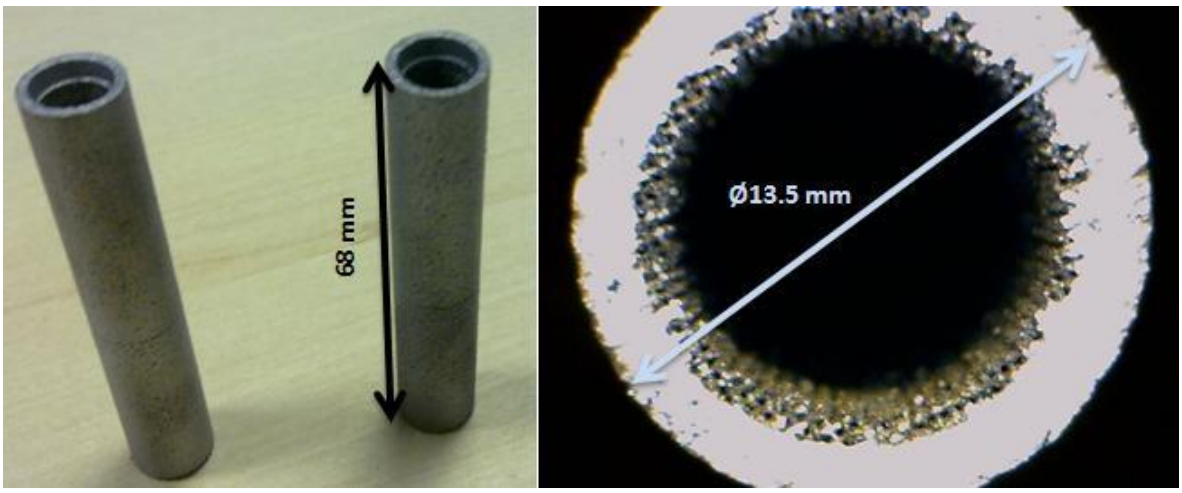

Figure 5- 1 Initial SLM heat pipes with annular sinter-style wick

5-2-1) Preparation of the initial samples and the test setup

In order to test these prototypes they had to be converted to test-able heat pipes. They had to be equipped to a so-called fill tube to be able to go through the conversion process. Fill tube allows the heat pipes to be filled with the working fluid and get sealed. Fill tube can potentially

be produced during the SLM process as an integrated part of the heat pipe although it was not possible in this project due to the restriction in the maximum working length of the SLM machine. Two sets of fill tubes were separately produced by SLM and with a conventional machining process. The former was to prove the capability of SLM to produce these but the latter was used for the rest of the process to facilitate the welding process due to its flatter surface and better tolerances. These are presented in figure 5-2.

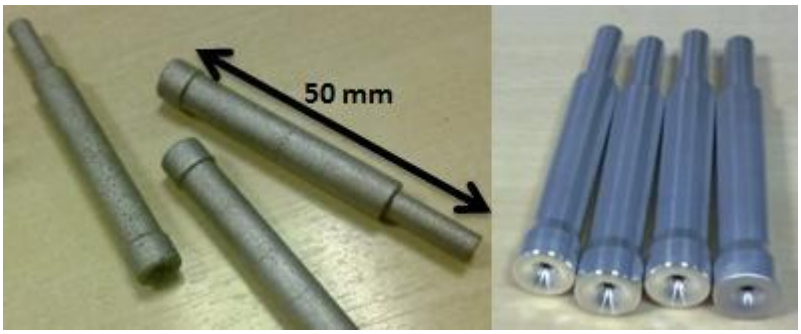

Figure 5- 2 Fill tubes produced by SLM (left) and a conventional machining method

Special shape of the fill tubes is to facilitate its welding to the heat pipe and sealing. The fill tubes were welded to the SLM HPs and the outer surfaces of the HPs were skimmed to provide a flatter surface as demonstrated in Figure 5-3. The welding process is an extremely delicate job and stimulates extremely precise tolerances for the fill tube and its housing cavity on the heat pipe. Discussing these details is out of the scope of this document.

Figure 5- 3 Fill tube welded to the SLM HP

And then the HP-fill tube assembly was equipped to a valve as shown in figure 5-4;

Figure 5- 4 SLM HP, fill tube and valve assembly

The heat pipe wall must be leak-free and also strong enough to withstand the maximum saturation vapour pressure of the working fluid at the maximum temperature that heat pipe is expected to be exposed to. For instance, if a heat pipe uses ammonia as the working fluid and the maximum temperature that it will be exposed to (operational or non-operational) is 50°C, it must be assured that the pipe does not deform at ammonia vapour saturation pressure at 50°C or 20 bar (0.8 bar for acetone).

The two welded samples were checked by a helium leak tester. In this instrument the pressure inside the tube is brought down to 10^{-9} Torr (1.333×10^{-7} Pa) and helium is blown over the outer surface. Any helium that leaks into the pipe is detected by the instrument. Only one of the two good samples passed this test and the other one failed due to the leak through the weld.

Figure 5- 5 Heat pipe sample is being tested on helium leak testing machine while is being heated by hot air gun to facilitate the extraction of any possible air trapped in the pores

The samples were also proof-pressure tested at 20bar for acetone experiments and then at 70bar in preparation for the final tests and passed the tests with no deformation. More details on this is given in Appendix A.

HP was then equipped to a circular fin structure to work as the condenser during the experiments. The test setup and temperature measurement points are presented in figures 5-6 and 5-7..

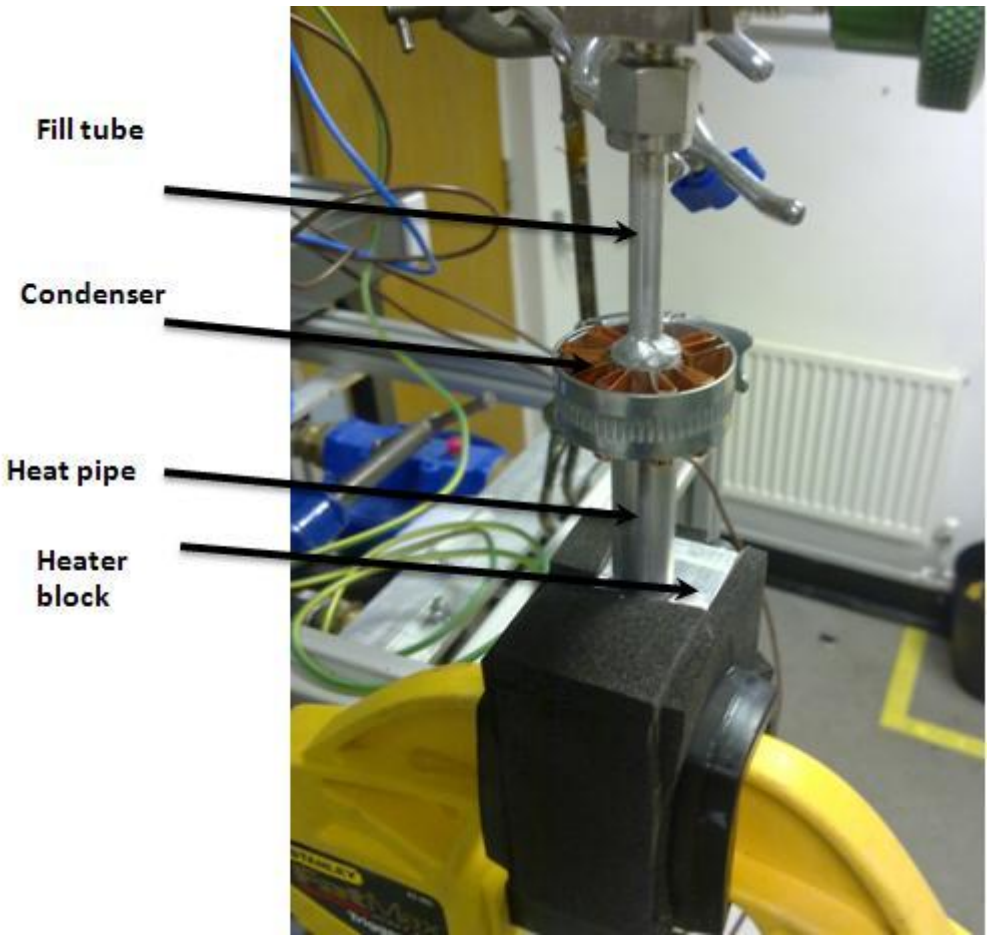

Figure 5- 6 Initial test set up

Figure 5- 7 Temperature measurement points for the initial tests

The main purpose of these experiments was to prove the feasibility of the SLM HP by demonstrating that the samples transfer the heat with a much lower temperature gradient than an identical pure conductor at the same conditions. This was met by comparing the temperature drop along the produced SLM heat pipe in two scenarios;

- When the pipe is filled (charged) and processed with acetone and works as a two phase system or a heat pipe
- When the pipe is empty (uncharged) and behaves as a pure solid thermal conductor

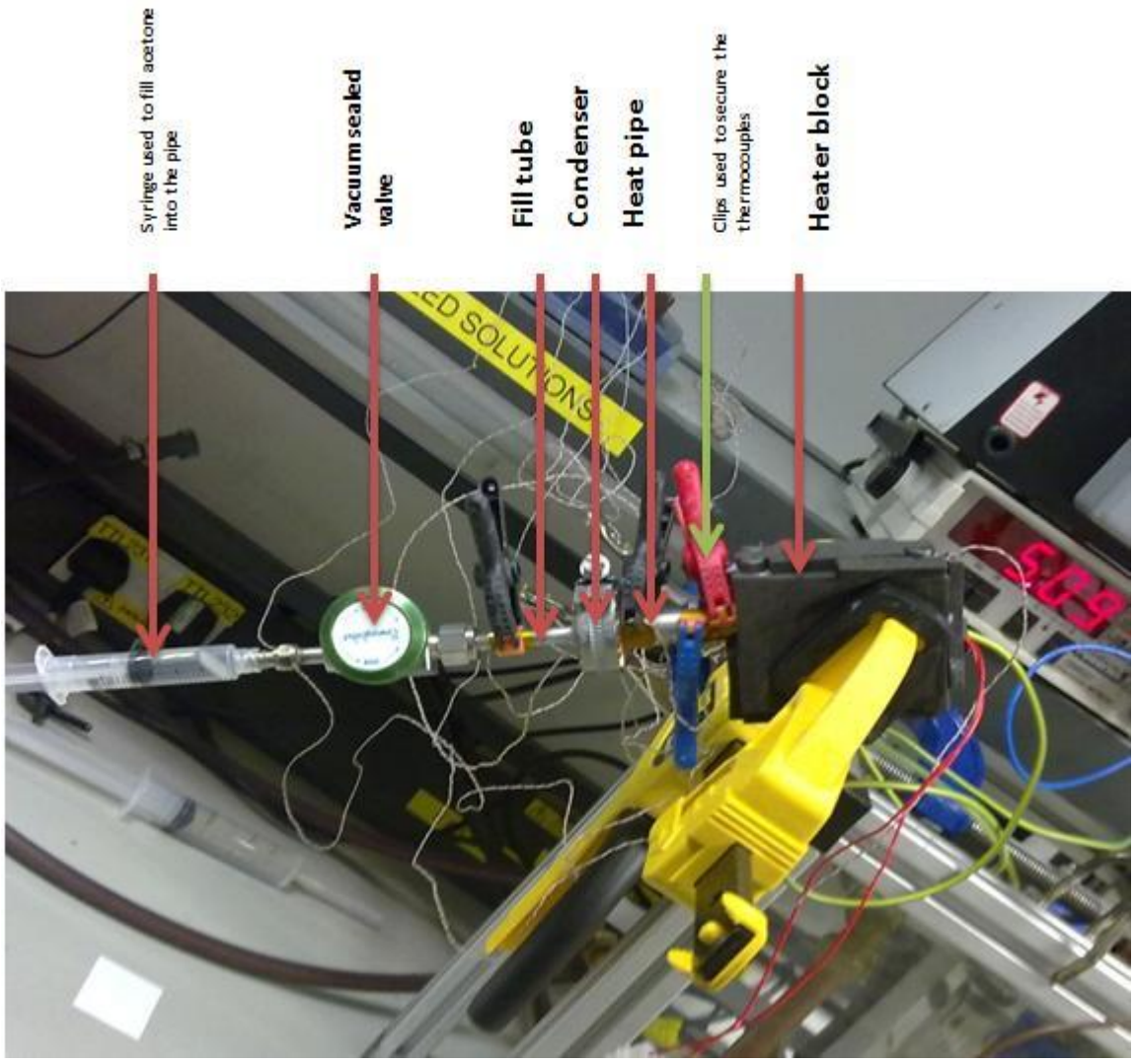

Figure 5- 8 Initial SLM HP test setup in operation

For charging the sample with acetone, the sample and the valve assembly is filled with acetone right to the top before connecting it to a syringe to minimize the amount of the air left in the system. Then the sample is heated up to above the acetone boiling temperature while the valve is shot. By quick opening of the valve acetone vapour rushes into the syringe and, on its way, pushes all the trapped air inside the pores into the syringe. By repeating this a few times all the air is extracted.

Then the sample is filled with what is theoretically calculated as the optimum fill volume. This is the volume of the pores all along the wick plus up to ten percent more. In our sample the wick

volume, considering that this sample is an annular wick sample with 500 micron regular wick and 58% porosity, is roughly 0.9 ml. So the sample was filled with around 1ml of acetone and with 5W power applied to the heater cartridge, temperatures were measured at different orientations. Then the pipe was vented (acetone was emptied and the sample with an open valve was left in the oven at 150°C for two hours to get completely dry inside out) and measurements were conducted again at the same orientations.

5-2-2) Initial test results

The test samples at this stage included;

- One functional (charged) sample
- Two un-functional (uncharged) samples

Temperature was measured at different orientations with CHARGED/UNCHARGED pipe @ 5W and the results are presented in Table 5-2. (In "orientation" column "+" sign means that pipe works with gravity or with its cold section above the hot region, and "-" denotes operation against gravity)

Table 5- 1 Initial SLM HPs test results – Comparison of the SLM HP performance in "charged" and "uncharged" states at various inclination angles and 5W

Scenario	orientation	Temp point 1 °C	Temp point 2 °C	Temp point 3 °C	Temp point 4 °C	Temp point 5 °C	Max temp difference °C (TP1 – TP5)
Acetone charged sample	+90	43.6	41.3	40.5	39.4	39.3	4.3
	+60	43.3	40.8	39.9	39.0	38.3	5.0
	+30	43.9	40.6	38.9	38.0	37.3	6.6
	-90	45.0	41.6	39.3	38.0	37.6	7.4
Uncharged (empty) sample	+90	46.9	43.9	41.5	37.5	35.6	11.3
	+60	46.6	43.3	40.6	36.1	34.2	12.4
	+30	46.6	43.2	40.5	36.1	33.9	12.7
	-90	46.6	43.2	40.5	34.0	33.7	12.9

For the uncharged scenario the values in Table 5-2 are mean values of the measurements on three different samples with a deviation of at most ±0.5°C. The values for the acetone charged scenario are the mean values of five repeated measurements on the same sample with a deviation of at most ±0.3°C. This is explained later in the error analysis section.

The objective of the experiment is clearly met by these results. In "uncharged" state the temperature gradient along the sample is almost independent of its inclination angle and is considerably higher than the "charged". In the "uncharged" state the heat transfer relies entirely on the conduction through the thickness of wall while in "charged" state, heat transfer is mostly by the evaporation and the circulation of the working fluid inside the tube. The SLM HP samples that are processed and charged with acetone work like any other heat pipe by transferring the heat with a low temperature drop.

As a side note, the performance of the SLM HP sample is relatively consistent at various inclinations which means the sinter-style wick provides good capillary. This is more investigated in the final experiments.

5-3) Experiments to prove that functional sinter-style aluminium/ammonia heat pipes can be produced by SLM and that they possess the main characteristics of the conventional sintered heat pipes

Final prototypes were converted into functional heat pipes and final experiments were conducted to prove that they possess the ability to work at inclination angles against gravity and can handle high surface heat fluxes as any other conventional sintered heat pipe.

The so-called final SLM heat pipe prototypes were produced with an H-shape cross section and then machined to the final required shape as explained in the previous chapter and demonstrated in Figure 5-9.

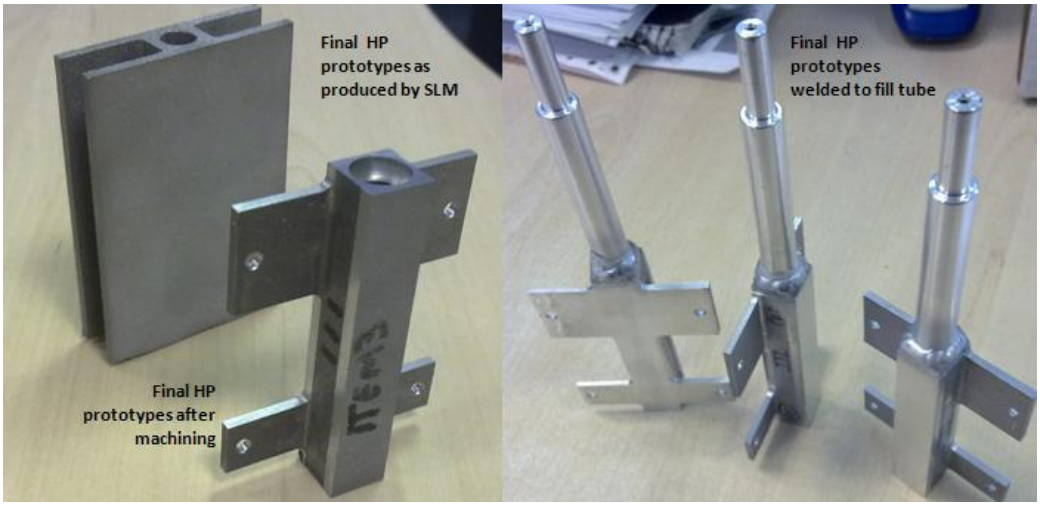

Figure 5- 9 Final SLM HP prototypes with annular sinter-style wick

5-3-1) Preparation of the final samples and test setup

These samples were also equipped to a fill tube and valve and leak-test and proof-pressure tested and filled with acetone with the same process explained before for the initial samples but were tested with the specially designed thermal test rig. The test setup is illustrated in Figure 5-10.

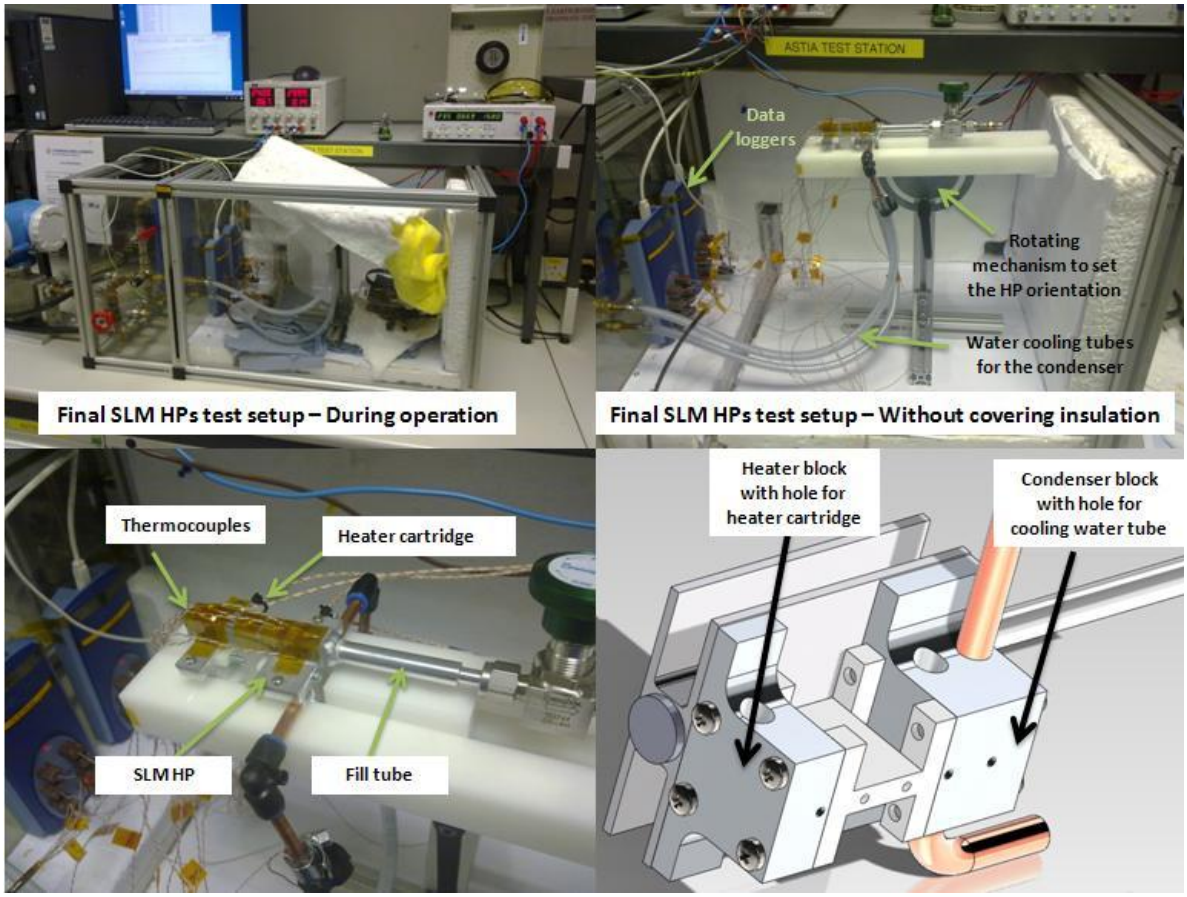

Figure 5- 10 Final SLM heat pipes experiments setup

Unlike the initial tests, final experiments were conducted using a liquid cooled condenser for higher accuracy. Temperature was measured at nine different points as per Figure 5-11 (point 9 is on the opposite side of the point five at the bottom of the heat pipe in the adiabatic section) plus the ambient temperature. The test lab ambient temperature was automatically controlled by the air conditioner, but for higher accuracy, the ambient temperature inside the test cube was recorded separately.

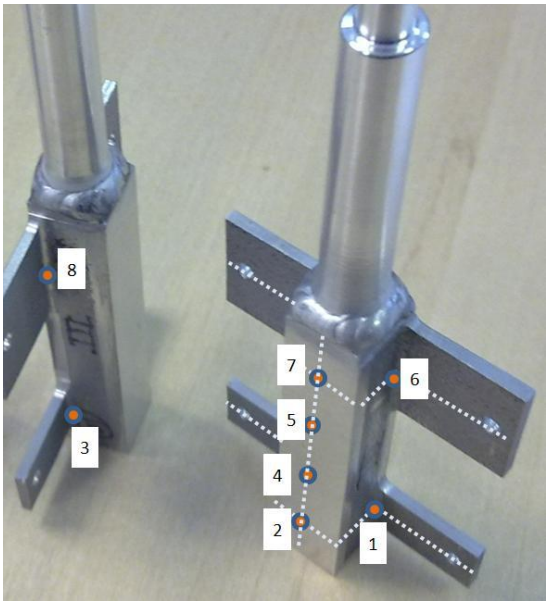

Figure 5- 11 Temperature measurement points on the final SLM HPs

Also, for comparison purposes, from an available extruded aluminium axially grooved heat pipe (AGHP) with identical external profile, two samples were cut to the same length as of the SLM HP prototypes and were processed and tested exactly the same way. These benchmark AGHPs are shown in figure 5-12;

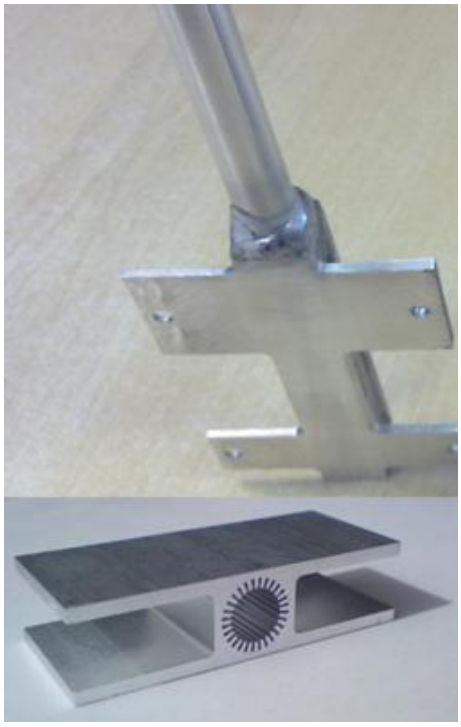

Figure 5- 12 AGHP benchmarks samples (externally identical to the SLM HP samples) were processed and tested at the same conditions for comparison purposes

The main objective of the final experiments was to prove that sinter-style aluminium heat pipes produced by SLM, compared to the available aluminium AGHPs, are able to work at inclination angles against gravity and achieve higher surface heat fluxes. Therefore the final experiments compare the performance of the available aluminium AGHPs with identical aluminium sinter style SLM HPs using acetone as the working fluid.

In each test the input power was increased from 1 to 16W in some steps and the final conclusions are made based on the maximum temperature drop along the pipe in each case. This is the maximum temperature in the evaporator minus the minimum temperature of the condenser or the maximum value between measurements at points 1, 2 and 3 minus the minimum value between measurements at points 6, 7 and 8. Water flow rate and inlet/outlet temperature were used to calculate the waste heat.

5-3-2) Final test results

Test samples at this stage included four externally and geometrically identical samples as follows;

- Two functional SLM HP samples with aluminium annular sinter-style wick
- Two functional extruded aluminium axially grooved heat pipe (AGHP) samples

All four samples were tested at various inclination angles and input powers and the results are presented in Figure 5-13.

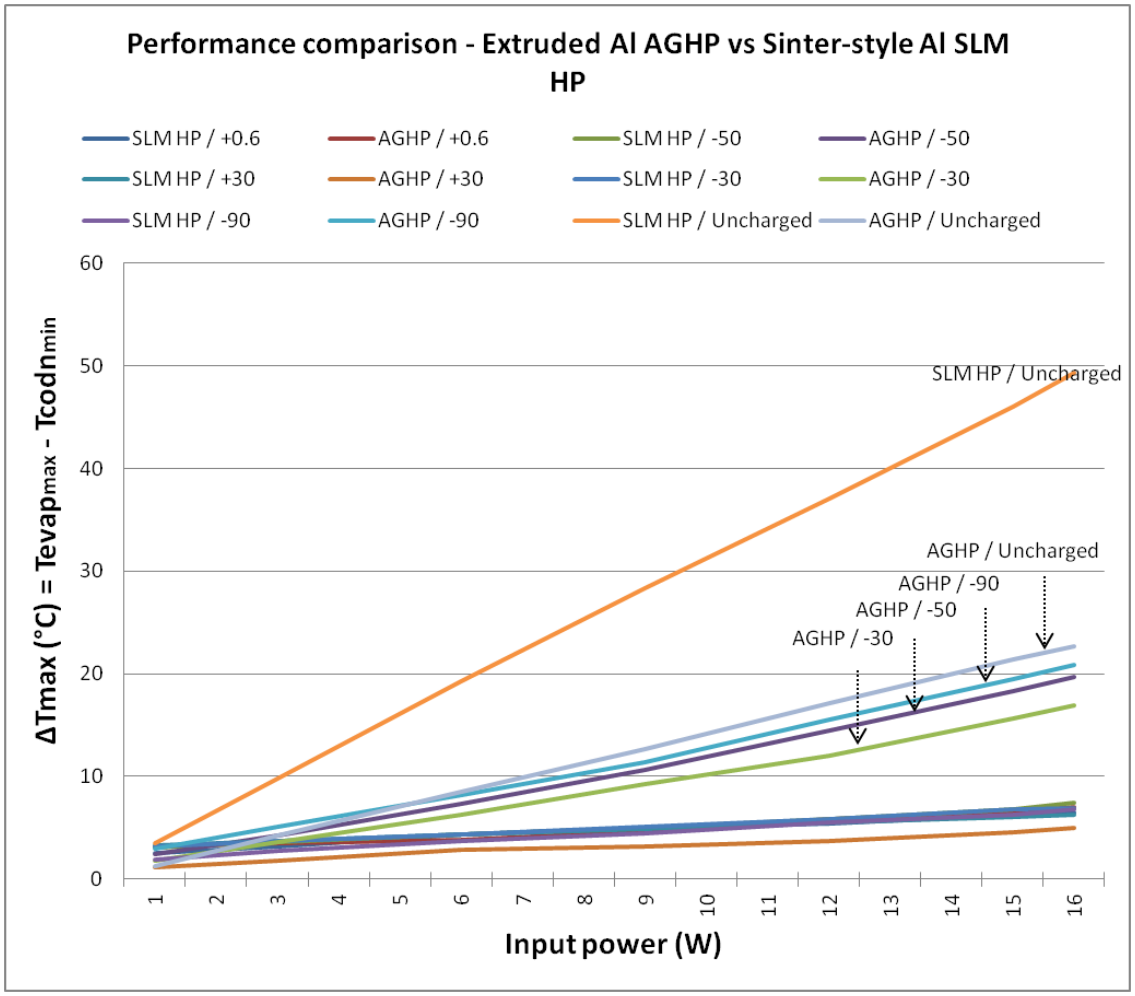

Figure 5- 13 performance comparison between Al AGHPs and sinter-style Al SLM HPs (In the chart's legend, the number after "/" indicates the inclination angle. "+" sign means that pipe works with gravity or with its cold section above the hot region, and "-" denotes operation against gravity)

These data are the mean values of different measurements on the samples as explained later. The most obvious information from the diagram is that the sinter-style SLM HP has a consistent performance in all operating angles while AGHP's temperature gradient increases considerably at inclination angles against gravity. At -90° or when it is in a vertical position with the cold region right below the hot section, AGHP temperature gradient gets very close to its performance at "uncharged" state which means there is no working fluid circulation and all the heat is transferred only by conduction through the wall.

This is more noticeable from the following graphs that show the axial heat transfer coefficients of the pipes versus the surface input heat flux.

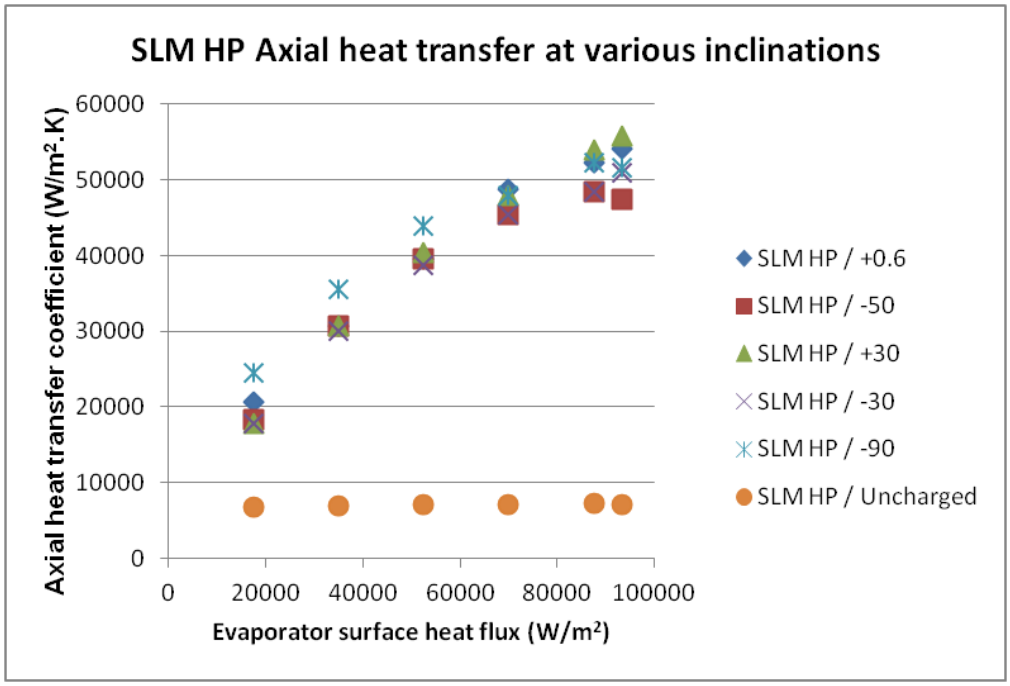

Figure 5- 14 Sinter-style SLM HP axial heat transfer coefficient at various inclination angles and surface input heat fluxes

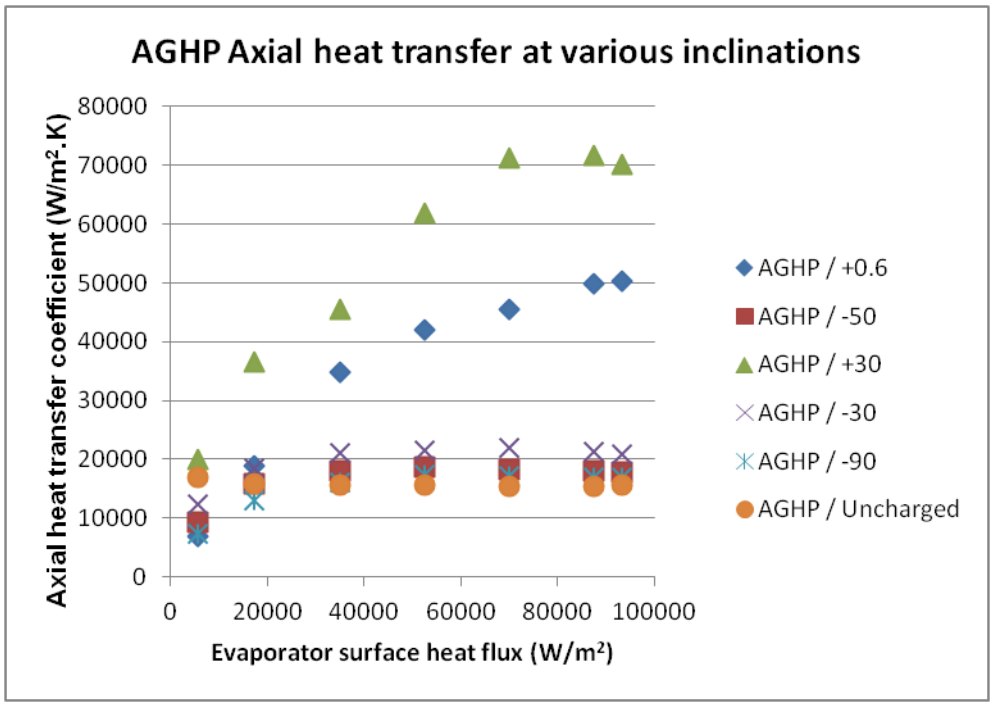

Figure 5- 15 AGHP axial heat transfer coefficient at various inclination angles and surface input heat fluxes

Surface input heat flux is the ratio of the input power to the evaporator surface area and the axial heat transfer coefficient is the input power divided by the product of the cross sectional area of the vapour channel times the temperature gradient along the pipe.

Several interpretations can be made from these graphs but the main purpose (and perhaps the most accurate one considering the limited samples) is to prove that the sinter-style SLM HP remains operational at inclination angles against gravity like any other sintered heat pipe produced by conventional HP manufacturing method.

The followings should also be noted when interpreting these data;

- These data have a ±0.65°C error margin for SLM HP prototypes and ±0.95°C for AGHP samples. This is discussed later in more details.

- HPs have been tested at uncharged (empty) state in horizontal orientation and charged and processed state at two orientations with gravity (0.6° and 30°) and three orientations against gravity (-30°, -50° and -90°). Selection of these certain angles has just been based on provision of a good set of data that clearly shows the performance alteration trend. Although most of the available data for the conventional AGHPs are for near horizontal operation with an angle of around +0.6° with gravity.

- Input power is what has been read by the power meter. This is not the actual power that is carried by HP. Some of it is wasted into the environment as explained later.

- The thermal mass of the rig dictates the required time before a certain test reaches the steady state situation after start and this time is considerably longer at very low powers of 1W-3W. Therefore the measurements for the power levels between 3W and 16W are perhaps more reliable and of more interest.

- Grooves provide a very limited capillary action so when the AGHP works against gravity the condensate is sucked up only to a certain length so the working fluid circulates only in a section of the pipe and the remaining length works only as a pure conductor. At against gravity operation, the higher the inclination angle, the shorter this effective circulation length would be until it gets close to zero when the pipe works reaches vertical orientation.

- Uncharged (empty) SLM HPs show a considerably higher temperature gradient than the extruded AGHPs. In uncharged case, pipes work as pure conductors so the higher temperature gradient of the SLM HPs can only be related to their lower thermal conductivity caused by the remaining pores and their special morphology which is the results of fusing separate powders together.

5-3-3) Partial dry-out of the SLM HP

It is believed that the SLM HPs have also been partially dried-out at high inclination angles against gravity. When capillary action is not enough the condensate is not returned all the way back to the other end of the heat pipe where the heat is applied, so the pipe starts to dry-out from that end. By increasing the power, this dried region extends further towards the condenser. Burn-out (or dry-out) starts from the very end of the evaporator section. The very short length of the heat pipes makes the identification of the exact moment that dry-out happens, impossible. The practical method to recognize this event is to attach several thermocouples in the evaporator region and record when the difference between two adjacent thermocouples starts to increase suddenly. In our experiments the very short length of the heat pipe prohibits this approach. Instead, at any orientation the power has increased from 1W to 16W at several steps allowing the temperature graphs to level out before recording the temperatures and the occurrence of the dry-out has been roughly guessed by random fluctuations that normally happen on the temperature of the condenser section and slight jump in the overall temperature gradient. For our sinter-style SLM HP the dry-out is believed to have been at 16W@-50°, 14W@-60°, 12W@-70°, 10W@-80° and 7W@-90°. For instance at -90° orientation the sinter-style SLM HP has been partially dried at the powers between 7W and 16W but the dried region has been so short (most likely only part of the 12mm length of the evaporator) that pure conduction in that section has compensated the lack of two-phase cycle and has made the pipe to show a relatively consistent performance in these high angle as seen in Figure 5-15. These data has later been compared against the theoretical values calculated by the numerical design tool.

5-3-4) Input surface heat flux

Input surface heat flux is the heat that enters the pipe divided by the heat input surface area. Although in the experiments, the heater block is attached to the entire width of the fin as demonstrated in Figure 5-16, but the actual heat input area into the core of the heat pipe is the circumferential area of the core in the evaporator region.

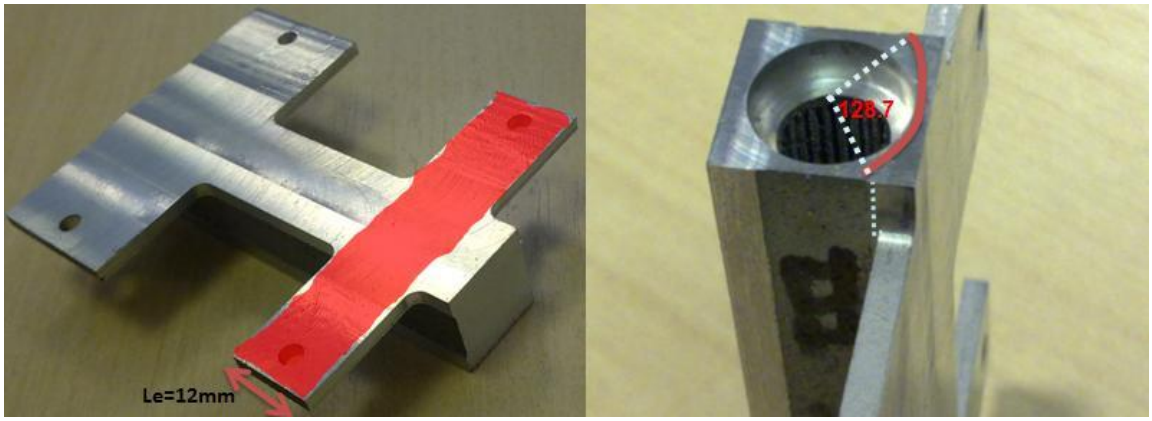

Figure 5- 16 heater block area and the actual heat input area

Using the evaporator length l_e of 12 mm and 12.7 mm outer diameter of the core, the actual input heat area would be;

$1.2 \times \pi \times 1.27 \times 128.7/360 = 1.7 Cm^2$

Input heat flux is calculated by dividing the power by the heat input or evaporator surface area and for any specific test conditions. For the above experiments it can safely be said that sinter-style SLM HPs handle a minimum nominal input heat flux of $16/1.7 = 9.4$ W/Cm^2 at -30° inclination angle against gravity and a 6.9°C temperature drop.

-30° inclination has been selected as it is known that at that angle, the sample has been fully functional in its entire length (and not partially dried out). It is called nominal because some of the heat is wasted into the environment and not carried by the pipe as discussed later.

Most of the reported AGHP input heat flux values in the literature have been obtained from testing AGHPs at slightly gravity aided orientation. The equivalent scenario in the above experiments is the +0.6° inclination angle case. For this case, the test results again show a minimum nominal value of $16/1.7 = 9.4$ W/Cm^2 and 6.5°C temperature drop. It should be noted that at these conditions, the pipe has still been fully functional at 16 W and, most likely, has been capable of handling higher powers but the cartridge heater could not be loaded was limited to 16W.

This is considerably higher than the values reported for conventional ammonia AGHPs and yet it is measured with acetone. Since the thermal properties of ammonia are better than acetone at this temperature range (a combination of liquid properties which is called "Merit Number" is a mean for ranking working fluids with higher Merit Numbers being more desirable and ammonia

merit number is much higher than that of acetone at this range), ammonia filled heat pipe test results are expected to show even higher heat input densities.

These results meet the second main objective of the project which was to prove that sinter-style aluminium heat pipes can be generated by SLM with the same characteristics attributed to the conventional sintered heat pipes (e.g. sintered copper heat pipes) including the ability to work at orientations against gravity and high input surface heat fluxes.

5-4) Results reliability and error analysis

As partly explained in the previous chapters, a huge amount of preparation was essential before the experiments on the final prototypes could be conducted. Mistakes and failures that happened at some stages plus the limited available time to use different resources, including the SLM machine or machining facilities, lead to only two successful functional samples to be produced. More than thirty HPs were produced by SLM with the final desired H-section profile but majority of them failed the leak test due to the wrong build strategy during the SLM process. Likewise, for the initial round cross section samples the welding jig and process were not fully developed yet and that meant the experiments had to be completed with only one fully functional sample.

The presented results are all mean values of several repeated experiments on the limited available good samples and the test results are believed to have answered the project questions very well. Some sources of errors were eliminated, some others were ignored considering the comparative nature of the experiments and some others were evaluated as explained below.

All the thermocouples were calibrated at the beginning of the experiments and necessary correction factors were applied into the data loggers' readings. All the measuring instruments including the flow meter, watt-meter, temperature and pressure data loggers and inclinometer had valid calibration certificates. Human errors were ignored based on conduction of all the experiments by the author and at the same conditions. Some of the other more important errors have been analysed below to provide a rough estimate for the accuracy of the results to the extent that is possible for the conditions of these experiments.

Ambient temperature variation

Most of the experiments were conducted between 8am and 4pm. Completion of each scenario takes a few hours for power step changes and stabilization times. It was noted that, during this time, the surrounding air temperature was changing by up to 1.2°C depending on the time of the

day although it was meant to be controlled by the air conditioning system at a constant 20°C temperature. The possible effect was examined by conducting an exemplary test, called test A, with the same conditions in the morning and afternoon of the same day as illustrated in figure 5-17.

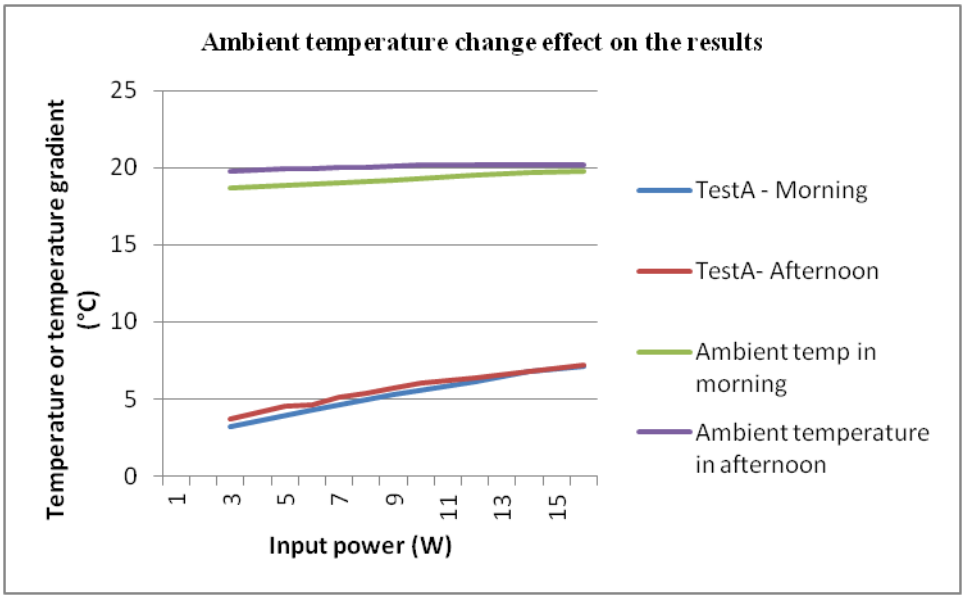

Figure 5- 17 Ambient temperature variation during an exemplary test at 8AM and 4PM and its effect on the test results

The test results show an increase of maximum 0.4°C in the measured HP temperature gradient @ 1.2°C increase in the lab temperature. Because normally the ambient temperature change was lower than this extreme, this effect was ignored in the final results.

HP performance change over the time

Heat pipes in general and aluminium heat pipes in particular are very delicate devices. Their long term performance is very sensitive to the details during their manufacturing and primarily the cleaning process. Any impurity leads to generation of non condensable gasses (NCG) that reduces the effective working length of the pipe. The samples for this project were only good enough to prove the project objectives and not as the qualification samples. Their preparation and filling process was far from ideal and therefore were expected to show a degraded performance over time. This was examined by repeating two exemplary tests (called test A and test B here) on a newly filled pipe and on the same pipe and the same conditions after six days.

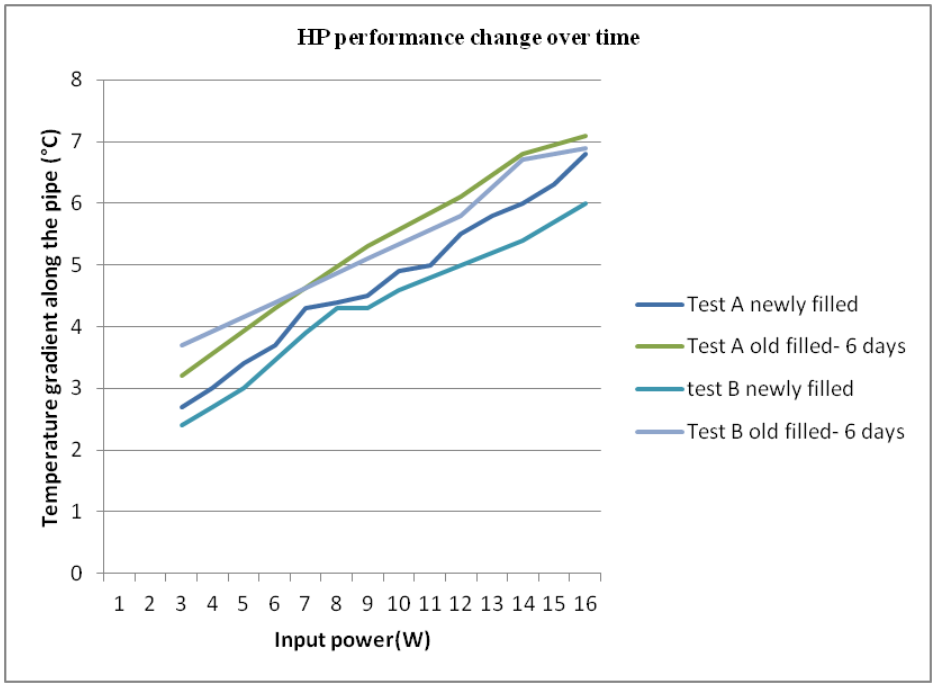

Figure 5- 18 Prototypes performance variation after six days

The results show up to 1.3°C higher temperature gradient after only six days at the worst case. Although this problem can be, almost fully, avoided in production by careful cleaning and filling process, there was no way round it in the limited time of the project so all the experiments on a specific prototypes were tried to be completed as quickly as possible or by venting and re-filling of the same.

Comparison of the performance of the two samples in each group together

Another source of error is the discrepancy between the performances of the samples in each group and the repeated tests on each individual sample. Final experiments were conducted on two SLM HP samples called "HP17SLM" and "HP20SLM" and two extruded AGHPs called "HP5E" and "HP2E". For the two samples in each group, their performance was compared for different scenarios.

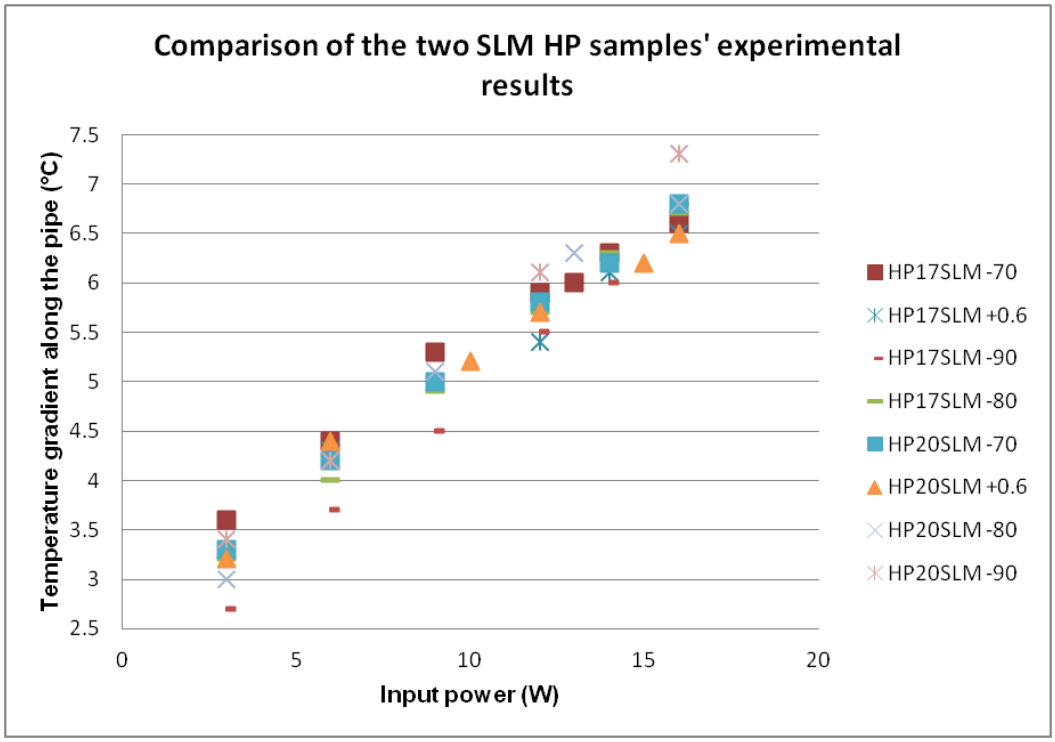

Figure 5- 19 Comparison of the performance of the two sinter-style SLM HP samples (In the chart's legend HP17SLM and HP20SLM are the two SLM HP samples, the number indicates the inclination angle and the sign denotes with or against gravity orientation)

The specific inclination angles have been selected only for provision of a good set of data to include possible maximum discrepancies. Maximum 0.7°C temperature difference is read from the diagram between the measured temperature gradients of the two SLM HPs at similar conditions. This maximum difference occurs @ -90° orientation and 3W.

The same comparison was performed between the two AGHP samples.

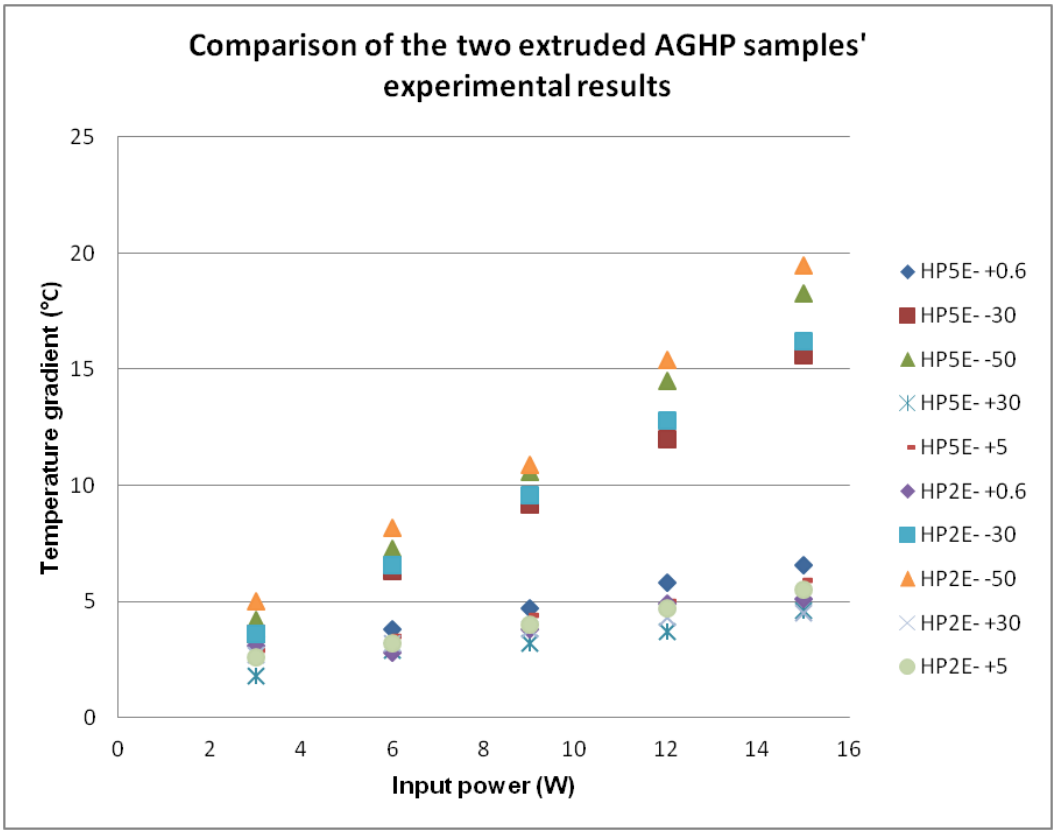

Figure 5- 20 Comparison of the performance of the two extruded AGHP samples (In the chart's legend H5E and H2E are the two AGHP samples, the number indicates the inclination angle and the sign denotes with or against gravity orientation)

The specific inclination angles have been selected only for provision of a good set of data to include possible maximum discrepancies. Maximum 1.5°C temperature difference is read from the diagram between the measured temperature gradients of the two AGHP samples at similar conditions. This maximum difference occurs @ +0.6° orientation and 15W.

Likewise repeated tests on a specific sample at the same conditions show a maximum deviation of ±0.3°C for SLM HPs and ±0.2°C for AGHPs. Therefore;

Max error of the mean values reported in Figures 5-13 and 5-14 for SLM HPs samples = 0.3+0.7/2=±0.65°C

Max error of the mean values reported in Figure 5-13 and 5-15 for AGHPs samples = 0.2+1.5/2=±0.95°C

All the thermocouples were calibrated before starting the experiments and correction factors were applied during the measurements therefore no error is considered for the inconsistency between the thermocouples. Other errors including the tools and human errors have not been taken into account.

Nominal and actual heat input

Although the entire test section was being covered during the tests by a relatively thick insulation layer yet some waste heat into the surrounding air is inevitable. The cooling water flow rate and input/output temperature were used to calculate this waste heat and the actual power that is carried by the heat pipe. Because the lab temperature and the cooling water flow rate were almost constant during all the experiments, the waste heat was a roughly constant value for each power level.

Therefore for each input power level read by the power meter and each cooling water flow rate, there is an equivalent power (heat) which is actually carried away by the heat pipe and the rest is wasted by radiation/convection into the lab environment. The nominal and actual powers were measured as per table 5-3.

Table 5- 2 Nominal and actual power levels

Nominal power (W)	1	2	3	4	5	6	7	8	9	10	11	12	13	14	15	16
Actual power (W)	0.9	1.8	2.6	3.5	4.4	5.3	6.1	7.0	7.9	8.8	9.7	10.5	11.4	12.3	13.2	14.0

5-5) Design tool validation based on the actual test results (temperature drop and dry-out)

The numerical design tool that was developed during the project is based on the formulas extracted from different sources. There are discrepancies between different sources especially for the maximum capillary limit which is the dominating factor in most of the operating temperature range of a heat pipe. Moreover, the calculation process employs empirical values that need to be specified for any type of heat pipe e.g. permeability, pore radii, contact angle, etc. therefore, as discussed before, a numerical design tool must be validated by a heat pipe manufacturer for its own specific range of products using a comprehensive set of experimental data. However, for this project, using the available experimental data and to the extent that it could be covered in the scope of the project, a comparison was performed between the design tool's predictions and the test results to validate the tool and determine its error margin.

Typically the main use of a design tool is before producing a heat pipe to specify the maximum power that the HP would be able to handle in a specific application before it hits one of its limits (very often the capillary limit) as well as the temperature gradient along the pipe.

First the design tool dry-out power predictions for different inclination angles and operating temperatures were compared against the experimental results as shown in table 5-4.

Table 5- 3 Dry-out power - comparison between the design tool predictions and experimental results

Operating angle (°) and temperature (°C)	Dry-out power (W) calculated by the design tool	Dry-out power (W) measured in experiments
-90° & 28°C	9.2	6.1
-80° & 33°C	9	8.8
-70° & 35°C	10.7	10.5
-60° & 38°C	13.6	12.3
-50° & 41°C	17.8	14

Dividing these values by the evaporator surface area of 1.7 Cm^2 to get the heat flux;

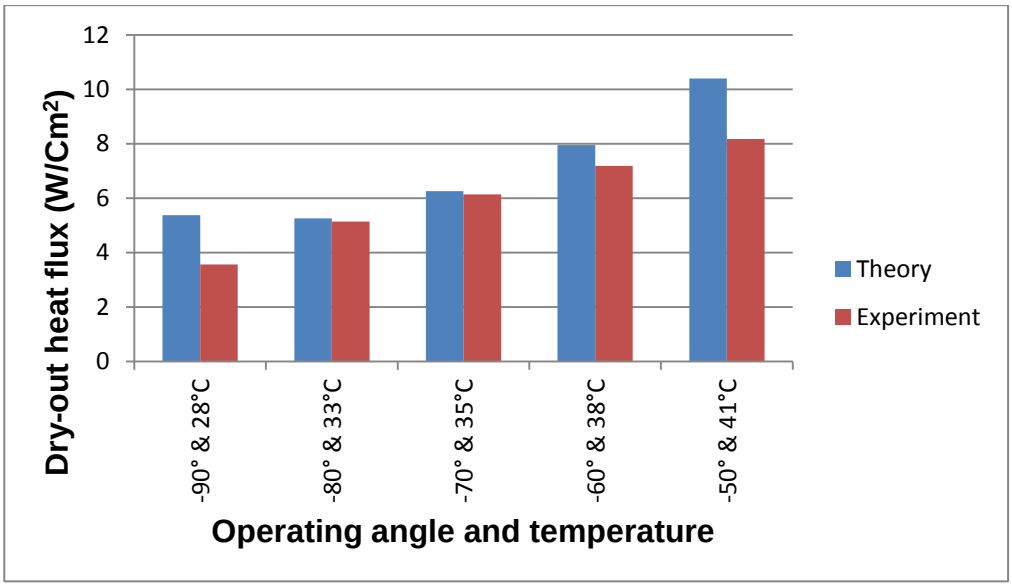

Figure 5- 21 Dry-out heat flux - Theoretical predictions and experimental results

As explained before, the very short length and limited number of the samples and other restrictions made the precise determination of the dry-out event during our experiments extremely difficult. No concrete conclusion can be drawn from these data in terms of the sources of discrepancies but the safest way is to extend the experimental results and perform this comparison in a much wider range of samples and experiment conditions and then apply some correction factors to the theoretical model once they are proved by repeated experiments. For now, and based on these data, one may conclude that theoretical predictions for maximum dry-out heat flux are higher than the experimental data and takes this error margin into account when designing an SLM HP. The discrepancies are due to inevitable ideal assumptions for some parameters especially the effective pore radius and permeability. Higher theoretical predictions for sintered wicks have also been reported by several other scholars including Hanlon & Ma (2003).

Design tool was also validated by comparing its temperature gradient predictions against the experimental results.

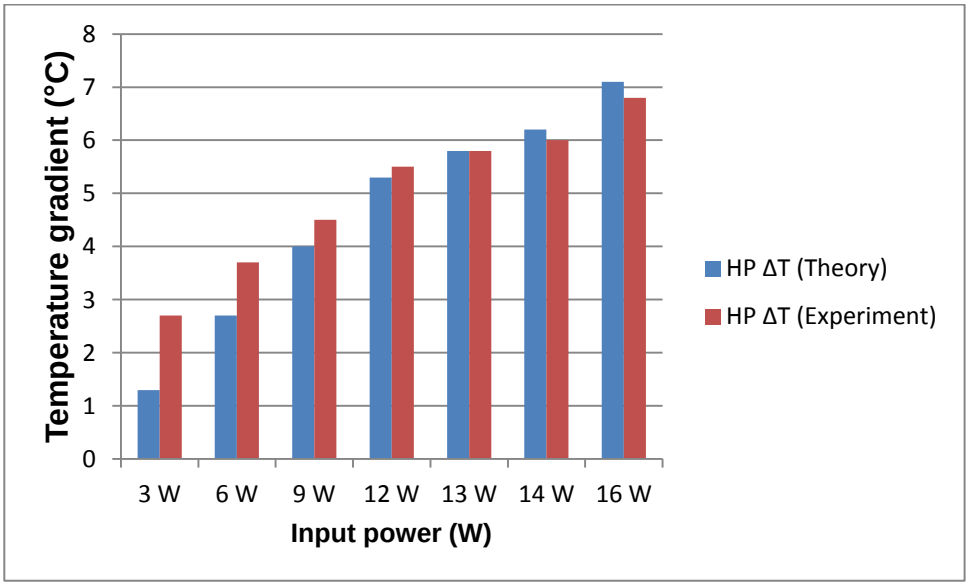

Figure 5- 22 HP temperature gradient vs. input power - Theory and experiment

The results show a reasonable accuracy of the theoretical values. The bigger difference at lower powers can be explained by the fact that the theoretical model only considers the temperature drops due to the heat passage through the wall and the wick in the evaporator and condenser and the thermal interfaces in these sections and assumes that the vapour channel is isothermal while specially at lower powers, in practice, there is a considerable temperature gradient between the condenser and the evaporator.

At higher powers the theoretical predictions begin to overestimate the temperature drops. This can be explained by the fact that at higher powers the condensate level in the evaporator wick drops and fluid evaporations happens from somewhere within the porous wick and not necessarily from the edge of the wick therefore heat does not need to travel all the thickness of the wick up to the edge of the vapour core. This can also be a confirmation for the quote made by Garimella, Iverson, et al. (2007) that "as input power is increased and more heat is dissipated by the wick, a relatively larger amount of this heat is dissipated by vaporizing the working fluid and a correspondingly smaller value is conducted along the solid matrix resulting in lower temperature gradient".

A novel heat pipe (HP) manufacturing method has been developed based on an additive layer manufacturing technique called "selective laser melting" or SLM. This innovation is expected to benefit current applications of aluminium/ammonia heat pipes in space and terrestrial projects as well as many new HP applications.

The project was jointly sponsored by the Northumbria University and Thermacore, a world leading heat pipe manufacturing company in the UK, and formed the feasibility stage of a much larger program in Thermacore aiming to develop the next generation of HPs for space applications. In this project, sinter-style aluminium SLM HPs have been produced and tested to prove their functionality and to provide an overall image of the new production process with regard to the major involved parameters.

It is believed that this is the first time that functional heat pipes are produced with this method and also the first time that functional aluminium HPs are produced with a sinter-style wick structure. Currently, aluminium heat pipes with aluminium sintered wick do not exist due to the impracticality of sintering aluminium powders on the internal walls of a heat pipe.

An SLM machine in the Liverpool University has been used to produce the prototypes. The prototypes have been processed and tested by the especially fabricated test rigs in Thermacore to prove their functionality and to demonstrate that they possess all the main attributes of the other sintered heat pipes (e.g. sintered copper HPs) including high surface heat flux and capability to work at inclination angles against gravity.

Several properties of the new heat pipes e.g. wick porosity, permeability and pore size; wall density, hardness, vibration resistance and optimum SLM build parameters have also been determined by the existing or especially developed rigs in Thermacore or Northumbria University laboratories including scanning electronic microscope (SEM), vibration table, permeability measurement rig, etc. Converting the SLM products into functional heat pipes involves many other steps which have also been completed and explained.

The project had four main objectives. First, to prove that functional heat pipes can be produced by SLM. This has been met by comparing the performance of the converted-to-HP samples

against unprocessed raw samples and demonstrating that they operate as a two-phase system which transfers the heat with low temperature gradient as expected from a HP.

Production of the first sinter-style aluminium SLM HP and to prove its operability was the second objective. To address this, appropriate prototypes were produced, converted to functional heat pipes and their performance was compared against identical extruded AGHPs in an especially designed rig. It was demonstrated by experiments, that they have the main attributes of any other sintered HP.

A numerical excel-based design tool was also developed to enable designing and parametric study of the SLM HPs. The theoretical predictions were compared against the actual test results and error margins were specified. This was the third project's objective and the fourth one was to identify the critical aspects and potentials of the new production process to be investigated in the future works. These have been pointed out throughout this document and are discussed later in this chapter.

The work showed that the SLM HP concept is confirmed to be indeed feasible with interesting advantages over the conventional methods including almost-unlimited flexibility and controllability especially on the wick structure that can pave the way for researchers to investigate advanced heat transfer structures while it is going through the qualification process for the use in real applications. It is now also understood that this innovation is not limited to aluminium heat pipes but to many other types of HPs as well since other material like Stainless Steel and Titanium are also established material for the use in SLM process.

However the new production method and heat pipes have a long way before being fully characterized and qualified especially for critical applications. There is vast number of parameters that investigating each one would require many resources and would be the subject of an entire project. Some of these parameters have been quickly analyzed through this project, within the limited available time and resources, in order to get a sense of the overall process and to identify the critical issues.

Although the ultimate use of the new heat pipes is expected to be in aluminium/ammonia HP applications, all the experiments were conducted using acetone since the required ammonia filling rig was not completed until the very end of the project. However this change of the working fluid makes no difference in the concluded results whatsoever as all the proving experiments have had a comparative nature.

Two successful functional samples were obtained and clear and precise answers were found to the project questions a reasonably good overall image of this new HP production process and the new HPs was provided through the conducted measurements and experiments.

Economics of the SLM HPs

Sintered aluminium heat pipes are currently unavailable therefore production cost comparison and economic justification of the novel sinter-style aluminium SLM heat pipes is not possible and of no value.

Moreover a very long qualification process is anticipated for the new SLM based process before it is established as an alternative HP production method and for SLM HPs to be fully characterized and meanwhile many of the involved economic figures may change. Therefore economy-based conclusions should not be made at this stage.

On the other hand, the new process is believed to be more suitable for producing HPs for high tech, low volume applications (at least in the short term) where the cost is not of the prime importance. The reasons for this high-tech applications suitability include the very high flexibility and controllability of the SLM process that enables the production of very complex wick structures, its capability to produce integrated HP-fill tube assemblies and irregular shaped heat pipes and the possibility of using titanium and Stainless Steel powders in the process as well.

However as a case study, and as the raw data for further investigations, the followings can be used. In the SLM machine which was used to build the samples for this project, the substrate disc is Ø125mm diameter and the maximum useful working height is around 70mm. On this substrate we managed to build 13 samples at one go as shown below;

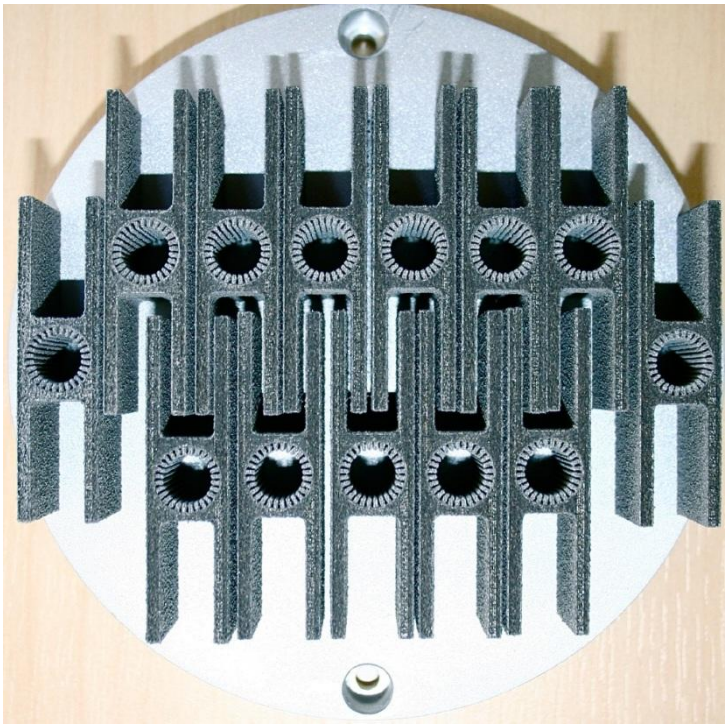

Figure 6- 1 Multiple SLM HP samples built simultaneously on a substrate

Build speed of the machine is between 5 to 30 Cm^3 per hour. This means building 13 of these samples (assuming Ø100mm x 70mm effective working area) takes between 18 to 110 hours depending on the build parameters e.g. laser exposure time, etc. Different tries to produce the samples for this project took between 36 to 60 hours. During this time the main power consumption of the system is for the laser which in this case has been 200W. Labour cost is minimal due to the level of automation and the overhead costs can probably be ignored assuming the process running in a heat pipe manufacturing company with many more larger-scale activities running in parallel.

More information on the economics of the established high volume products of the additive layer manufacturing techniques (e.g. medical implants) can be seen at (Violante, Juliano, et al. 2007) and (Tuck & Hague, 2006) and a case study of the cost comparison between injection moulding and SLS (Selecting Laser Sintering) techniques to build a plastic part comprising four parts has been presented in Atzeni & Salmi, (2012).

Identified challenges and critical issues – Suggestions for future works

This project forms the feasibility stage of a much larger program for development of the next generation of space heat pipe. Prompted by the results of the project, several issues should be considered for future builds and in continuation of the program. These are explained below;

- *SLM build strategy and applicable extent.* Like any other technique, SLM has limited applicability range although its full capabilities are not fully explored yet. Certain metallic powders are well established for the process e.g. titanium and Stainless Steel, some others can potentially be used but their optimum build parameters are not fully examined yet e.g. Al6063 and some other aluminium alloys and some can not be used mostly due to their high laser reflectivity that avoids the full powder melting e.g. copper. Also, each SLM machine has a certain work volume that dictates the maximum possible dimensions of the product with the largest being in the range of $1m^3$. This range should be very well defined if SLM is to be established as an alternative HP manufacturing method.

  Moreover remaining residual stresses in the SLM products is a major issue. Different strategies and build directions can be employed during the process as long as each powder layer, during the build, is supported by a preceding layer and there is no sudden protrusion that makes the build physically impossible. At further distances from the substrate and for thin walls, the geometry has to be supported by virtual pillars that are cut from the object after build to avoid deformation of the product. For the prototypes of this project, these supports proved to create stress concentration points that consequently lead to creation of micro-cracks in the product. Several prototypes failed the leak test due to the leakage through micro-cracks that are believed to have been generated by these supports. Therefore the build strategy should be carefully investigated in future builds.

- *Density of the SLM solid structures.* SLM solid structures are generated by fully melting the powders together inside the borders of the section of the geometry that has been defined as solid. This process so far has been associated with some remaining pores that can affect both the rigidity of the structure and, for the purpose of building HPs, the thermal conductivity and leak-freeness of that. Optimizing the laser build parameters increased this density for this project's prototypes to near 98% for AlSi12 aluminium alloy but further investigations are needed especially if other alloys such as Al6063 are to be used in the process. This has already been the subject of several researches reported in the literature.

- *Thermal conductivity of the SLM structures.* Final experiments of the project showed a considerably higher temperature gradient along the uncharged AlSi12 SLM HP samples compared to uncharged Al6063 AGHPs at the same conditions that can only be related to the lower thermal conductivity of the SLM samples. There is no considerable

difference between the value of this for the two alloys in raw form hence the lower conductivity of the SLM products should (at least partly) be related to their morphology and possible molecular alterations during the melting/fusing process. As the first step, SLM built samples can be measured separately to determine their thermal conductivity value for the use in design calculations instead of using the value of the raw material.

- *Remaining loose powder.* The remaining loose powder in SLM products is normally shaken out after the end of the build process. Appropriate provisions must be made in the design of a product and in the SLM build strategy to facilitate this. The difference between the actually measured and theoretically calculated values of the permeability and pore size in the project porous samples is believed to be related to the blockage of some of the pores by the trapped loose powder.

- *Flatness and appearance of the SLM products*. SLM products have a porous appearance as seen in the project pictures. For heat pipes, since a good contact with the hot and cold medium is essential, an extra machining/skimming process must be done on the SLM HPs. Considerations should be taken in the initial design and provisions should be made for this.

- *SLM HP to functional HP conversion process.* In this project, the prototypes were produced with separate fill tube with an extra welding process involved but even if SLM HPs are produces with an integrated fill tube, still a conversion process of cutting from the base plate, machining, cleaning and filling is needed before obtaining a functional heat pipe. Provisions must be made for each of these steps at the HP design stage.

- *Contamination.* Scanning electronic microscope (SEM) images revealed the existence of titanium content in the ALSi12 samples. The contamination is believed to have caused by the titanium powder left in the SLM machine funnel and lab environment from previous builds. Especially for ammonia heat pipes this can have disastrous effect in the short or long term performance of the pipe by generating non condensable gasses through the reaction of ammonia with the unexpected contaminants.

- *Optimal SLM porous properties.* The minimum possible SLM unit cell size is currently in the range of 300 μm. This, along with the laser power, laser movement controlling parameters, material and the base geometry of the porous structure dictates the achievable porosity and pore size of the porous structures. For this project the porous structures were of an octahedral base geometry. Parametric study of all the involved

parameters simultaneously to enable generation of porous structures with any desired porosity, permeability and pore radii and also working with smaller unit cell sizes for the use in building other anticipated types of heat pipe such as "loop heat pipes" should be considered as a subject for future works.

- *Shock and vibration resistance.* The project samples were tested only in a narrow range of vibration by the available resources to prove their rigidity to withstand the normal forces during the build, conversion and testing process as well as the vibration level in many normal non-critical applications. But for shock and vibration full qualification especially for critical space applications, a comprehensive study must be done.

- *Test layout and prototype design.* The very special H shape of the final prototypes of this project was to enable a direct comparison against the at-the-time available axially grooved profile heat pipes. While the design was good for this purpose but if the heat input/output areas are symmetrical during the experiments, more useful results can be concluded. Also the very short length of the prototypes makes some of the characterizing experiments impossible. For future works it is suggested the prototypes be produced using a larger SLM machine and perhaps with a different build strategy that enables production of longer samples.

Hardness of the SLM solid structures

Hardness of the SLM solid structures was measured on four pieces with two different densities. Two of the samples belonged to the latest prototypes built using the modified machine parameters for improved density and the other two from the initial lower density solid samples. Measurements were done using two different instruments, HT-1000A and MH310 in Brinell or HB units and three readings were done on each sample by each instrument.

As the samples were very light weight, they were laid on a heavy aluminium slab using some yellow grease between them and clamped in place as instructed in the manuals. This can explain the inconsistency between readings on a sample by the same instrument. The results are presented in Table A-1.

Table A- 1 Hardness measurement results on SLMbuilt AlSi12 structure. H denotes the high density samples and L, the lower density ones

Sample / Instrument	HT-1000A	MH310
4H	81, 94, 85	93, 100, 81
5H	81, 80, 78	76, 78, 91
4L	81, 85, 96	89, 94, 112
5L	85, 83, 83	80, 82, 86

It is important to note that because SLM products are generated by melting the material in a powder shape and re-fusing them together, the mechanical, thermal and physical properties of the resulted products can be considerably different from those of that material in its original slab form. For comparison purpose, the hardness of Al6063-T6 which is the most common material for extruded AGHPs is 73HB (Ref: ASM International) while all the measured values for AlSi12 samples are above this with an average value of roughly 83HB. The results show no point of concern about AlSi12 SLM HPs with regard to their hardness.

Yield strength/yield point of the SLM solid structures

Yield strength or yield point is the stress at which a material starts to deform permanently. In designing parts, this parameter is vital as it specifies the maximum load that can be applied to them.

For ammonia charged AGHP's, yield strength is a critical parameter to consider in their design to ensure the wall material can withstand the very high saturation vapour pressure of ammonia at the maximum operating temperature. In this project five AlSi12 solid samples were tested along with four samples of a high strength aluminium magnesium alloy (for reference) using an Instron 3382 Tensometer. The samples were machined to dog-bone shapes and clamped into the Tensometer jaws. The force on the component is increased until the sample yields and finally breaks. This process is shown in the Figure A-1.

Instron 3382 used for the tensile strength measurements

Samples cut to a dog-bone shape

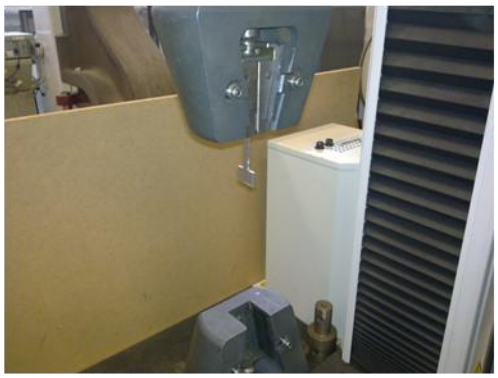

Sample is pulled by the two jaws of the machine

Samples after the test

Figure A- 1 Yield strength measurement process

The stress-strength curves developed by the machine for different samples are shown below and final table shows the samples' dimensions and the calculated yield point for each one.

Yield point calculation process was as follows;

- The width and thickness of each sample, in the narrow section, was measured in two points. The highest of these two measurement values was used for yield strength calculation

- Samples 1 to 4 (magnesium aluminium alloy reference samples) have an elastic region as shown in the diagrams. For all of them the maximum yield force was 3.3KN.

- Samples 5-9 (SLM built AlSi12 samples) break with almost negligible deformation and that is a known property of AlSi12 parts. As it is shown in the diagrams for samples 5-9 there is no difference between the peak and break load.

- The loading diagram for samples 2 to 9 is shown in Figure A-2.

- Samples 1-4 material are from a magnesium alloy of aluminium (used here only to show the elastic region) and samples 5-9 are made of AlSi12 by SLM.

- The experiments were done in a normal lab environment of 22°C. This value changes by temperature and aging of the material.

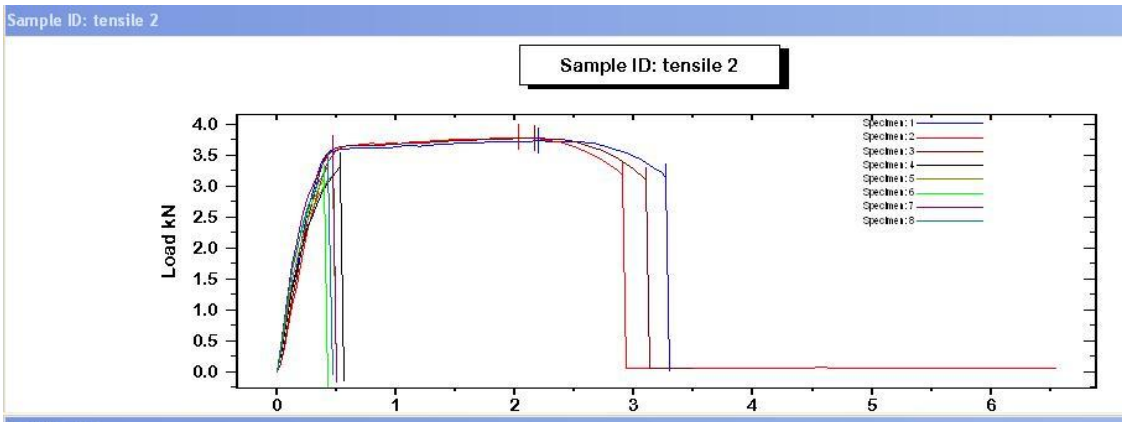

Test Results

Sp No	Load@Peak (kN)	Disp@Peak (mm)	Brk. Load (kN)	Brk. Disp (mm)
1	3.730	2.200	3.147	3.267
2	3.783	2.033	3.186	2.900
3	3.772	2.167	3.090	3.100
4	3.317	0.533	3.317	0.533
5	3.176	0.467	3.176	0.467
6	3.122	0.400	3.122	0.400
7	3.597	0.467	3.597	0.467
8	3.317	0.433	3.317	0.433

Figure A- 2 Yield strength measurement on SLM built AlSi12 structures and samples of a reference magnesium alloy of aluminium

Table A- 2 Results of the yield strength measurement on SLM produced AlSi12 samples (5 to 9) and reference aluminium alloy samples (1 to 4)

				Sample No:								
Description	Specification	'+' Tol	'-' Tol	1	2	3	4	5	6	7	8	9
Width	5.00	0.50	0.50	5.187	5.123	5.142	5.112	5.402	5.564	5.218	5.540	5.497
Width	5.00	0.50	0.50	5.191	5.124	5.151	5.097	5.288	5.538	5.412	5.632	5.325
thickness	2.00	0.50	0.50	1.989	1.989	2.028	2.077	2.356	2.284	2.408	2.352	2.393
thickness	2.00	0.50	0.50	1.996	2.007	2.039	2.067	2.396	2.331	2.427	2.344	2.427
Yield Strength	UNIT	MPa		318	321	314	311	256	245	238	271	249

AlSi12 SLM produced structures are very brittle and do not have an elastic region under load. The average value of the yield strength for these samples is 238 MPa. For comparison purpose, the yield tensile strength for Al6063-T6 (used to build most of the available AGHPS) is 214 MPa (REF: ASM, Aerospace Specification Metals Inc.). The results show no point of concern about AlSi12 SLM HPs with regard to their yield strength.

Welding fixture

A special welding jig was designed and manufactured for welding fill tubes to the machined SLM heat pipes. This is shown in Figure A-3. The fixture holds the pipe firmly for precise welding of the fill tube and also provides passages for hot and cold water for heating and cooling of the sample at different stages during welding.

Figure A- 3 Welding fixtures to assist welding fill tube to the SLM HP

Shock and vibration fixtures and experiments

Shock and vibration testing are used to simulate the extreme conditions that a product may face during operation and determine the ruggedness of a product. The test conditions are defined based on the standards of the target application for the product.

SLM has been used in this project for the first time to produce heat pipes. Through the project it is proved that SLM is capable of producing different types of heat pipes for various applications depending on the heat pipe material, wick structure and working fluid. Aluminium ammonia heat pipes that are the focus of the project are currently used mainly in space and some terrestrial applications as mentioned before. Like many other parameters, full characterization of SLM heat pipes needs a comprehensive set of experiments depending on the final application which is outside the scope of this project. For this project and to get a rough idea of the SLM heat pipes' resilience in high vibrating environments, a European space agency (ESA) standard (ECSS, 2010) was used to define the test conditions. However conducted tests were very restricted comparing to the standard's requirements due to the limited available time and resources. Experiments were done only for vibration and not shock, only non-functional samples were tested and vibration limits were narrower than the standard requirements and were only sinusoidal and not random due to the limited capability of the available shaker. ESA requirements for sinusoidal vibration are listed in Table A-3.

Table A- 3 Sinusoidal vibration qualification test levels according to ESA standard

Frequency (Hz)	Level	First frequency > 100 MHz	First frequency ≤100 MHz
5 to 21	11 mm (0 to peak)	No notching	With notching
21 to 60	20 g (0 to peak)	No notching	With notching
60-100	6 g (0 to peak)	No notching	With notching

Instron E3000 electromechanical dynamic and static testing machine (Figure A-4) was implemented for sinusoidal vibration tests. Although E300 main use is static testing in a tensile or compression mode within a single frame but most of the dynamic tests can also be done by it by hanging samples from the upper jaw. Since this machine was the only available resource and benefited from the most up-to-date technology and controlling software, it was used for conducting these tests.

Figure A- 4 Instron E3000 Electromechanical testing machine

Vibration tests were planned as below;

1. To test the SLM porous structures to make sure that they will not break apart in a vibrating environment. For this purpose the permeability samples shown in figure 4-19 and 4-20 were used and a fixture was designed for them as shown by Figure A-5. The objective was to observe/measure any generated loose powder inside each of the four cavities after shaking.

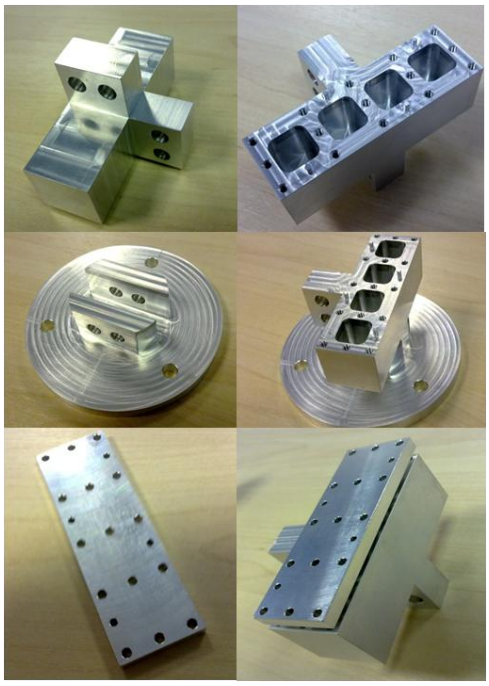

Figure A- 5 SLM porous structures vibration test fixture

2. To test un-functional final heat pipes. The objective was to observe/measure any generated loose particles inside the pipe after vibration as well as testing the strength of the tube-fill tube weld. Another fixture was designed for this as shown below;

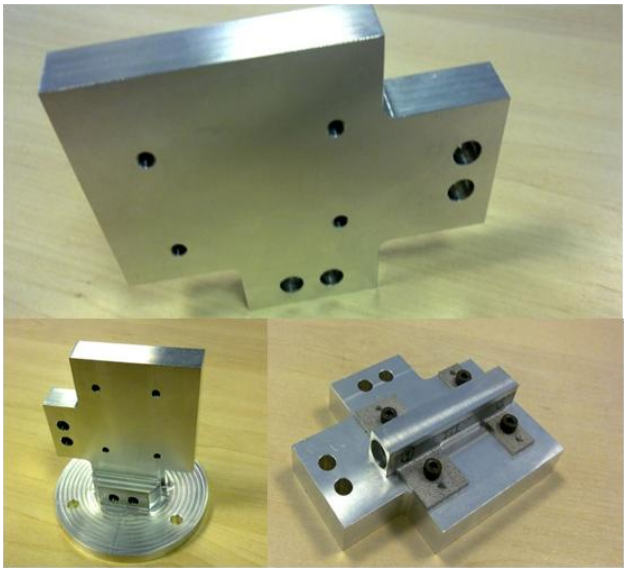

Figure A- 6 SLM HP vibration test fixture

The test plan is shown in Table A-4.

Table A- 4 Test plan for sinusoidal vibration of the SLM HPs

	Title	Prototype / fluid	Description	Pass / Fail criteria
Phase 1	SLM porous structure integrity / rigidity test	SLM various porous structures	This test aims to identify any possible failure of the porous structures built SLM under the sinusoidal vibration conditions specified by ESA	The porous structure must remain intact or with minimal damage after the test
	Non-functional heat pipe sinusoidal vibration test	Un-processed heat pipe	This test aims to identify the possible effect of the specified sinusoidal vibration on just the structure of the non-filled (unprocessed) SLM HPs as The possible effect(s) can be damage to the wick or generation and propagation of cracks due to the remaining	The sample(s) must remain intact and pass the Leak testing, proof pressure and burst pressure testing and , when applicable, the

Table A- 4 Test plan for sinusoidal vibration of the SLM HPs				
			pores in the heat pipe container and end cap, damage to the heat pipe-fill tube weld or the container deformation.	results must be identical to the results of a sample that has not undergone the vibration tests

Phase II would be to test the functional heat pipes (in operation) which should be done in future works.

Test Results

Considering the following equation;

$$Acceleration\ in\ (g) = \frac{r\omega^2}{9.81} \quad \text{(Eq. A. 1)}$$

Where;

r : Amplitude in meters

$\omega = 2\pi f$ where f is the frequency

the sinusoidal vibration requirements of Table A-3 is represented by the following diagram. But because the instrument used for the tests was limited in performance, the actual vibration curve was different as shown in Figure A-7.

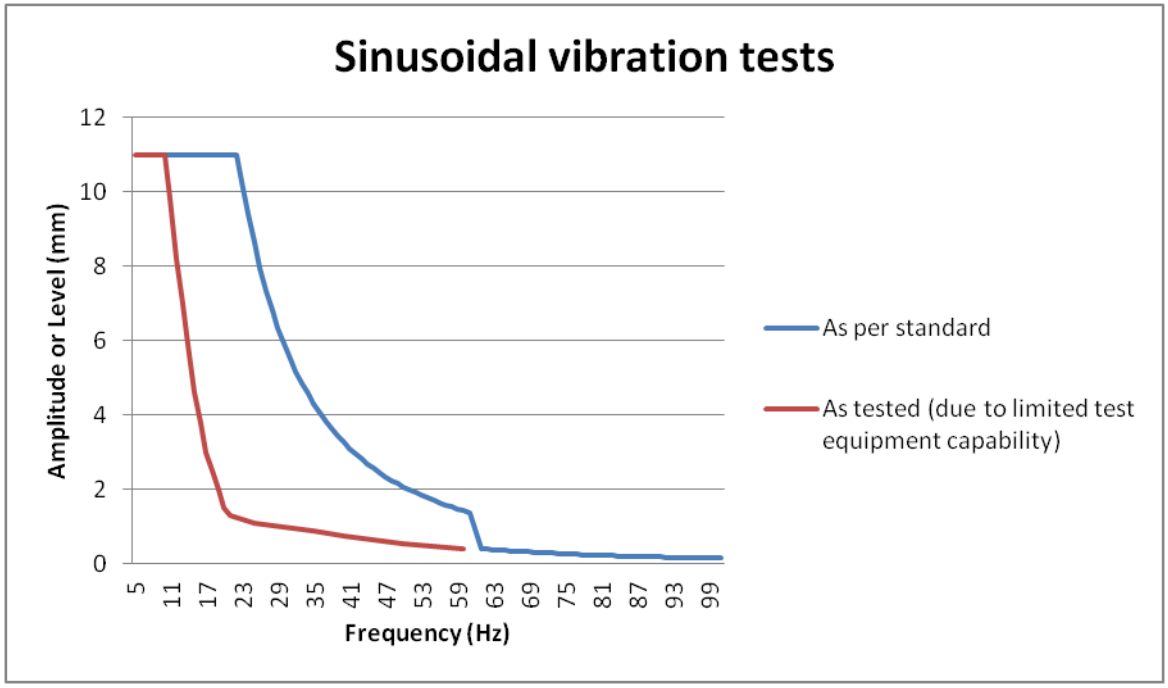

Figure A- 7 Standard and actual vibration tests diagrams

Testing at frequencies above 60 Hz was impossible by this instrument and at frequencies below 60Hz as well, amplitude had to be reduced (from what specified/calculated by the standard) in order to avoid the machine hitting its performance limits. For example for a frequency of 30 according to the above formula;

$$Amplitude\ r = \frac{20 \times 9.81 \times 1000}{(2\pi \times 30)^2} = 5.52\ mm$$

But in reality at a frequency of 30Hz maximum achievable amplitude (before the machine hit its performance limit and emergency shuts down) was 1mm.

Heat pipe sample opening end was blocked by a rubber bond and it was tested at two different axes and two different stages, one at the frequency band of 5 to 21 Hz and then at the frequency band of 21 to 60Hz. It was weighed before the tests and after each frequency band and after shaking any possible generated loose powder out (possible damage to the structure) and no difference and no damage was observed.

Porous structures were tested the same way. At two different axes and two different stages corresponding to two frequency bands and were weighed at three stages before the tests and after each stage. No difference in the weight or damage was observed.

Table A- 5 SLM HP and SLM porous structures sinusoidal vibration test results

	Initial weight (g)	Weight after the sinusoidal vibration tests in two axes from 5 to 21Hz (gr)	Weight after the sinusoidal vibration tests in two axes from 21 to 60Hz (gr)
Heat pipe	20.49	20.48	20.48
Porous structure 1-300 regular	5.99	5.99	5.99
Porous structure 1-300 random	5.83	5.84	5.84
Porous structure 1-500 regular	3.11	3.11	3.10
Porous structure 1-500 random	3.45	3.45	3.45

Although the tested vibration limits have been lower than the ESA requirements, still the applied vibration has been quite higher than what actually exist in many terrestrial applications. These tests just provided enough insurance that SLM HP are rigid enough to go through the full production and test process as well as many possible real applications for them but full characterization of SLM HP and ultimately using them in space applications needs a comprehensive shock and vibration test that should be done in future works.

Contact Angle – Wettability

Capillary pressure is the main driving force in a heat pipe that transports the condensed working liquid through the wick to the evaporator. Capillary pressure is generated by the difference between the curvature radius of the working fluid menisci inside the pores in the evaporator and condenser regions of a heat pipe. The curvature radius in turn is dictated by the contact angle between the liquid and solid surface.

The contact angle of the liquid and the solid walls inside a pore depends on the liquid surface tension and the adhesion force between the liquid and the solid. If the adhesion force is greater than the surface tension, the liquid near the solid wall is pulled up and the liquid surface tension causes the bulk of the liquid to move up to keep the surface intact.

Evaporation in the evaporator causes the menisci's radius of the curvature to decrease while condensation in the condenser increases this radius.

$$\Delta P_c = \sigma\left(\frac{1}{R_e} + \frac{1}{R_c}\right) \quad \text{(Eq. A-2)}$$

Where Re and Rc are the radii of curvature in the evaporator and condenser respectively (Peterson, 1994). Maximum capillary pressure happens when both of the radii curvatures to be minimum. For a circular pore;

$$(R_e, R_c)_{min} = \frac{r_c}{\cos\theta} \quad \text{(Eq. A-3)}$$

and as a result,

$$\Delta P_{c,max} = 2\sigma\frac{\cos\theta}{r_c} \quad \text{(Eq. A-4)}$$

This is the same as equation 3-5.

Wetting fluids are the ones with a contact angle between 0 and 90 degree while non-wetting liquids have a contact angle between 90 and 180 degree. This is shown in figure A-8.

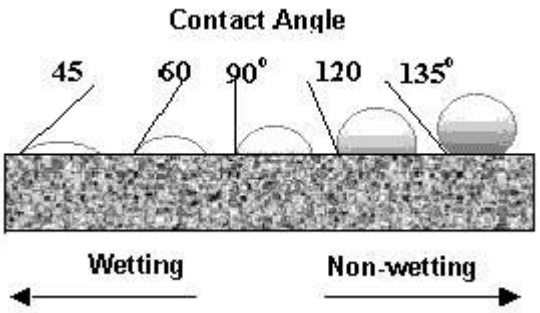

Figure A- 8 Wetting and non-wetting fluids

All the working fluids used in heat pipe have to be wetting for the heat pipe material. According to equation A-4, for a certain capillary radius, contact angle is only a function of the surface tension while this is only valid for completely flat surfaces. The wetting mechanism is still an active research area mainly for development of super-hydrophobic surfaces (non-wetting surfaces for self-cleaning, drag reduction and other applications) but it is known that the contact angle is not only influenced by surface tension but also by the surface structure (roughness and morphology). In reality contact angle depends on how the fluid is delivered and formed on a surface and it changes with surface roughness.

Because in this project AlSi12 aluminium alloy was being used to build heat pipes to work with ammonia (acetone in the experiments), it was essential to get an idea of the wet-ability of these fluids on this aluminium alloy. Like other parameters, precise measurements of the contact

angles needs much more comprehensive studies and resources that is out of the scope of this project. This contact angle and wet-ability was measured only for acetone since for ammonia, special measuring equipments are needed as it is not in its liquid form at normal ambient temperature and the following droplet method can not be used for that. The measured value has been used in the developed design tool explained in the previous chapter.

In this project the conventional method of measuring contact angle was implemented by dropping a droplet on the surface of the SLM heat pipe prototypes and measuring its left and right contact angles.

Figure A-9 shows the measurement rig setup;

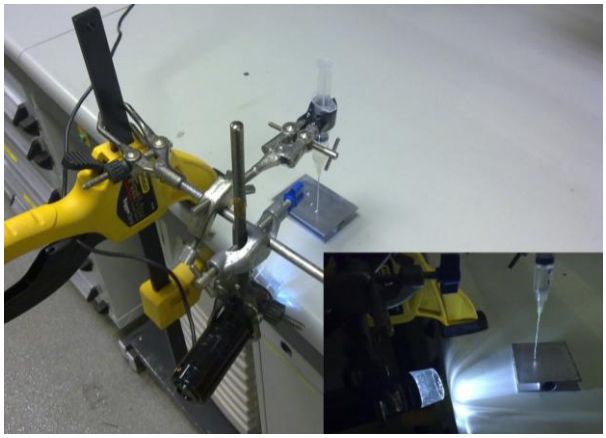

Figure A- 9 Contact measurement test set up

Two SLM heat pipe samples were used, one with the natural finish as it is produced by the SLM machine and one with a polished surface;

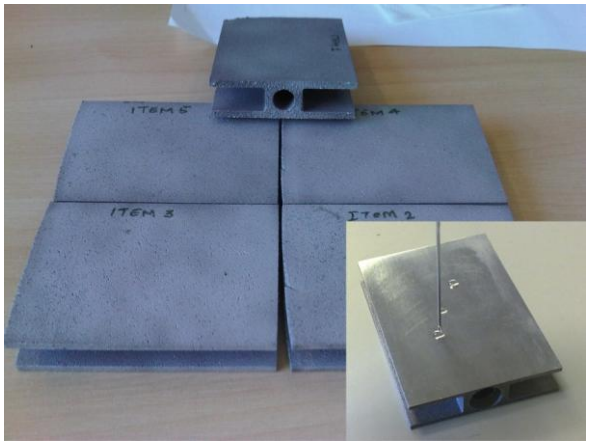

Figure A- 10 SLM HP samples - Natural surface finish and machined surface (in inset)

Several drops of acetone were introduced to different locations on each of the two surfaces and their contact angle was measured on both sides as depicted in Figure A-11.

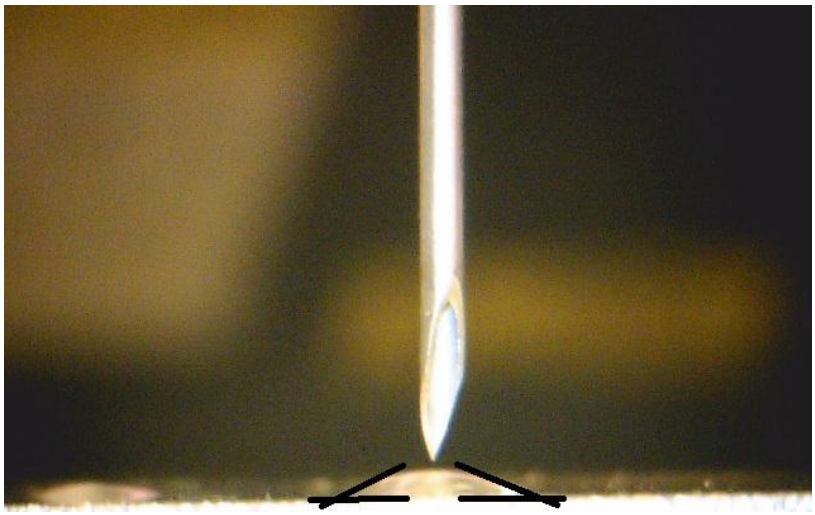

Figure A- 11 An acetone drop on the surface to measure its left and right contact angles

The results are presented in Table A-6.

Table A- 6 Contact angle measurement for acetone drops on natural and machined surfaces of SLM ALSi12 samples

Surface	Left angle °	Right angle°	Surface	Left angle°	Right angle°
Machined-drop1	22	21	Natural-drop1	21	18
Machined -drop2	20	19	Natural-drop2	25	22
Machined -drop3	20	18	Natural-drop3	22	14
Machined -drop4	18	15	Natural-drop4	20	20
Machined -drop5	18	16	Naural-drop5	21	19
Machined -drop6	22	25	Natural-drop6	12	17

All drops were tried to be similar and to be delivered in the same way but generating identical droplets and measuring conditions was impossible due to the test rig setup method. Moreover surface flatness slightly differs at different area and acetone evaporates quickly in the lab environment so the time spent to generate the droplet and to take each photo could have

affected the measurements. These justify the variations in measurements. No meaningful difference is seen between the natural and machined surfaces. This might be due to the fact that the droplets have been much bigger than the average roughness. For the calculations in this project the average value of all the above measurement or 19.4 degree has been used.

Development of the ammonia filling rig

The process to fill the working fluid into heat pipes varies considerably depending on the type of the heat pipe and the fluid. This process for the copper-water heat pipes was explained in section 3-6 but for aluminium/ammonia heat pipes it is considerably more complicated.

The first issue is that ammonia is in its gaseous state at normal ambient temperature unlike water or acetone. Moreover working with ammonia is associated with serious safety hazards and needs specially designed environment and equipment and on top of that, aluminium is extremely reactive with the smallest traces of oxygen (that also exist in any remaining water content in ammonia) so purity of ammonia and cleanliness of the process is of prime importance to avoid short or long terms failure of the pipe due to generation of non condensable gasses inside the pipe.

One of the major activities during almost the entire project was to develop an ammonia filling rig in a specially designed ammonia laboratory in Thermacore, the industrial partner of the project. The operation principle of the rig is to evaporate the anhydrous ammonia from the ammonia tank, condensing and measuring the required volume inside an intermediate tank, called Ullage tank and then evaporating the measured volume of the ammonia from the Ullage tank and condensing it inside the heat pipe and then repeating this process for several time by filling and flushing the pipe to ensure that any remaining air or impurity has been extracted from the pipe.

This process stimulates several cooling and heating circuits, vacuum tight precision valves, connections and measuring instruments as shown in Figure A-12 schematically.

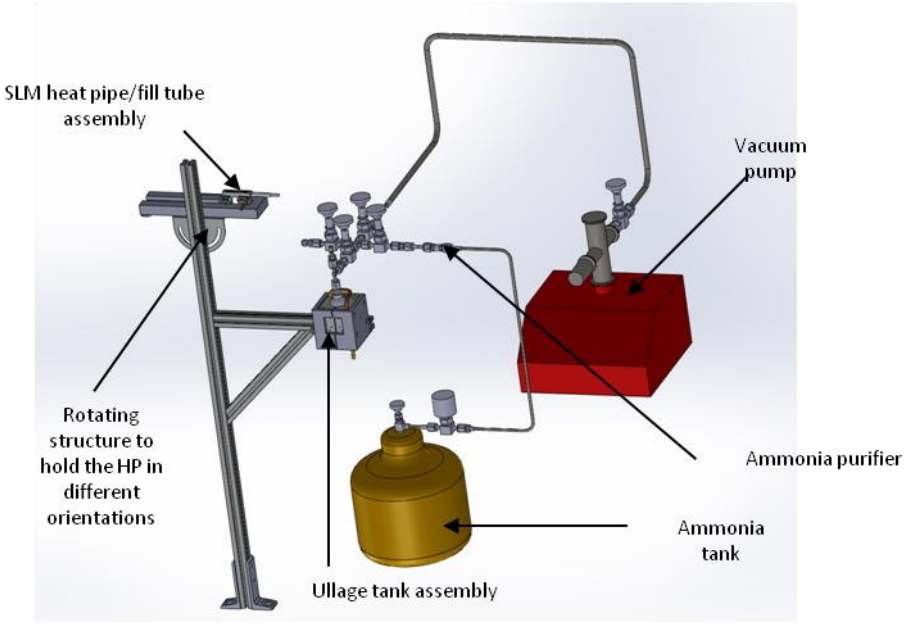

Figure A- 12 Ammonia filling/venting rig

An Ullage tank assembly including the heating/cooling features were designed for this rig as shown in Figures A-13 and A-14.

Figure A- 13 Ullage tank and its cooling/heating jacket

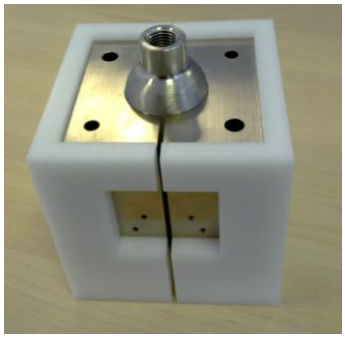

Figure A- 14 Ullage tank assembly. Two of the holes shown are the passages for the liquid from Chiller for cooling the Ullage tank and the other two are fitted with heater cartridges for heating

Figure A-15 demonstrates the completed ammonia filling rig.

Figure A- 15 Completed ammonia filling rig to fill ammonia into SLM HPs

Proof pressure test

Proof pressure tests were conducted on all the samples to ensure that they will not deform (or burst) at the maximum temperature that they will be exposed to, in a functional or un-functional state. For the acetone experiments, the samples were proof-pressure tested at 20bar and then at 70 bar in preparation for the ammonia tests although the latter was not conducted. All the samples passed the proof pressure tests with no deformation. Following is a description of the process in each test.

For initial thermal performance tests with acetone, the heat pipe temperature is not expected to go above 150°C. Acetone saturated vapour pressure at 150°C is around 4 bar. With a high safety factor, the sample was proof-pressure tested at 20 bar. To do this, the sample is marked and measured at several point before and after the test. The difference between these measurements reveals any possible deformation of the sample. This is to recognise if any section of the pipe has bulged or distorted at that pressure. Pressure is increased at 5 bar increments with a few minutes stop at each increment and fifteen minutes hold at 20 bar pressure. The test layout, measurement points and measured results are shown below;

Figure A- 16 Proof pressure test layout

Figure A- 17 Dimension measuring points on the sample before and after proof pressure test

Table A- 7 Initial sample dimensions before and after proof pressure test @ 20bar						
Location ID	Left-to-right			Top-to-bottom		
	"Pre"	"Post"	Ratio (post/pre)	"Pre"	"Post"	Ratio (post/pre)
A	13.513	13.512	1.000	13.507	13.496	0.999
B	13.530	13.529	1.000	13.531	13.530	1.000
C	13.525	13.522	1.000	13.521	13.521	1.000
D	13.521	13.519	1.000	13.522	13.520	1.000
E	13.508	13.508	1.000	13.510	13.510	1.000
F	13.515	13.515	1.000	13.516	13.516	1.000

Table A- 7 Initial sample dimensions before and after proof pressure test @ 20bar						
Location ID	Left-to-right			Top-to-bottom		
	"Pre"	"Post"	Ratio (post/pre)	"Pre"	"Post"	Ratio (post/pre)
G	13.383	13.382	1.000	13.383	13.382	1.000
H	13.383	13.384	1.000	13.392	13.392	1.000

Measurement results show no sensible deformation at any point of the sample at 20bar.

Appendix B – List of the electrical instruments used for the experiments in Thermacore Europe for experiments traceability

Picco data logger		
Picco data logger		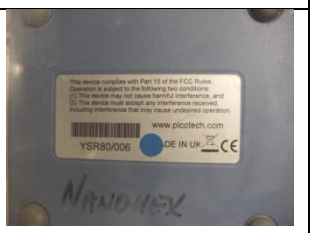
DC power supply		
Power meter		
Water pump		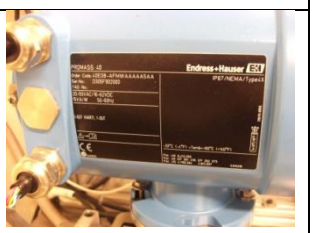

- Abd El-Baky, M. A., & Mohamed, M. M. (2007). Heat pipe heat exchanger for heat recovery in air conditioning. *Applied Thermal Engineering*, *27*(4), 795-801.
- Ahmed, Y. M. Z., M. I. Riad, et al. (2007). "Correlation between factors controlling preparation of porous copper via sintering technique using experimental design." Powder Technology **175**: 48-54.
- Almeida, R. (2004). NOVEL, COMPOSITE WICKS (FOR TWO-PHASED LOOPS), European Space Research and Technology Centre.
- Application of heat pipe technology in frozen soil safety. (2010). Retrieved May 01, 2013, from http://shengnuo-heatpipe.com/product/350-application-of-heat-pipe-technology-in-frozen-soil-safety---8b92/
- Arima, H., J. H. Kim, et al. (2010). "Local boiling heat transfer characteristics of ammonia in a vertical plate evaporator." International Journal of Refrigeration **33**: 359-370.
- Aronson, R. B. (1976). The heat pipe-Hot new way to save energy. *Machine Design*, *48*, 52-56.
- Atzeni, E., & Salmi, A. (2012). Economics of additive manufacturing for end-usable metal parts. *The International Journal of Advanced Manufacturing Technology*, *62*(9-12), 1147-1155.
- Bai, L., Lin, G., Wen, D., & Feng, J. (2009). Experimental investigation of startup behaviors of a dual compensation chamber loop heat pipe with insufficient fluid inventory. *Applied Thermal Engineering*, *29*(8), 1447-1456.
- Barantsevich, V., & Shabalkin, V. (2003). Heat pipes for thermal control of ISS solar battery drive. *Applied thermal engineering*, *23*(9), 1119-1123.
- Barthau, G. (1977). "Experimental investigation of convective boiling of ammonia at high pressure." Haet And Mass Transfer Source Book **Fifth**: 106-119.
- Bayasan, R. M., Korotchenko, A. G., Volkov, N. G., Pustovoit, G. P., & Lobanov, A. D. (2008). Use of two-phase heat pipes with the enlarged heat-exchange surface for thermal stabilization of permafrost soils at the bases of structures. *Applied Thermal Engineering*, *28*(4), 274-277.

- Bear, J. (2013). *Dynamics of fluids in porous media*. DoverPublications. com.
- Bertoldo J., Vlassov V., Candido P A., Genaro G., (2012). "Experimental performance comparison of axially grooved heat pipes charged with acetone and ammonia", 16th internal heat pipe conference, Lyon, France, May 20-24.
- Built environment. 2013. in *Collinsdictionary.com*. Retrieved July 9, 2013, from http://www.collinsdictionary.com/dictionary/english/built-environment?showCookiePolicy=true
- Carson, J. K., Lovatt, S. J., Tanner, D. J., & Cleland, A. C. (2005). Thermal conductivity bounds for isotropic, porous materials. *International Journal of Heat and Mass Transfer*, *48*(11), 2150-2158.
- Chen, Y., Zhang, C., Shi, M., Wu, J., & Peterson, G. P. (2009). Study on flow and heat transfer characteristics of heat pipe with axial "Ω"-shaped microgrooves. *International Journal of Heat and Mass Transfer*, *52*(3), 636-643.
- CHEN, Y., ZHU, W., ZHANG, C., & SHI, M. (2010). Thermal characteristics of heat pipe with axially swallow-tailed microgrooves. *Chinese Journal of Chemical Engineering*, *18*(2), 185-193.
- Chi, S. W. (1976). Heat pipe theory and practice: a sourcebook.
- Chiu, L. H., Wu, C. H., & Lee, P. Y. (2007). Comparison between oxide-reduced and water-atomized copper powders used in making sintered wicks of heat pipe. *China Particuology*, *5*(3), 220-224.
- Combs, S. K. (1978). "An Experimental Study of heat Transfer Enhancement forr Ammonia Condensing on Vertical Fluted Tubes." Technical Report, ORNL-5356, Oak Ridge National Laboratory.
- Combs, S. K. (1979). "Experimental Data for Ammonia Condensation on Vertical and Inclined Fluted Tubes." Technical Report, ORNL-5488, Oak Ridge National Laboratory.
- Cotter, T. P. (1965). "Theory of Heat Pipes", Los Alamos Scientific Laboratory Report No. LA-3246-MS.
- Dobre, T., Pârvulescu, O. C., Stoica, A., & Iavorschi, G. (2010). Characterization of cooling systems based on heat pipe principle to control operation temperature of high-tech electronic components. *Applied Thermal Engineering*, *30*(16), 2435-2441.
- Domingo, N. and J. W. Michel (1981). "Ammonia Condensation Experiments at Oak Ridge National Laboratory." Technical Report, CONF-810622-1, Oak Ridge National Laboratory.

- Domingo, N. (1982). "Condensation of Ammonia on the Outside of Smooth and Fluted Tubes at Various Tube Positions." Technical Report, ORNL-5826, Oak Ridge National Laboratory.
- Dullien, F. A. (1991). *Porous media: fluid transport and pore structure*. Access Online via Elsevier.
- ECSS, European cooperation for space standardization, (2010). "Qualification of two-phase heat transport systems", ECSS-E-ST-31-02C, Noordwijk, The Netherlands, ESA-ESTEC Requirements & Standards Division.
- Eggers P. E., Serkiz A. W., Burian R. J., (1971). "Development of high power density ammonia heat pipes", ASME winter annual meeting, Washington, D.C. November 28-December 2.
- ESDU (1979). "Heat Pipe Properties of Common Small Pore Wicks." ESDU 79013.
- Faghri, A. (1995, July). Heat pipe science and technology. In *Fuel and Energy Abstracts* (Vol. 36, No. 4, pp. 285-285). Elsevier.
- Hanlon, M. A., & Ma, H. B. (2003). Evaporation heat transfer in sintered porous media. *TRANSACTIONS-AMERICAN SOCIETY OF MECHANICAL ENGINEERS JOURNAL OF HEAT TRANSFER*, *125*(4), 644-652.
- Harwell, W., Mcintosh, R. (1981). "The OAO heat pipes - 8 1/2 years of flight data". Conference proceedings, Advances in heat pipe technology; London; September 7-10, 1981. (A82-42091 21-34) Oxford, Pergamon Press, 1981, p. 601-618.
- Hayley, D. W. (1982). Application of heat pipes to design of shallow foundations on permafrost. In *Fourth Canadian Permafrost Conference: National Research Council of Canada, Ottawa* (pp. 535-544).
- Heuer, C. E. (1979). *The application of heat pipes on the Trans-Alaska Pipeline* (No. CRREL-SR-79-26). COLD REGIONS RESEARCH AND ENGINEERING LAB HANOVER NH.
- Hoa, C., Demolder, B., & Alexandre, A. (2003). Roadmap for developing heat pipes for ALCATEL SPACE's satellites. *Applied thermal engineering*, *23*(9), 1099-1108.
- Iverson, B. D., Davis, T. W., Garimella, S. V., North, M. T., & Kang, S. S. (2007). Heat and mass transport in heat pipe wick structures. *Journal of thermophysics and heat transfer*, *21*(2), 392-404.
- Jiao, A. J., Ma, H. B., & Critser, J. K. (2007). Evaporation heat transfer characteristics of a grooved heat pipe with micro-trapezoidal grooves. *International journal of heat and mass transfer*, *50*(15), 2905-2911.

- Jones J. A., (1983) “Aluminium/Ammonia heat pipe gas generation and long term system impact for the space telescope’s wide field planetary camera”, Applied mechanics technology, Jet propulsion laboratory.
- Kaya, T. (2009). Analysis of vapor–gas bubbles in a single artery heat pipe. *International Journal of Heat and Mass Transfer*, *52*(25), 5731-5739.
- Kerrigan K., O’Donnell G. E., Jouhara H., Robinson A. J., (2012). “A high power density and low water content heat pipe natural convection heat exchanger for domestic heating application”, 16th international heat pipe conference, Lyon, France, May 20-24.
- Kreeb, H., Groll, M., & Zimmerman, P. (1973). Lifetest investigations with low-temperature heat pipes. *Proceeding of 1stIHPC, Sttutgart, Germany, October1973, Paper*, (4), 1.
- Larkin B.S., Dubuc S., (1975). “Self de-icing navigation buoys using heat pipes”, Division of mechanical eng. national research council Ottawa, Canada.
- Leong, K. C., Liu, C. Y., & Lu, G. Q. (1997). Characterization of sintered copper wicks used in heat pipes. *Journal of Porous Materials*, *4*(4), 303-308.
- Li, C., G. P. Peterson, et al. (2006). "Evaporation/Boiling in Thin Capillary Wicks (l)—Wick Thickness Effects." Journal of Heat Transfer **128**: 1312.
- Li, Y., Xiao, H., Lian, B., Tang, Y., & Zeng, Z. X. (2008). Forming method of axial micro grooves inside copper heat pipe. *Transactions of Nonferrous Metals Society of China*, *18*(5), 1229-1233.
- Lips, S., Lefèvre, F., & Bonjour, J. (2009). Nucleate boiling in a flat grooved heat pipe. *International Journal of Thermal Sciences*, *48*(7), 1273-1278.
- Liu, D., G. Tang, et al. (2006). "Modeling and experimental investigation of looped separate heat pipe as waste heat recovery facility." Applied Thermal Engineering **26**: 2433-2441.
- Liu, Z., Chong, P. H., Skeldon, P., Hilton, P. A., Spencer, J. T., & Quayle, B. (2006). Fundamental understanding of the corrosion performance of laser-melted metallic alloys. *Surface and Coatings Technology*, *200*(18), 5514-5525.
- Loh, C. K., Harris, E., & Chou, D. J. (2005, March). Comparative study of heat pipes performances in different orientations. In *Semiconductor Thermal Measurement and Management Symposium, 2005 IEEE Twenty First Annual IEEE* (pp. 191-195). IEEE.
- Louvis E., Fox P., Sutcliffe C. J. (2011). “Selective laser melting of aluminium components”. Journal of Materials Processing Technology 211 275–284.

- Maydanik, Y. F. (2005). Loop heat pipes. *Applied Thermal Engineering*, *25*(5), 635-657.
- McGlen, R. (2011). Next generation Heat pipes for Thermal Management in Space, Thermacore Europe.
- McIntosh, R., Ollendorf, S. T. A. N. F. O. R. D., & Harwell, W. (1975). The International Heat Pipe Experiment. *AIAA Paper*, (75-726).
- Mercelis, P., & Kruth, J. P. (2006). Residual stresses in selective laser sintering and selective laser melting. *Rapid Prototyping Journal*, *12*(5), 254-265.
- Munzel, W. D., & Savage, C. J. (1976). Lifetests of artery heat pipes for low temperature range. *Heat Pipes*, *1*, 383-392.
- Murr, L. E., Gaytan, S. M., Medina, F., Lopez, H., Martinez, E., Machado, B. I., ... & Bracke, J. (2010). Next-generation biomedical implants using additive manufacturing of complex, cellular and functional mesh arrays. *Philosophical Transactions of the Royal Society A: Mathematical, Physical and Engineering Sciences*, *368*(1917), 1999-2032.
- Noie-Baghban, S. H., & Majideian, G. R. (2000). Waste heat recovery using heat pipe heat exchanger (HPHE) for surgery rooms in hospitals. *Applied Thermal Engineering*, *20*(14), 1271-1282.
- Okihara T., Kanamori M., Kamimura A., Hamada N., Matsuda S., Buturlia J., Miskolczy G., (1980). "Design, Testing, and shipboard evaluation of a heat pipe de-icing system", AIAA Pap AIAA Thermophys Conf, 15th.
- Ollendorf S., McIntosh R., Harwell W., (1973). "Performance of Heat Pipes in Zero Gravity", 2nd International Heat Pipe Conference
- Panchal, C. B., E. H. Buyco, et al. (1980). "A spirally fluted tube heat enhancement as a condenser and evaporator on a vertical fluted surface." Numer Heat Transfer **3**: 357-371.
- Peterson, G. P. (1994). An introduction to heat pipes. Modeling, testing, and applications. *Wiley Series in Thermal Management of Microelectronic and Electronic Systems, New York, Chichester: Wiley,| c1994*, *1*.
- Prado P., Mishkinis D., Kulakov A., Radkov A., Torres A., Tjibtahardja T., Merino A., (2012). "Performance of an ammonia loop heat pipe operating at temperatures up to 125°C", 16th international heat pipe conference, Lyon, France, May 20-24.
- Pruzan, D. A., Klingensmith, L. K., Torrance, K. E., & Avedisian, C. T. (1991). Design of high-performance sintered-wick heat pipes. *International journal of heat and mass transfer*, *34*(6), 1417-1427.

- Ranjan, R., Murthy, J. Y., & Garimella, S. (2009). Analysis of the wicking and thin-film evaporation characteristics of microstructures.
- Reay, D., & Kew, P. A. (2006). *Heat pipes: Theory, design and applications*. Butterworth Heinemann.
- Riehl, R. R., & Dutra, T. (2005). Development of an experimental loop heat pipe for application in future space missions. *Applied Thermal Engineering*, *25*(1), 101-112.
- Riffat, S. B., & Gan, G. (1998). Determination of effectiveness of heat-pipe heat recovery for naturally-ventilated buildings. *Applied Thermal Engineering*, *18*(3), 121-130.
- Rosenfeld J. H., Sanzi J. L., (2012). "Analysis results of a ten year sodium heat pipe life test", 16th international heat pipe conference (16th IHPC), Lyon, France, May 20-24.
- Sabin, C. M., H. F. Poppendiek, et al. (1977). "Heat Transfer Enhancement for the OTEC Evaporator Technical Report." GLR.197 Geoscience, CA.
- Savage, C. J. (1976). Development of artery heat pipes in Europe under ESA sponsorship. *Heat Pipes*, *1*, 373-381.
- Semenic, T., Lin, Y. Y., Catton, I., & Sarraf, D. B. (2008). Use of biporous wicks to remove high heat fluxes. *Applied Thermal Engineering*, *28*(4), 278-283.
- Semenic, T. and I. Catton (2009). "Experimental study of biporous wicks for high heat flux applications." International Journal of Heat and Mass Transfer **52**: 5113-5121.
- Shao, L., & Riffat, S. B. (1997). Flow loss caused by heat pipes in natural ventilation stacks. *Applied thermal engineering*, *17*(4), 393-399.
- Shigehid Takagi and S. Yamauchi (1990). Porous Ceramic Material and Process for Preparing some. United States.
- Somchai, J., D. John, et al. (2007). Heat Pipe Application. Encyclopedia of Energy Engineering and Technology - 3 Volume Set (Print Version), CRC Press**:** 807-813.
- Soylemez, M. S. (2003). On the thermoeconomical optimization of heat pipe heat exchanger HPHE for waste heat recovery. *Energy conversion and management*, *44*(15), 2509-2517.
- Spindler, K. (2010). "Overview and discussion on pool boiling heat transfer data and correlations of ammonia." International Journal of Refrigeration **33**: 1292-1306.

- Sviridenko, I. (2008). "Heat exchangers based on low temperature heat pipes for autonomous emergency WWER cooldown systems." Applied Thermal Engineering **28**: 327-334.
- Thermacore. from http://www.thermacore.com/products/extreme-temperature.aspx.
- Thermacore. "Axially Grooved Heat Pipes." from http://www.thermacore.com/products/axially-grooved-ammonia-heat-pipe.aspx.
- Thermacore. "Heat Pipe Technology." from http://www.thermacore.com/thermal-basics/heat-pipe-technology.aspx.
- Thome, J., L. Cheng, et al. (2008). "Flow boiling of ammonia and hydrocarbons: A state-of-the-art review." International Journal of Refrigeration **31**: 603-620.
- Tuck, C., & Hague, R. (2006). The pivotal role of rapid manufacturing in the production of cost-effective customised products. *International Journal of Mass Customisation*, *1*(2), 360-373.
- Vasiliev L., Grakovich L. P., Pylilo L. E., (1978). "Application of heat pipes for freezing grounds", The A. V. Luikov heat and mass transfer institute, Minsk, USSR.
- Vasiliev, L. L. (1998). REVIEW PAPER State-of-the-art on heat pipe technology in the former Soviet Union. *Applied thermal engineering*, *18*(7), 507-551.
- Vasiliev, L. L. (2005). Heat pipes in modern heat exchangers. *Applied thermal engineering*, *25*(1), 1-19.
- Vasiliev, L., & Vasiliev Jr, L. (2005). Sorption heat pipe—a new thermal control device for space and ground application. *International journal of heat and mass transfer*, *48*(12), 2464-2472.
- Vasiliev L., Grakovish L. P., Rabetsky M. I., Vasiliev L. Jr., (2012). "Grooved heat pipe evaporators with porous coating", 16th international heat pipe conference, Lyon, France, May 20-24.
- Violante, M. G., Iuliano, L., & Minetola, P. (2007). Design and production of fixtures for free-form components using selective laser sintering. *Rapid Prototyping Journal*, *13*(1), 30-37.
- Vlassov, V. V., de Sousa, F. L., & Takahashi, W. K. (2006). Comprehensive optimization of a heat pipe radiator assembly filled with ammonia or acetone. *International journal of heat and mass transfer*, *49*(23), 4584-4595.
- Wan, J. W., Zhang, J. L., & Zhang, W. M. (2007). The effect of heat-pipe air-handling coil on energy consumption in central air-conditioning system. *Energy and buildings*, *39*(9), 1035-1040.

- Wang, Y. X., & Peterson, G. P. (2003). Analytical model for capillary evaporation limitation in thin porous layers. *Journal of thermophysics and heat transfer*, *17*(2), 145-149.
- Weibel, J. A., Garimella, S. V., & North, M. T. (2010). Characterization of evaporation and boiling from sintered powder wicks fed by capillary action. *International Journal of Heat and Mass Transfer*, *53*(19), 4204-4215.
- Weinbrandt, R. M., & Fatt, I. M. (1969, June). Scanning electron microscope study of the pore structure of sandstone. In *The 11th US Symposium on Rock Mechanics (USRMS)*.
- Wong, S.-C., J.-H. Liou, et al. (2010). "Evaporation resistance measurement with visualization for sintered copper-powder evaporator in operating flat-plate heat pipes." International Journal of Heat and Mass Transfer **53**: 3792-3798.
- Yadroitsev, I., Bertrand, P., & Smurov, I. (2007). Parametric analysis of the selective laser melting process. *Applied surface science*, *253*(19), 8064-8069.
- Yau, Y. H., & Ahmadzadehtalatapeh, M. (2010). A review on the application of horizontal heat pipe heat exchangers in air conditioning systems in the tropics. *Applied Thermal Engineering*, *30*(2), 77-84.
- Zhang, H., & Zhuang, J. (2003). Research, development and industrial application of heat pipe technology in China. *Applied thermal engineering*, *23*(9), 1067-1083.
- Zhang, E., & Wang, B. (2005). On the compressive behaviour of sintered porous coppers with low to medium porosities—Part I: Experimental study. *International journal of mechanical sciences*, *47*(4), 744-756.
- Zhang, C., Chen, Y., Shi, M., & Peterson, G. P. (2009). Optimization of heat pipe with axial "Ω"-shaped micro grooves based on a niched Pareto genetic algorithm (NPGA). *Applied Thermal Engineering*, *29*(16), 3340-3345.
- Zhang, L., & Lee, W. L. (2011). Evaluating the use heat pipe for dedicated ventilation of office buildings in Hong Kong. *Energy Conversion and Management*, *52*(4), 1983-1989.

- {da Silva Lima}, R. J., J. {Moreno Quibén}, et al. (2009). "Ammonia two-phase flow in a horizontal smooth tube: Flow pattern observations, diabatic and adiabatic frictional pressure drops and assessment of prediction methods." International Journal of Heat and Mass Transfer 52: 2273-2288.
- Anderson, W. G., P. M. Dussinger, et al. (2008). "High Temperature Titanium-Water and Monel-Water Heat Pipes." Aerospace: 1-12.
- Azad, E. (2008). "Theoretical and experimental investigation of heat pipe solar collector." Experimental Thermal and Fluid Science 32: 1666-1672.
- Bourdoukan, P., E. Wurtz, et al. (2008). "Potential of solar heat pipe vacuum collectors in the desiccant cooling process: Modelling and experimental results." Solar Energy 82: 1209-1219.
- Fang, G., X. Liu, et al. (2009). "Experimental investigation on performance of ice storage air-conditioning system with separate heat pipe." Experimental Thermal and Fluid Science 33: 1149-1155.
- James, C. and S. J. James (1999). "The heat pipe and its potential for enhancing the freezing and thawing of meat in the catering industry ´ s dans l ' industrie alimentaire , pour la Le caloduc et ses possibilite ´ lation et la de ´ conge ´ lation de la viande conge." International Journal of Refrigeration 22: 414-424.
- Kerrigan, K., H. Jouhara, et al. (2010). "Heat pipe-based radiator for low grade geothermal energy conversion in domestic space heating." Simulation Modelling Practice and Theory: 1-10.
- Ling, Z. (2004). "A study on the new separate heat pipe refrigerator and heat pump." Applied Thermal Engineering 24: 2737-2745.
- Max, A. (2006). Ammonia. Ullmann's Encyclopedia of Industrial Chemistry, Weinheim: Wiley-VCH: 143.
- Malek, A. and R. Colin (1983). "Ebulition de l'ammoniac en tube long. Transfer de chaleur et pertes de charges en tubes vertical et horizontal " Centre Technique des Industries Mecaniques, Senlis, France CETIM-14-011: 1-65

- Marcus, B. D. and G. L. Fleischman (1977). Flat-Plate Heat pipe. U. S. Patent. United States, The United States of America as represented by the Administartor of the National Aeronautics and Space Administration, Washington, D.C. 4046190.
- Ohadi, M. M., S. S. Li, et al. (1996). "Critical review of available correlations for two-phase flow heat transfer of ammonia Synthese critique des corr61ations disponibles pour le transfert de chaleur lors de l ' 6coulement biphasique de l ' ammoniac." Science 19: 272-284.
- Oliveti, G. and N. Arcuri (1997). "Solar Radiation Utilizability Method in Heat Pipe Panels." Solar Energy 57.
- Riffat, S., S. Omer, et al. (2001). "A novel thermoelectric refrigeration system employing heat pipes and a phase change material: an experimental investigation." Renewable Energy 23: 313-323.
- Riffat, S. and X. Zhao (2004). "A novel hybrid heat-pipe solar collector/CHP system—Part II: theoretical and experimental investigations." Renewable Energy 29: 1965-1990.
- Shabgard, H., T. L. Bergman, et al. (2010). "High temperature latent heat thermal energy storage using heat pipes." International Journal of Heat and Mass Transfer 53: 2979-2988.
- Tundee, S., P. Terdtoon, et al. (2010). "Heat extraction from salinity-gradient solar ponds using heat pipe heat exchangers." Solar Energy 84: 1706-1716.
- Yau, Y. (2008). "The use of a double heat pipe heat exchanger system for reducing energy consumption of treating ventilation air in an operating theatre—A full year energy consumption model simulation." Energy and Buildings 40: 917-925.
- Zhao, X., Z. Wang, et al. (2010). "Theoretical investigation of the performance of a novel loop heat pipe solar water heating system for use in Beijing, China." Applied Thermal Engineering 30: 2526-2536.
- Ziapour, B. M. and A. Abbasy (2010). "First and second laws analysis of the heat pipe/ejector refrigeration cycle." Energy 35: 3307-3314.